SYNTHESIS OF GROUND-WATER DISCHARGE DEPOSITS NEAR YUCCA MOUNTAIN

J.B. Paces[1], R.M. Forester[1], J.F. Whelan[1], S.A. Mahan[1], J.P. Bradbury[1], J. Quade[2], L.A. Neymark[1], L.M. Kwak[1]

[1]U.S. Geological Survey, Denver, CO
[2]University of Arizona, Tucson, AZ

ABSTRACT

Distinct, fine-grained (silt to fine sand), eolian deposits containing varying amounts of calcareous or siliceous cements and fossils are scattered throughout the Amargosa Valley and adjacent areas. These deposits have been examined in reconnaissance fashion, and sampled for geochronologic, isotopic, and paleontological studies to provide evidence for their origin and timing. Uranium-series disequilibrium, thermoluminescence and radiocarbon dating techniques have been applied to a wide range of materials including nodular and tabular carbonates, insect-burrow casts, calcified and silicified plant petrifactions, mollusc shells, and the silts themselves. Results are generally concordant with both stratigraphy and between methods. These data indicate that latest activity at all sites occurred between 10 and 15 ka. The consistency of young ages by all three methods strongly indicate a primary age significance. Materials younger than 9 to 15 ka have not been identified indicating that activity ceased around 12 to 15 ka in up-gradient sites, and slightly later (~9 ka) down-gradient at lower elevations. At sites with vertical exposure, $^{230}Th/U$ ages span the last two glacial cycles. In general, ages of deposits span a period of about 15 to 60 ka, and an older episode of about 90 to 180 ka. The break between these two time spans appears to be related to lithologic breaks at several sites. Consistency of dating results between scattered deposits indicates that regional rather than local controls dominate the activity at these sites.

Carbonates from discharge deposits show a limited range of $\delta^{18}O$ values of about 19±1‰ for samples least effected by surface evaporation. A larger range is apparent for $\delta^{13}C$, however differences are generally related to the type of sample: nodular carbonates and calcite cements typically have higher $\delta^{13}C$ (to +2‰) than mollusc shells and plant petrifactions (-10 to -5‰). Oxygen isotopes are distinct from carbonates associated with active discharge of water from deep carbonate aquifers (Grapevine Springs, Nevares Spring, Devils Hole) characterized by $\delta^{18}O$ of 13 to 16‰. Temperatures for the effluent at these springs is typically elevated above mean annual temperature and indicates equilibration with deeper geotherms during transit. The higher $\delta^{18}O$ values observed for Amargosa Valley discharge deposits are consistent with cooler temperatures, recharge at lower elevations, or both, and are compatible with shallower and shorter ground-water flow paths relative to currently active springs.

Ostracode and diatom assemblages from Amargosa Valley discharge deposits indicate that paleodischarge supported a variety of paleoenvironments. These can be generally classified as seeps, flowing springs and spring-supported standing water (pools, wetlands). Reconstruction of paleoenvironments is based on comparing fossil assemblages with modern equivalents typically found in northern Nevada or higher latitudes.

Isotope (initial $^{234}U/^{238}U$, $\delta^{87}Sr$ and $\delta^{13}C$) and paleontological data indicate that a surface-water source for discharge deposits is not possible. Data also discount short-flow-path, perched aquifer systems associated with local recharge in adjacent highlands as a ground-water source. Instead, regional, saturated-zone ground water most-likely supplied discharge during pluvial episodes. This conclusion requires the regional water table to fluctuate up to about 100 to 120 m between pluvial and interpluvial periods. Fluctuations of the same magnitude occurred over the last two glacial cycles. The discharge record corresponds well to other climate proxies in the region and represents a rapid response of the saturated-zone to changes in mean annual precipitation, net infiltration and recharge. Over the past several hundred thousand years, data from discharge sites do not support the concept of a monotonically-declining water table in the region based on tectonic-driven factors. Indeed, much of the late Pleistocene was characterized by higher water tables (as much as 60 to 80% of the last 200 ka). Therefore, this it is anticipated that this hydrologic state will recur in the future.

TABLE OF CONTENTS

1. INTRODUCTION:

Effective isolation of high-level radioactive waste at the potential Yucca Mountain site requires not only a characterization of present-day hydrologic conditions, but also an understanding of the changes in those conditions that are likely to be encountered during the functional life span of the potential repository. Regional climate conditions in southern Nevada have changed dramatically over the past several hundred thousand years as a complex function of global climate factors. Past-climate proxy records from throughout the southern Great Basin clearly demonstrate that episodes of higher effective moisture relative to present-day conditions were resident about 70 to 80 percent of the time during the last 2 million years (Forester et al., 1996). An understanding of how increased amounts of surface water translate to ground-water dynamics is of great importance to the issue of radioactive waste isolation in the potential geological repository at Yucca Mountain. One means of providing reasonable bounds for the range of post-closure hydrologic conditions expected at the site is to characterize the record of conditions experienced in the region over the last four hundred thousand years.

The potential repository horizon is located approximately 200 to 400 m above the present-day water table. However, evidence for higher saturated-zone (SZ) water levels at some time in the past has been suggested based on secondary mineral occurrences (Levy, 1991) and Sr isotopic variations (Marshall et al., 1993) from borehole data and hydrologic models involving increased recharge (Czarnecki, 1985) in the Yucca Mountain regional flow system. Although evidence from these studies suggests a maximum increase in water-table elevation of 100 to 150 m, the timing of these fluctuations remains unconstrained. In addition to determining the maximum extent and timing of water-table fluctuations, dated paleohydrologic information from the saturated zone provides information on how rapidly ground-water hydrologic systems responded to changes in Pleistocene climate and indirectly may delineate changes in areas of significant recharge, flow paths and travel times.

Sparse vein materials from drill cores provide geological evidence for water-table fluctuations at Yucca Mountain. Ground-water discharge deposits are, however, commonly exposed in southern Crater Flat and the central Amargosa Valley (Figure 1). Those deposits are down-gradient from and within 15 to 20 km to central Yucca Mountain. This report is an attempt to compile and synthesize much of the data that are available for paleodischarge sites near Yucca Mountain. It builds upon reconnaissance data obtained by the USGS in previous years that concentrated on the geochronological determinations indicating the youthfulness (<20 ka) of parts of these deposits (Paces et al., 1993, Paces et al., 1994, Paces 1995). Additional information incorporated for the first time in this report include attempts to establish

working stratigraphic frameworks at individual sites, stable isotope data and micro-paleontological data. These data are used to develop a paleodischarge model that accounts for the history and origin of the deposits. The discharge model links hydrologic variations to climate change and will be used as input to both paleoclimate synthesis and as a natural test of the hydrologic response to future-climate scenarios.

2. STRATIGRAPHY AND GEOCHRONOLOGY

Ground-water discharge deposits from five separate areas in and adjacent to the Amargosa Valley have been studied (Figure 1) including the Crater Flat Deposit[1] (CFD), Crater Flat Wash Deposit (CFW, a.k.a., Root Cast Deposit), Lathrop Wells Diatomite Deposit (LWD; a.k.a., Horse Tooth Deposit, a.k.a. Highway 95 White Bed), State Line Deposits (SLD), and Indian Pass Deposit (IPD). The deposits all show general lithological and morphological similarities, typically consisting of whitish-gray to pale green fine-grained sandy to silty loam units. Coarse clastic material is conspicuously absent from most of the present exposures, although coarse gravel units may be inter-bedded locally or at depth. Where deposits adjoin gravelly alluvium (CFD, CFW and LWD) they often have a thin veneer of young gravel covering the up-slope areas during the time since the discharge was last active. The absence of coarse clastic material readily distinguishes discharge deposits from alluvial and colluvial deposits associated with surface water transport (Taylor, 1991; Quade et al., 1995). Particle size distribution within the discharge deposits is dominated by fine-sand and silt fractions. Bedding is typically massive, punctuated by occasional laterally-discontinuous layers of authigenic materials such as carbonate-rich nodules or mat-like layers, casts of insect burrows or plant petrifactions. Authigenic calcite and lesser silica produce a wide range of cementation from soft, barely-calcareous silt to contorted hard nodules to dense limestone containing regularly-spaced, sub-vertical tube-like voids that are probably plant-stem molds. Much of the layered or nodular limestone typically contains fine-grained siliciclastics (clays), which often complicates 230Th/U geochronologic interpretations. A one- to two-meter thick bed of white to whitish-gray diatomite is unique to the LWD deposit. Plant petrifactions, mollusc shells, ostracodes, vertebrate fossils and Native American artifacts (flints, scrapers) have been observed at most sites.

Observed features at the five sites resemble those described by Quade and others (1995) for more-laterally extensive deposits flanking the nearby Spring Mountains. Those deposits were interpreted as the result of eolian detritus captured by vegetation associated with wet, marshy ground or small, open water bodies along with authigenic minerals deposited from calcium- and silica-rich ground waters (Quade et al., 1995).

All samples are from natural surfaces and exposures or from shallow (<1.5 m) hand-dug pits. Although easily erodible, deposits are generally not deeply dissected. Several deposits expose a maximum of 1-2 m of stratigraphic thickness (CFW, CFD, IPD). A maximum stratigraphic thickness of 5-7 m is available in several arroyos that cut through the high terrace of the SLD near Franklin Well, and at the LWD, although not in a single section. Multiple lithologic units can be identified at each of the deposits, however systematic detailed mapping of these units has not yet been conducted. Qualitative observations indicate that some units may be laterally continuituous over tens to hundreds of meters. However, mound-like morphologies, multiple orifices, rapid facies changes, lack of distinct marker beds, multiple episodes of deposition and erosion, and the absence of trenching combine to frustrate simple geologic reconstruction at any of the sites.

A new set of stereographic air photographs at a scale of 1 to 2400 (1 cm = 24 m) have been obtained for three of the sites closest to Yucca Mountain (CFD, CFW and LWD). These photographs were used to locate previously-collected samples and served as the base for more-detailed stratigraphic examinations. Local stratigraphic sections were constructed at several of the sites, however attempts to characterize the overall stratigraphy at each site are deferred until more thorough maps of the deposits and trenches are available. Nevertheless, sketch maps showing sample locations and localized stratigraphic columns showing available geochronological information are presented below on a site-by-site basis.

2.1 Lathrop Wells Diatomite Deposit (LWD):

The LWD constitutes one of three discharge deposits flanking the low set of hills bounding southern Crater Flat. Figure 2 shows the surface distribution of fine-grained discharge deposits along with

[1] All locality names are informal and are only intended to facilitate discussion of the deposits in this report.

station locations (sample locations are given in Appendix 1). The deposit occurs low on the piedmont slope at an elevation of about 790 to 800 m. The up-slope portions of the deposit are partially covered by gravelly alluvium and colluvium consisting predominantly of tuff and lesser dark Paleozoic carbonate derived from the adjacent ridge. Down-slope portions are extensively eroded resulting in conspicuous bright-white badlands just north of the highway. Currently, discharge deposits are exposed over an area of about 600 by 400 m.

In the main area of exposure (eastern-most portion with abundant stations in Figure 2), the deposits are constructed of three major units that appear to be reasonably continuous: a lowermost green sandy unit, a middle diatom-rich unit, and a capping hackly siliceous to marly calcareous unit. Stratigraphic sections were measured at Stations 6 and 8 and are represented in Figures 3 and 4. Areas further west exhibit very poor exposure and no attempt is made to correlate units to the main badlands area. Deposits in the main badlands area contain a sparse distribution of carbonate- or silica-rich materials (plant petrifactions, nodular carbonate, and mollusc shells) that have been analyzed by uranium-series disequilibrium and radiocarbon dating techniques. Silts constituting the fine-grained eolian components of these deposits have been analyzed by thermoluminescence dating techniques. Geochronological results are summarized in Figures 3 and 4 and are briefly discussed below for each unit.

2.1.1 Capping marl: The uppermost thin (<1 m) capping marl unit is preserved as patchy, discontinuous occurrences on the up-slope side of the deposit. The unit contains abundant carbonate-opal plant petrifactions[2] as well as minor nodular carbonate of possible biogenic origin. These materials have been dated by uranium-series disequilibrium and yield a range of ages from 11 to 17 ka (Table 1, Figure 3). Plant petrifactions contain the highest U/Th ratios requiring only minimal detrital-^{230}Th corrections to measured isotope ratios (see Appendix 2 for correction methods). Therefore, propagated uncertainties are much smaller for these materials relative to ages calculated for samples of nodular carbonate with much higher detrital components and larger detrital-^{230}Th corrections (small versus large error ellipses, respectively, in Figure 5). Age estimates for plant petrifactions range from 12.3 to 16.0 ka with 2 sigma uncertainties of 0.1 to 0.3 ka and are shown on an uranium-series disequilibrium evolution plot of "most reliable" analyses (Figure 6) that excludes samples of nodular carbonate with similar ages but much greater uncertainties due to larger detrital-^{230}Th corrections. Initial $^{234}U/^{238}U$ (extrapolated $^{234}U/^{238}U$ back to the time of mineral formation) calculated for these same samples range from 3.7 to 3.9. Slightly higher and lower values are obtained for nodular carbonates with larger detrital corrections (3.4 to 4.3), but the greater uncertainties introduced by higher amount of the unmeasured detrital component (large error ellipses between the 10 to 20 ka isochrons on Figure 5) limit the usefulness of these analyses.

Three of four terrestrial gastropod shells (*Succinid*, *Vertigo Berryi*, and *Vallonia*) from the same unit have calibrated[3] radiocarbon ages of 16.2 to 16.3 ± 0.2 ka (Table 2); nearly identical to uranium-series disequilibrium results. Resolvably older ages of 16.8 and 16.9 ±0.2 ka were obtained from aquatic molluscs from the same sample location. The slightly older ages of these organisms is likely related to incorporation of part of their carbon from dissolved aquifer bicarbonate (Riggs, 1984) containing "dead" carbon acquired from old (Paleozoic) carbonates along the flow path or aging of aquifer water during transit between recharge and discharge sites (Brennan & Quade, 1995). One terrestrial snail sample (Vallonia) yielded a intermediate radiocarbon age of 16.7 ka ± 0.2 ka. In addition to the mollusc shells, a single analysis of a small, but very well-preserved silica/carbonate plant petrifaction was submitted for radiocarbon. Two uranium-series disequilibrium ages of 12.3±0.2 and 14.7±0.6 were obtained for this same sample (HD1385-1). However, unlike the mollusc-shell results, the radiocarbon age of 6.51±0.2 ka (Table 2) is significantly younger than uranium-series disequilibrium ages. The sample was collected from an exposed surface and may record the effects of carbon exchange with atmospheric carbon in solution in surface waters.

[2] Calcite- or opal-fossilized root and stem fragments showing moderate to excellent degrees of preservation of original biological textures and structures. The term rhizolith, although technically restricted to a petrified root, is used synonymously in data tables and elsewhere in this report.

[3] Conventional radiocarbon ages (corrected for isotopic fractionation using measured $\delta^{13}C$) less than about 20 ka were recalculated to calibrated radiocarbon ages using the CALIB 3.0.1 program of Stuiver and Reimer (1993) and data sets therein to account for variations in atmospheric production rates.

2.1.2 Diatomite: Much of the upper portion of the main badlands area at the LWD site consists of a white-gray, non-calcareous powdery loam containing abundant diatoms. A crude attempt to separate and date the diatoms directly by uranium-series disequilibrium failed due to relatively low U contents (1.11 ppm), and high Th contents (3.65) resulting in an analysis with an excessively-high detrital-Th correction. Although a high-purity diatom separate was not obtained, the measured U and Th contents indicated that the organisms do not appear to preferentially incorporate U from solution into their siliceous tests as observed in other forms of opal from these deposits.

Without a means of directly dating diatoms, samples were collected from the upper and lower thirds for thermoluminescence (TL) analysis. Resulting ages for the two samples from the diatomite at the Station 6 section (TL-65 and TL-66) yield identical ages within error overlap of 29±3 and 30±6 ka (Table 3, Figure 3). TL ages for both samples appear robust on the basis of uniform values for estimated dose determined at multiple temperatures (Figure 7) (plateau test, see Appendix 2). The constant ratio between natural and artificial glow-curves over the plateau region indicates that there has been negligible leakage of electrons out of traps over the duration of exposure to the ambient radiation field. Ages for the two samples indicate an accumulation of about 1.3 m of diatom-rich sandy loam over a relatively short interval (less than one to several thousand years). Although a TL age from the overlying capping marl is not available, the TL ages of 30 ka for the underlying diatomite are consistent with the 14 to 16 ka ages obtained by U-series and radiocarbon on the overlying marl.

In addition, the basal 20-30 cm of the diatomite contains small, hard fragments of mineralized plant debris. These materials are finer and lack the well-preserved internal structure observed in larger plant petrifactions. They consist of silica-replaced branching tubules with sand-rich sheaths that were removed prior to analysis. Only two fragments from the Station 6 section were analyzed (HD1970, Figure 3): one had low uranium (4.4 ppm) and high thorium (4.6 ppm) whereas the second had a similar thorium content, but much higher uranium (22 ppm). The high uranium analysis yields a relatively low-error age of 42±2 ka compared to the low-uranium analysis with a calculated age of 56±6 ka (Table 1, Figure 3). The presence of high-uranium material bodes promise for additional analyses in the future. These ages from the base of the diatomite are consistent with the younger TL age estimates higher up in the unit.

2.1.3 Green-sand unit: The whitish-gray diatomite unit is separated from the underlying green-sand unit by a distinctly-sharp contact over much of the main badlands area. The unit consists of a series of alternating hard green sands and mud-cracked silts containing common, but isolated, angular tuff chips. Overall grain-size is coarser than the diatomite, and sorting varies from moderate to very good. The upper portion is non-calcareous, however calcite content increases with depth. Several distinct nodular-carbonate zones are present within the unit and have been used to crudely correlate areas of non-continuous exposure. However, these zones do not have unique characteristics or appear to exhibit lateral continuity greater than 10 to 30 meters making confident correlation problematic.

The uppermost 20-30 cm of the green-sand unit contains fine petrified plant debris and nodular material replaced by silica. Two analyses were obtained from the Station 6 section (HD1971, Figure 3) on a composite small rhizolith sample (115±3 ka) and a small, hard nodular fragment (152±3 ka). The two analyses were both enriched in uranium and required minimal detrital-Th correction. The older of the two exhibits a low initial $^{234}U/^{238}U$ relative to most other materials in the deposit (discussed below) and may indicate a potential problem with the material. Additional analyses of uranium-enriched materials in the sample should allow a more-precise geochronological characterization in the future. Plant fragments are assumed to have been mineralized in place rather than having been reworked from older beds. They show no obvious effects of rounding by transport. In addition, other coarse, exogenous clastic material indicative of fluvial transport is absent suggesting that transport-energy levels were insufficient to rework older sediments.

The nodular zone at the base of the box-pit at the Station 6 section contains small, irregular, rounded concretions of dominantly calcite with lesser amounts of silica. Two analyses with high uranium and low thorium yield reasonably precise ages of 186±3 ka and 173±14 ka that overlap within error. Both have initial $^{234}U/^{238}U$ within the range clearly defined by younger materials from the capping marl. The agreement of both age and initial ratios provide a high degree of confidence that the U and Th in

these materials have behaved in a closed system since deposition.

Other nodular zones within the green-sand unit have been crudely correlated to the nodular zones within the Station 6 section box pit. These materials have been collected from surface exposures or from shallow, hand-dug pits (Figures 3 and 4). Many analyses tend to have low U/Th resulting in large detrital corrections and associated errors, and show evidence of secondary mobility of U. Uranium is readily oxidized to the hexavalent state and is transported as a variety of species in aqueous solution whereas tetravalent Th remains non-transportable under most surface conditions. As a result, U can be mobilized subsequent mineral formation yielding higher $^{230}Th/^{238}U$, apparent old ages (or non-calculable if ^{230}Th exceeds the limits of in situ production), and anomalously high calculated initial $^{234}U/^{238}U$. These effects are apparent on uranium-series disequilibrium evolution plots (Figure 5, for example) by increasing the $^{230}Th/^{238}U$ at constant $^{234}U/^{238}U$. Sample HD1974, a coarse nodular carbonate at Station 13, yields four analyses of increasing age and initial ratio from 120 to 193 ka and from 4.5 to 5.2, respectively (Figure 5). Although the analysis with an age of 120 ka may still exhibit effects of secondary U mobility, its age is interpreted to be closest to the age of deposition. Likewise for sample HD1464 from the same stratigraphic level beneath the diatomite at Station 7; the age of 164 ka and initial ratio of 5.4 is assumed to show the effects of U-loss, whereas subsamples with ages of 129 and 136 ka are assumed to be closer to the age of deposition although they too have high initial ratios of 4.9 and 4.6.

The section at Station 8N (Figure 4) is interpreted to represent a deeper level of exposure relative to the Station 6 section (Figure 3) based both on geological and geochronological correlation. Nodular carbonate from this section contained analyses with excess ^{230}Th (HD1978), or with finite ages affected by U-loss (HD1980). Several radiocarbon analysis of terrestrial and aquatic mollusc shells give conventional radiocarbon ages (not calibrated for variation in ^{14}C production rate) of 35 to 42 ka (Table 2). Although the dated shells have been hand-picked to exclude fragments with observable secondary calcite overgrowths, the percentage of modern carbon in these materials varies only between about 1 and 0.5. They are therefore sensitive to small amounts of contamination with a recent source of carbonate.

Although nodular carbonate from the base of the Station 8N section did not allow reliable U-series age determinations, possible correlation to nodules at about the same elevation 40 to 50 m west at Station 9 (Figure 2) may provide a more reliable age for the base of the section. Sample HD1976 consists of a dense limestone nodules scattered at the surface that are similar in shape and size to other nodular carbonate in the deposit, but are much harder and denser. A single large nodule was slabbed and subsampled from three separate areas of darker and denser carbonate accumulation relative to the lighter, softer matrix. Ages of 140±3, 211±8 and 244±7 ka were obtained with initial ratios of 3.5, 3.9 and 3.9, respectively. Although the range of subsample ages within the same 10 cm slab are difficult to reconcile, initial ratios are all within the range observed for most recent deposits. Additional nodules must be analyzed before interpretation of this spread of numbers can be adequately evaluated, however, a simple model of U-loss as described above cannot explain the difference between subsamples with ages of 211 and 244 ka.

Additional support of the older ages observed in HD1976 comes from a broad area containing coarsely-banded, tufa-like limestone south of the main badlands area closer to Highway 95. Sample HD1977 from Station 9s consists of a 15 to 20 cm thick slab that was cut and then subsampled with depth from the exposed surface. The stratigraphically highest subsample from several mm below the exposed outer surface yields an age of 140±3 ka, material at 1.5 to 2.0 cm below the surface yields an age of 172±3 ka, and two separate subsamples from the same layer at a depth of 3.0 to 3.5 cm yield identical ages of 208±5 and 204±4 ka. All four of these analyses have initial $^{234}U/^{238}U$ that are somewhat lower than most material analyzed at LWD (2.95 to 3.24 instead of 3.5 to 4.0. The array of points form a reasonably straight line on a U-series evolution plot (Figures 5 and 6) and could be explained by U-loss in the deeper material relative to the surface (considered unlikely due to the dense nature of sampled materials and probability of greater interaction of outermost layers with post-deposition solutions), or, more likely, by mixing of younger and older materials deposited during different climate cycles. A similar explanation is possible for subsamples of HD1976 accounting for the difference between the subsamples with ages of 140 and 210 ka, but not for the difference between subsamples with ages of 210 and 244 ka. A stipulation for a

mixing model in both samples is the requirement that the 140 ka calcite in both samples have different, but lower initial ratios than the rest of the associated subsamples.

An example of the complex stratigraphy present in this deposit is readily apparent near the southern end of the main badlands area where material exposed in a box-pit at Station 8, a mere 10 m south of Station 8N across a shallow drainage, bears little resemblance to the measured section at Station 8N. A schematic section is given in Figure 4b for comparison to deposits at approximately the same elevation as those in the section at Station 8N shown in Figure 4a. The capping brown hackly unit bears some resemblance to the latest Pleistocene capping marl on the up-slope side of the deposit, however its origin and relation to the underlying green sand is unclear. A robust age of 90.9±1.2 ka with an initial $^{234}U/^{238}U$ of 3.78 was obtained on a fragment of petrified plant debris in the middle of the exposed green sand unit. Other materials from this same horizon gave much older ages with anomalously high initial $^{234}U/^{238}U$ (7.4 and 13) and are suspected of having experienced U-loss. A better understanding of the stratigraphy at Station 8 and its relation to other parts of the deposit awaits better exposure through trenching activities.

In addition to U-series geochronology samples, four samples from various positions within the Green-sand unit were collected for thermoluminescence analysis. All samples were processed similarly and yielded similar age estimates between about 30 and 40 ka calculated for dose rates at half of their moisture-saturation values (Table 3, Figures 3 and 4). Dates from this unit may be slightly older than the two samples from the overlying diatomite (29 and 30 ka), but are very close to being within error overlap. Partial bleach results yield ages that are within analytical uncertainty of total bleach results for the three samples completed suggesting adequate resetting of TL traps prior to latest burial.

The six TL samples from throughout the deposit that produced reliable estimated dose plateaus have ages that appear to be in general agreement with stratigraphy. These apparent ages suggest a single episode of eolian activity between 29 and 42 ka that deposited 5 to 7 m of sand and silt with only very minor age differences between the green-sand and overlying diatomite units. However, these ages conflict with the older dates from authigenic cements in the green-sand unit that must be the same age or younger than the matrix materials in which they form. TL ages of 32 to 42 ka are strikingly younger than U-series ages on carbonate and silica from the same horizons, ranging between 115 and 186 ka in the box pit at Station 6, and between 91 and 244 ka elsewhere. Results from the two techniques cannot be resolved even when using the lowest calculated dose rates obtainable by assuming complete water saturation during their burial history. In this case, TL ages increase to between about 40 to 50 ka (Table 3).

Reasons for the discrepancy between geochronological methods are not understood at present. These deposits represent the first time in several years of collaborative study of colluvial and alluvial surface deposits as well as other discharge deposits (see below) where such a large discordance exists between methods. Agreement between U-series and radiocarbon dates for samples in the capping marl, as well as the gross uniformity of calculated initial ratios between oldest and youngest materials provide no indication of methodological errors for U-series dates. Also, the presence of major unconformity seen in U-series dates occurring at a very clear lithologic break provides some additional reassurance that older U-series ages are not the result of sample or analytical artifacts.

The most striking difference between deposits at the LWD and elsewhere in the Yucca Mountain area is the presence of common to abundant diatoms composed of opal. The most common species present, *denticula valida*, and its associates exhibit a range of grain sizes of several microns to several tens of microns, overlapping the 4 to 11 micron fraction used for TL. No attempt was made to preferentially remove diatoms during processing of silts for TL. The hydrous, non-crystalline form of silica may behave quite differently than the much more typical quartz in the sense of the type, presence, and stability of electron traps. If these traps are not capable of holding on to a stable TL signal, they will not contribute significantly to the luminescence measured in the laboratory, derived mainly from eolian silicate material (feldspars and quartz). Alternatively, traps may spontaneously empty without exposure to light or heat. In either case, the result will be a decrease in the estimated dose that yields an apparent age that is younger than the true age. Other factors also represent potential sources of TL age underestimates including excess ^{234}U in materials contributing to ambient radiation field, possible post-

depositional mobility of potassium or uranium, non-anomalous response of laboratory radiation, inadequate sample pre-heat routines, translocation of fines, or presence of soil diatoms that form after sediment burial.

2.2 Crater Flat Deposit (CFD):

The CFD occurs on the northern side of the set of low hills separating Crater Flat from Amargosa Valley. It represents the northernmost exposure of fine-grained paleodischarge deposits under investigation and, as such, is the closest to the potential repository (approximately 15 km to the north east). It also represents the highest elevation at about 840 m above sea level. Present-day distribution of deposits occurs mostly south and up-slope of the southernmost major wash near the confluence where the three major wash systems that drain the entire Crater Flat basin converge and exit through the narrow water gap to the south and slightly east (Figure 1). Figure 8 shows the surface distribution of fine-grained discharge deposits along with station locations (sample locations are given in Appendix 1). The deposits occupy a broad, gently-sloping apron derived from the low hills to the south. As at the LWD, the up-slope portions of the deposit are partially covered by sandy and gravelly alluvium, colluvium and eolian deposits, with gravel clasts composed predominantly of tuff and lesser dark Paleozoic carbonate. The deposit is not well-dissected, and therefore exhibits little stratigraphy that can be easily examined. Currently, CFD deposits cropout over an area of about 700 by 300 m, but they may extend substantially further west under a thin mantle of alluvium or colluvium. Two trenches were excavated in the early 1980's as part of the work by Swadley and Carr (1987) in an attempt to delineate strand-lines associated with a possible Lake Amargosa. Neither of these two trenches (informally called East Trench and West Trench) transect fine-grained discharge deposits typical of the bulk of the deposit. They expose sandy alluvial materials that may exhibit ground-water overprinting. Unfortunately, the relations between fluvial units in trenches and eolian materials constituting the bulk of the fine-grained deposits on natural surfaces are not exposed.

Without benefit of trenches, the lack of vertical exposure precludes attempts to define any broad stratigraphy at the site. Most samples were collected from surface exposures. These include a variety of plant petrifactions and nodular carbonate materials. Large, very well-preserved plant petrifactions from surface lag at Station 3 yield U-series ages of 15.1±0.6, 15.8±0.8, 19.0±1.0 and 21±2 ka with initial $^{234}U/^{238}U$ of 2.87 to 3.03 (Table 4, Figure 10). A radiocarbon age subsampled from one of the same petrifactions yielded a calibrated age of 16.0±0.3 ka for carbonate from the innermost portions of the petrifaction (Table 5) and is in very good agreement with younger U-series ages. A calibrated radiocarbon age of $8.33^{+0.09}/_{-0.16}$ ka for carbonate from the outer layers of the same petrifaction suggests that carbonate was added to outer surfaces at substantially later times or that the carbon in outer layers shows the effects of post-depositional atmospheric exchange. Dark organic material outlining cell walls is still observable in thin section and SEM backscatter images suggesting that replacement by carbonate occurred during or very shortly after plant death in order to preserve delicate plant structures and organic matter. An attempt to radiocarbon date the organic matter in one of these petrifactions yielded an age of $6.01^{+0.1}/_{-0.06}$ ka. This material was anticipated to date the age of the original plant equivalent to or older than the oldest carbonate age. Although outer surfaces hosting lichen were removed by grinding prior to analyses, it is likely that some modern organic matter extended into this sample and contaminated the small amount of carbon available from the original plant. No further work was done to better understand the role of organic matter in these petrifactions.

Station 6 also provided a suite of smaller, but well-preserved carbonate-rich plant petrifactions. U-series ages of 10.3±1.3 and 12.9±0.6 ka (Table 4) from two of these fragments are significantly younger than the materials at Station 3, but have identical initial $^{234}U/^{238}U$ of 2.9. A sample of nodular carbonate collected at the surface from the same site has a much higher ^{232}Th content than the plant petrifactions ($^{230}Th/^{232}Th$ of 2.4 compared to 10) and requires a larger detrital correction. The resulting age of 18±5 is within error overlap of the other petrifactions at both stations, and yields an identical, albeit more uncertain, initial $^{234}U/^{238}U$ of 3.1.

A shallow (1.5 m) pit (CFD Pit 1) was hand-dug on top of one of the most prominent low mounds in the southeastern portion of the deposit (Figure 8). The measured section is shown in Figure 9 and includes a sequence of loamy units with variable degrees of carbonate cementation. Surface lag at this site consists of nodular carbonate and well-cemented insect burrow casts. None of these materials were

analyzed, therefore correlation to other surfaces dated between 11 and 20 ka has yet to be confirmed. Two TL samples were collected from non-cemented horizons at about 10 to 20 and 100 to 110 cm depth. Both samples had low field-moisture dose rates between 3.0 and 3.7 grays/ka; substantially lower than any other surface or discharge deposits measured in the Yucca Mountain vicinity (typically 7.5 to 10 grays/ka). These low dose rates were confirmed with additional field measurements as well as laboratory gamma counting analysis.

TL results (Table 6) from the younger sample, TL-21, exhibit stable plateaus for both total and partial bleach experiments. A total-bleach age of 30±3 ka is obtained for half-saturation moisture contents with a nearly identical age for partial-bleach experiments. The deeper sample, TL-20, also shows stable plateaus for both experiments (Figure 11), although the partial bleach exhibited one temperature interval that was well outside the average equivalent dose value. Although the half-saturation total-bleach age of 39±5 ka for this sample is older than the overlying sample, the uncertainties in the moisture history of these clay-rich discharge samples allow a much larger range of ages than the propagated analytical uncertainties. If the lower sample remained near saturation throughout much of the late Pleistocene, an age estimate closer to 50 ka would be more appropriate (48±6 ka for dose rates determined for saturated moisture contents).

Two carbonate-cemented layers interpreted as vegetative mats bound the silty argillic zone sampled by TL-20. Both contain substantial amounts of detrital Th ($^{230}Th/^{232}Th$ of 1.7 to 3.0) which severely limits the precision of $^{230}Th/U$ age determinations (large error ellipses on Figure 10). There does, however, appear to be a reproducible difference between the two units which is consistent with their relative position. Five subsamples derived from total digestion of whole rock and different grain-size fractions from the overlying unit (HD1607) yield ages between 53 and 64 ka with large errors, whereas five large-error age estimates from the underlying unit (HD1606) range between 99 and 119 ka. Both units exhibit initial $^{234}U/^{238}U$ that are within the range of values commonly observed in ground waters, but are somewhat higher than those observed for the latest Pleistocene materials analyzed elsewhere at this deposit (3.3 to 4.0 rather than 2.9 to 3.1). Weighted averages of both units yield age estimates of 60±5 and 108±7 ka (Figure 10). Although these averaged ages should not be substituted for more-precise determinations on low-Th materials, they are interpreted as an indication that older material is present in the deeper portions of the pit. These ages are viewed as being generally consistent with both breaks in lithology (including the two argillic zones exhibiting reddish-brown oxidation) as well as TL ages, especially if saturation moisture contents are considered.

Samples of well-sorted medium-grained sand, variably-cemented with carbonate were collected from the West Trench for TL and U-series analysis. The physical morphology of this 1.5 to 2 m thick unit does not appear similar to the bulk of the fine-grained discharge deposits to the east, however the lack of coarse clastic material and the presence of dense, nodular-like cementation is unlike most other sandy alluvial or pedogenic deposits observed elsewhere in the Crater Flat basin. Age relations between this eolian or fluvial sand unit and the discharge deposits to the east are not apparent from outcrops along the drainage. Unfortunately, analyses of the carbonate cement did not yield useful geochronological information due to very high Th contents and associated large detrital corrections. A TL sample (TL-23) did yield an adequate TL plateau for the total bleach experiment resulting in an age of 51±5 ka calculated at 3% moisture content (Table 6). A stable plateau was not obtained for the partial bleach, however an estimate of equivalent dose in the normal temperature range results in an age estimate on the order of 61 ka. Lack of a plateau for the partial bleach may indicate an inadequate resetting of the TL signal during transport (especially if of fluvial origin). The unit also contains sparse, poorly-preserved rhizoliths towards the northern end of the trench. An individual rhizolith was analyzed for U and Th isotopes (HD1733). The resulting age of 56±3 is within error of the TL determination of the host sand. It also yields an initial $^{234}U/^{238}U$ that is much lower than those unambiguously associated with discharge deposits. Therefore, although data are minimal, the sand unit exposed in the West Trench is considered to be contemporaneous with discharge 300 to 600 m to the east, however there is no evidence that this deposit is genetically linked to the same processes responsible for discharge deposits.

2.3 Crater Flat Wash deposit (CFW):

Crater Flat Wash deposit occur low on the sediment apron flanking the hills on the western side of

the drainage out of Crater Flat. The deposits are similar in scale to the both LWD and CFD sites (Figure 12), but are notable for the lack of dissection of the lowing-lying terrace. The deposit consists of fine-grained loamy units similar to other sites, with a conspicuous lack of carbonate. However, only a very small amount of stratigraphy is apparent; exposures are restricted to no more than 1 to 1.5 m of vertical relief. The site is at an elevation identical to LWD of about 790 m above sea level.

The lack of exposure has limited the amount of information available from this site. Several stations were identified and sampled (Figure 12), but detailed descriptions or analytical data collection have not yet been performed. The only exception are U-series analyses (HD1750) of two individual, small plant petrifactions found in abundance in scattered areas. Petrifactions are largely siliceous and have relatively high U and low Th ($^{230}Th/^{232}Th$ of 16 and 69). Resulting ages of 19.9±0.6 and 15.2±0.2 ka (Table 7) require little detrital-Th correction and are very similar to late Pleistocene ages obtained from the three previously-described sites. Initial $^{234}U/^{238}U$ activity ratios of about 4.2 are higher than observed in the carbonate-rich, silica-poor CFD, but similar to or slightly higher than values observed in the more silica-rich deposits at LWD.

2.4 State Line Deposits (SLD):

Satellite images of the Amargosa Valley clearly show a large area of light-toned, fine-grained deposits west of Ash Meadows near Franklin Well that are comparable in scale and reflectance to non-active portions (non-vegetated) of the Ash Meadows discharge area (Figure 1). The deposits occur at the distal southern end of the large alluvial fan of Fortymile Wash and are bounded to the south by the Amargosa River which appears to be deflected southward towards the southern end of the Funeral Mountains. The modern-day water table is closer to the surface in this same area relative to other stretches along the Amargosa River as indicated by the presence of localized mesquite thickets. Both of these features suggest a complex interaction of the two fluvial and associated ground-water flow systems (Amargosa and Fortymile Wash). Stratigraphic variability due to facies changes, as well as structural controls in this part of the fan system are likely causes of localized past dischage in this area.. The deposits cover a broad, gently-sloping area approximately 10 to 15 km by 5 km at an elevation between 700 m above sea level on the northwest end and 670 m to the southeast.

Exposure is limited by the low-lying nature of the deposits. On the southeastern side, just north of Franklin Well, the deposits form a high-terrace approximately 5 to 6 m above the river bottom. The southern margin of this terrace is dissected by several short arroyos which provide reasonable exposure of a 3 to 4 m thick stratigraphic section which has been examined and sampled in reconnaissance fashion. A schematic cross-section in one of these arroyos is shown in Figure 13a. The uppermost unit consists of a carbonate-rich cap extending over much of surface where examined to the north and west. Under this cap are a sequence of whitish-gray to greenish-gray silty loams exhibiting varying amounts of carbonate or silica cement and discontinuous denser carbonate lens that may represent vegetative mats.

U-series data are sparse for this section. Much of the nodular or mat-like carbonate-rich materials have high ^{232}Th contents, or exhibit excess ^{230}Th abundances (^{230}Th in greater amounts than what is supported by available ^{238}U in secular equilibrium) that may be related to the effects of U-loss. Three analyses of materials from the capping carbonate provide reliable results (Figure 14). A single analysis of a densely-cemented insect burrow cast (HD1854) occurring as lag at the uppermost surface yields an age of 32±4 ka with an initial $^{234}U/^{238}U$ of 3.1 (Table 8). Near the southern end of the arroyo, the capping carbonate becomes less porous, increasing in density to hard, limestone-like material. A single analysis of this Th-poor material (HD1711-A1) yields a relatively robust age of 49.2±1.4 with an initial $^{234}U/^{238}U$ of 3.09, identical to the younger burrow cast. Vugs and fractures in this capping biogenic limestone are coated with thin coatings of secondary botryoidal opal. Analysis of this high-U, low Th material (HD1711-A2) yields a precise age of 37.8±0.3 ka with an initial $^{234}U/^{238}U$ of 3.03 requiring negligible detrital correction. These dates suggest that discharge was active between 30 and 50 ka forming the upper portions of the terrace deposits.

The whitish-gray loam underlying the capping carbonate was sampled for TL analysis (TL-45). Equivalent doses measured for this sample gave a stable plateau over a wide temperature interval for the total bleach procedure (Figure 15) resulting in a TL age of 26.5±2.5 ka calculated at half-saturation moisture content (Table 9). Saturated moisture content of 58 percent for this sample yields an age of

33±3 ka. A similarly stable equivalent dose plateau was obtained for the partial bleach of this sample resulting in slightly older ages. Although this unit underlies the capping carbonate, TL and U-series ages are interpreted to be grossly compatible considering the higher moisture contents observed in the sample.

A thick, non-calcareous, silica-cemented greenish silty unit underlies the whitish-gray silt and contains an abundance of small fragments of well-preserved plant petrifactions. These materials are largely replaced by silica, and preserve very delicate internal structures. Three individual fragments (HD1737) from near the top of this unit contain high U (10 to 12 ppm), low Th (0.06 to 0.36 ppm) and thus require negligible detrital correction ($^{230}Th/^{232}Th$ activities of 140 to 880). Resulting ages cluster between 97 and 105 (Table 8) with initial ratios between 3.02 and 3.11. Together with analyses from the capping carbonate, U-series results from this section plot along a tightly-constrained evolution curve (Figure 14) spanning a period of at least 70 k.y. where source water $^{234}U/^{238}U$ compositions where remarkably constant between 3.0 to 3.1.

A similar, but softer, green silt unit lacking cement and abundant plant fragments underlies the hard, ledge-forming, green silt. Sample TL-44 was collected from this unit within 50 cm of the upper contact. A stable plateau of equivalent doses was obtained for the total bleach procedure resulting in an age of 94±18 ka calculated for a half-saturation moisture content of about 30%. Saturated moisture contents of 61% yield an age of 120±23 ka. An adequate plateau was not apparent for partial bleach procedure of the same sample. The most reasonable estimate of an equivalent dose results in a somewhat older partial bleach age, however the larger propagated uncertainties obtained for both procedures allow the age discrepancies to fall within error overlap. Anomalous fading tests done on this sample indicate that fading was less than 10% over a 28 day period. This is the oldest TL date obtained for discharge deposits and, unlike the conflicting results observed at LWD, the age is concordant with approximate 100 ka ages obtained by U-series dating.

The low-lying area north of Franklin Well and just above the river bottom consists of a broad, flat exposure of brown silts found to contain gastropod shells (Figure 13b). The river bottom deposits appear to be inset within the high-terrace deposits and contain mollusc shells collected for radiocarbon and potential U-series analyses. The assemblage contained both terrestrial and aquatic species. Two samples of terrestrial *Succind* shells yielded statistically-identical calibrated radiocarbon ages of 9.02±0.26 and 9.24±0.2 ka (Table 10). A single analysis of an individual aquatic *Planorbid* shell gave a resolvable older age of $10.8^{+0.2}/_{-0.3}$ ka. The 1.5 to 2.0 difference in ages contrasts to the 0.5 to 0.6 age difference between terrestrial and aquatic snail shells observed at LWD. Differences in ages between terrestrial snails that obtain most of the carbon in their shells from the atmosphere or emergent vegetation, and aquatic snails in the same deposit that obtain most of carbon from dissolved ground-water bicarbonate, have been interpreted to represent aging of ground water in transit from recharge areas (Brennan and Quade, 1994). Many factors may complicate this simple model, however the small differences in ages sharply contrast to the 27 ka apparent ages obtained from living snail shells from artesian springs at Ash Meadows in a Paleozoic carbonate-dominated flow system (Riggs, 1984).

A single snail shell from this same unit was also analyzed by U-series (HD1738, Table 8) and the silts by TL (TL-46, Table 9). The aquatic *Planorbid* shell had relatively high U content (3.7 ppm) and low Th (1.6 ppm) yielding an age of 11±2 ka which is within error of ^{14}C ages from the terrestrial snail shells. The initial $^{234}U/^{238}U$ of 3.3±0.2 is within error of materials analyzed from the high-terrace deposits. Agreement of the age with radiocarbon and initial $^{234}U/^{238}U$ with other U-series results suggests that these types of snail shells in this environment may provide a viable means of extending mollusc-shell dating beyond the 40 ka limit of radiocarbon. Luminescence results from TL-46 silts gave stable plateaus for both total and partial bleach procedures. The sample was collected within 20 to 30 cm of the surface and had a field-moisture content of 22% and a saturated-moisture content of 45%. The high field-moisture value (typical values of 1 to 8%) is undoubtedly due to collecting the sample during a wet winter shortly after precipitation events. Therefore, use of the field-moisture dose rate is thought to represent a typical half-saturation condition. The resulting TL age of 12.1±1.8 ka is within error of the U-series snail date and very nearly overlaps the 9 ka radiocarbon ages. Since the moisture history is largely limited to the drier conditions of the Holocene, a dose rate based on moisture conditions intermediate between dry and half-saturation may be

more appropriate. This would result in a slightly younger age in complete agreement with ages obtained from both of the other two geochronometers.

2.5 Indian Pass Deposit:

Satellite imagery shows a substantial patch of white deposits similar in reflectance to other discharge deposits and covering an area of approximately 3 by 1 km on the south side of the Amargosa River in the central Amargosa Valley. These deposits occur on the northwest flank of Lees Peak, a bedrock outlier that constricts the Amargosa Valley southeast of Big Dune. The deposits occur at an elevation of 780 m above sea level en route to Indian Pass, a low saddle separating the southeastern and northwestern Funeral Mountains. The deposits are similar in nature to those elsewhere in the vicinity described above, however only reconnaissance observations have been made to date. A hand-dug water well, presumably dating to prospecting activities in the late 19th or early 20th century, is present at the site and attests to the proximity of ground water to the surface in this area.

The only detailed information available at the present time comes from a measured section in the central portion of the deposit (Figure 16). A natural dry-wash exposure of about 2.5 m consists of two distinct units (Figure 17); a lower green silty unit and an upper brown siliceous marl. The section was sampled for both U-series and TL geochronology to test whether the deposit also reflected a late Pleistocene history of discharge as seen elsewhere in the Amargosa Valley. Plant petrifactions (HD1984) and nodular carbonate (HD1985) lag from the upper surface of the exposure yielded $^{230}Th/U$ ages of 15.9±0.3 and 14±4 ka, respectively (Table 11). The large difference in uncertainties reflects the variable detrital-^{230}Th corrections necessary for the different materials. Individual, sub-vertically-oriented rhizoliths collected in place from the underlying brown siliceous marl yield $^{230}Th/U$ ages of 10.9±0.2 and 20.8±1.0 ka. The large range in ages probably reflects an extended episode conducive to plant growth, although the possibility of U-loss for the oldest rhizolith cannot be discounted (higher measured $^{230}Th/^{238}U$ activity for a constant measured $^{234}U/^{238}U$ activity, Figure 18). Initial $^{234}U/^{238}U$ activity ratios of 3.0 to 3.1 for all four samples fall in the range commonly observed for many other Amargosa Valley discharge deposits.

Results for sample TL-71 collected from the top of the underlying green-silty unit are consistent with U-series dates for the overlying unit (Table 12). A broad, stable plateau was obtained for the total bleach procedure resulting in a half-saturation age (25%) of 19±1.4 ka. The half-saturation moisture dose rate estimate is viewed as a reasonable model considering the wetter conditions dominant in the late Pleistocene and drier conditions throughout the Holocene. Partial bleach procedures have not yet been completed, however they are expected to provide concordant data considering the robust behavior of the total bleach plateau. A second TL sample from the green sand unit at the base of the section (TL-70) also provided a good total bleach plateau (Figure 19) resulting in a half-saturation age of 41±3 ka. The calculated age at saturation-moisture dose rates is 50±3 ka. Anomalous fading tests for both IPD TL samples show no detectable fading (<5%) over a 40 day period.

Nodular carbonate is also present at the base of the measured section. Two analyses from samples collected about 50 cm vertically apart (HD1981 and HD1982) have high Th relative to U and require large detrital-Th corrections to obtain statistically identical $^{230}Th/U$ ages of 28±6 and 27±7 ka for the lower and upper sample, respectively. Initial $^{234}U/^{238}U$ activities of 3.3±0.3 and 3.4±0.4 are higher than, but within error of, those observed for materials in the capping brown silt. These ages are consistent with stratigraphy and TL ages in that they are older than the value of about 18 ka obtained for TL-71. The large $^{230}Th/U$ uncertainties for these samples plus the significant uncertainty surrounding the choice of the most appropriate moisture history controlling the time-integrated dose rate for TL age estimates allow U-series and TL ages of the basal part of the section to be nearly within error overlap. Conversely, the age difference may be real representing earlier sediment burial followed by subsequent concretionary carbonate precipitation from carbonate-saturated ground water.

2.6 Conclusions from Geochronologic data:

Current geochronological investigations provide a reconnaissance-level framework of discharge activity at sites in southern Crater Flat and the Amargosa Valley. The overall concordance between results from three independent chronometers are shown in Figure 20 and supports the following interpretations:

- Discharge occurred during the latest glacial cycle between 10 to 20 ka. The consistency of

the young ages obtained using the three independent methods strongly indicate a primary age signature as opposed to any scenarios involving partial resetting of older deposits by more-recent surface processes (i.e., climate-induced pedogenic overprinting).

- Discharge activity between 10 and 20 ka at all five sites are consistent with a regional phenomenon rather than isolated activity related to local hydrologic conditions.
- At least the ^{230}Th/U evidence indicates that activity was cyclic and includes deposits associated with the penultimate glacial cycle as well as the last glacial cycle. Deposits related to this cycle are only exposed in the more-deeply dissected sites at LWD and SLD, with a possible hint of the older materials from the base of shallow (1.5 m), hand-dug pit at CFD. Elsewhere, the older deposits are either not exposed, removed by erosion prior to the deposition of the last cycle, or have not yet been identified. In general, ages of deposits span a period of about 15 to 60 ka, and an older episode of about 90 to 180 ka. The break between these two time spans appears to be related to lithologic breaks at several sites.
- Materials younger than about 10 to 16 ka have not been identified from any of the sites, including surface-lag deposits that form as these badland-type deposits are deflated. The absence of Holocene material indicates that the last discharge activity ceased around 12 to 15 ka at up-gradient sites, and slightly later (~9 ka) down-gradient at lower elevations (i.e., SLD). This time corresponds to the cessation of the last cycle of spring activity in the Las Vegas and Pahrump Valleys (Quade et al., 1995) and reflects initiation of the hotter and dryer conditions typical of much of the Holocene interglacial.

3. STABLE ISOTOPE DATA:

Stable carbon and oxygen isotopes in carbonates from sites associated with ground-water discharge provide information on the source of the discharging water ($\delta^{13}C$) and the temperatures at which recharge and discharge took place ($\delta^{18}O$). Carbonate occurs in spring deposits as cements, nodules, both aquatic and terrestrial mollusc shells, calcified plant petrifactions, and, in the instances of bicarbonate-rich discharge, as tufas and travertines. Calcite is the dominant carbonate phase with the exception that many invertebrate shells are aragonite. At present, $\delta^{13}C$ and $\delta^{18}O$[4] data exist for most of the carbonate occurrences found in the reconnaissance sampling of these past discharge deposits (Table 13).

Spring deposits can be crudely classified by their discharge temperatures and authigenic mineralogy. Information concerning flowpaths and (or) aquifer depths and lithologies should be inferable from mineralogical and isotopic study of paleo-discharge deposits. In general, warmer waters will contain higher concentrations of dissolved components and have a greater capacity to deposit authigenic minerals than cooler waters. Tufa and travertine formation is controlled by the extent of calcite supersaturation in the discharging ground water with calcite formation often limited by the availability of the dissolved Ca^{+2} ion. In southern Nevada, springs discharging from deep, warm carbonate-rich Paleozoic carbonate aquifers typically have substantial concentrations of both bicarbonate and calcium. Calcite often lines the walls of discharge conduits (banded travertine veins) or forms tufa mounds at the surface. Shallower (and cooler) aquifers hosted by less calcareous rocks will form less voluminous deposits characterized by local carbonate cementation of clastic beds and sporadic occurrence of calcareous plant and animal fossils. Volume of water discharge also varies significantly and impacts the morphology of resulting deposit. High-volume, discharge focused at long-lived spring conduits often form substantial, dense limestone edifices, whereas low-volume or more diffuse discharge forming wetland seeps and marshes provide an environment favoring accumulation of sand and silt with little if any inorganic carbonate mineralization (Quade et

[4] Stable isotope compositions are reported as the per mil (‰) deviations of the samples from the International standards VPDB (for C) and VSMOW (for O). Calcite (C and O) stable isotope determinations were performed according to approved technical procedures based on techniques developed by McCrea (1950). $\delta^{13}C$ and $\delta^{18}O$ values were measured by mass spectrometry at the Isotope Geology Branch of the USGS in Denver. Mineral $\delta^{13}C$ and (or) $\delta^{18}O$ values reported here are routinely reproducible to ±0.1 and ±0.15‰, respectively. However, ninety-eight aliquots of NBS-19 (or its in-house equivalent, TS-1) analyzed during the course of data collection had average $\delta^{13}C$ and $\delta^{18}O$ values of 1.91 ± 0.02‰ and 28.32 ± 0.15‰, respectively, compared to accepted values of 1.92 and 28.65‰. All $\delta^{18}O$ values reported in Table 13 have been adjusted by +0.30‰ to accommodate our deviation from the accepted value for NBS-19.

al., 1995). Although these sediments are only locally calcite cemented, biogenic carbonates may still be present.

3.1 Carbonate travertine and tufa deposits

Where deep regional carbonate aquifers discharge at the surface, they frequently deposit subsurface travertine veins and associated tufa mounds. Inorgaincally-precipitated travertine vein calcite preserves the most direct record of the chemical and isotopic composition of the depositing waters without modification through surficial processes. Because calcite deposition occurred from deep-circulating aquifers where discharge temperatures are likely to remain constant, the record of changing $\delta^{18}O$ compositions has the potential to preserve high resolution records of variations in recharge water compositions that are, in turn, a reflection of global climate variation (Devil's Hole calcite record, Winograd et al, 1988, 1992). The $\delta^{13}C$ and $\delta^{18}O$ values of calcite deposited by several of these carbonate depositing springs are shown in Figure 21.

Grapevine Springs on the northeastern side of Death Valley consists of several square kilometers of thick tufa mounds constructed over numerous sites of past and active discharge. Vein-travertine calcites have $\delta^{13}C$ for values ranging from -4.6 to 0.7‰ and $\delta^{18}O$ values of 13.8 to 19.0‰. This range of $\delta^{13}C$ is characteristic of calcite precipitated from regional ground water hosted by marine carbonate rocks. These values for $\delta^{18}O$ are typical for calcites deposited in warm (modern discharge temperatures range from about 25 to 35°C) discharge settings, whereas the variability in $\delta^{18}O$ records changes in the averaged meteoric water $\delta^{18}O$ compositions at sites of ground water recharge. Abundant exposures of travertine veins at the Grapevine Springs deposits provide an opportunity to study long-term records of variations in average meteoric water, which, if dated, may prove useful for helping to calibrate other long-term climate records obtained from lacustrine sedimentary sequences in the region (e.g., Death Valley and Owens Lake cores currently under study within the Lakes, Playas, and Marshes activity).

Nevares Spring in central Death Valley consists of an actively forming tufa mound that is well-exposed where it has been cut along its southern flank by a small stream. These tufas have $\delta^{13}C$ and $\delta^{18}O$ values of -2.5 to -1.3‰ and 14.7 to 18.9‰, respectively (Figure 21). These $\delta^{18}O$ values are consistent with the fairly warm temperatures observed at active discharge sites (36 to 38°C, Perfect et al., 1995). Values for $\delta^{13}C$ reflect the carbonate host rocks of the aquifer. The distinct positive covariance between $\delta^{13}C$ and $\delta^{18}O$ values of these calcites result from the combined effects of CO_2 evasion, evaporation and cooling after discharge at the surface.

Calcites from feeder veins and overlying tufa deposits exposed at the deeply-dissected section at Travertine Point near Furnace Creek Wash east of Death Valley, California show strong isotopic similarities to the Grapevine Springs system. The Travertine Point system apparently ceased hydrologic activity at about 1 million years ago (Winograd et al., 1985). Calcite from Devils Hole (splits provided by I.J. Winograd, USGS), are isotopically similar to the system at Nevares. Extensive work on variations in $\delta^{13}C$ and $\delta^{18}O$ in calcites from Devils Hole core DH-11 by Coplen and others (1994) and Winograd and others (1992) shows a very high degree of inverse covariance, where $\delta^{13}C$ ranges from -1.5 to -3.0 at the same time that $\delta^{18}O$ changes from 13.0 to 16.0. These authors suggest that the dissolved inorganic carbon signal documents climate-induced changes in plant communities linked to temperature changes either on a global or local scale.

A small, but prominent carbonate mound just north of Highway 95 within Rock Valley (Fig. 1), approximately 200 m^2 and 15 m high, is currently mapped as an outcrop of undivided lacustrine beds of the Tertiary Pavits Spring and Horse Spring Formations (Frizzell and Schulters, 1990). However, the mound consists of nearly pure limestone with textures and bedding similar to tufa deposits at Nevares Spring and elsewhere. Sub-horizontal to draped beds of tufa-like limestone are also cut by abundant banded travertine veins that are macroscopically indistinguishable from those at Grapevine Springs or in the Travertine Point area.

Values of $\delta^{13}C$ and $\delta^{18}O$ for calcite from the Rock Valley mound, as well as from a low outcrop of bedded limestone just across Highway 95 to the south (Fig. 21 and Table 13), do not allow unequivocal assignment of the materials to a spring or lacustrine origin. Vein-travertine calcite (sample HD-1118) has $\delta^{13}C$ and $\delta^{18}O$ values of -2.5 to -4.7‰ and 17.5 to 18.1‰, respectively, whereas the tufa and bedded limestone calcite ranges from -1.8 to 0.7‰ and 18.4 to 22.9‰. Carbon isotopic results for this single mound span a wider range of $\delta^{13}C$ values than most of the other tufa mounds of unquestioned ground-water origin. The Rock Valley mound also

has consistently higher $\delta^{18}O$. Although stable isotopic compositions for limestones of unequivocal Pavits Spring and Horse Spring Formations are unavailable at present, distribution of $\delta^{13}C$ and $\delta^{18}O$ of calcite within the carbonate mound in Rock Valley bears a strong resemblance to compositions from calcite in the wetland-type discharge deposits discussed below. Should geochronologic investigations of the Rock Valley mound indicate Pleistocene or Holocene activity, then further investigations of the origin and saturated-zone hydrologic implications are warranted.

3.2 Amargosa Valley discharge deposits

Stable isotope results from the five paleodischarge sites in the Amargosa Valley vicinity show a large range in both oxygen (18 to 27‰) and carbon (-10 to +1‰) delta values (Fig. 22). A positive covariance between C and O values in the several suites of carbonates (Figure 23) indicates that additional processes of CO_2 evasion and evaporation occurred after ground waters discharged at the surface. The lowest inorganic carbonate $\delta^{18}O$ values, representing materials least-effected by surface processes, cluster around 19±1‰. Unlike $\delta^{18}O$, the range of $\delta^{13}C$ remains large for carbonates with minimum $\delta^{18}O$ values: a feature that reflects mixing between the primary carbon inputs to these environments. Carbonate cements and nodules likely reflect the dissolved inorganic carbon in discharging waters and have $\delta^{13}C$ values from -4 to +1‰. In contrast, biogenic carbonates (mollusc shells, plant petrifactions) commonly have lower $\delta^{13}C$ values between -10 to -5‰. Observed carbon compositional differences for a large suite of samples from LWD are attributed to differences in sample type (Figure 23). No systematic differences in $\delta^{13}C$ are apparent between biogenic samples from both the latest or penultimate glacial-cycle age from LWD, nor between carbonate cements from both LWD and CFD that span both glacial-cycles.

Compared to the carbonate tufas and travertines described in the preceding section (shaded field in Figure 22), carbonate cements and nodules from the Amargosa Valley discharge deposits have similar $\delta^{13}C$ values, but higher $\delta^{18}O$ values. Increase in the temperature of calcite formation will decrease the oxygen isotope fractionation between calcite and water resulting in lower calcite $\delta^{18}O$ values. An additional difference between modern, high-volume springs and paleodischarge sites is that carbonates associated with relatively low-discharge in marsh and wetland environments can show extreme enrichments in $\delta^{18}O$ with values ranging from 18‰ to as high as 25 to 27‰. This range of isotopic compositions, plus the positive covariation between $\delta^{18}O$ and $\delta^{13}C$, is consistent with evaporative enrichment of ^{18}O in waters present in shallow pools and marshy areas.

Minimum $\delta^{18}O$ values of carbonate from each deposit most-closely reflect the temperature and isotopic composition of the discharging waters. At the carbonate-poor paleodischarge deposits, these minimum $\delta^{18}O$ values are roughly 3‰ higher than those from the carbonate mounds at active sites such as Ash Meadows and Devils Hole. This difference reflects either cooler temperature or higher $\delta^{18}O$ discharge, or both, at the carbonate-poor sites. If near-equal discharge $\delta^{18}O$ values for the two types of deposits is assumed, then the discharge at the carbonate-poor sites would have had water temperatures of 0 to 16°c, significantly cooler than those at the modern springs. Discharge from a shallower flow path would have temperatures closer to mean annual temperature, which was 5 to 10°C cooler during the last glacial maximum relative to present (see discussion under Lakes, Playas, and Marshes above). If near-equal discharge temperatures are assumed, then the 3‰ lower values for discharge at the carbonate-poor sites probably reflects recharge at lower elevations than the carbonate-depositing sites. Regardless of the exact reason, both cooler temperatures or lower elevation recharge are more compatible with shallower and shorter ground-water flow paths.

4. PALEONTOLOGICAL DATA AND PALEOENVIRONMENTAL INTERPRETATIONS:

4.1 Ostracodes:

4.1.1 Lathrop Wells Diatomite: Ostracodes in the LWD samples (see listing in Appendix 3) indicate the discharge environments at this site typically ranged from highly-ephemeral seeps to flowing springs. Samples LWD-7 (upper unit) and LWD-11 contain no ostracodes, but aquatic and terrestrial molluscs are common indicating the possibility of ephemeral seeps. Samples LWD 10 and 13 contain a few species of ostracodes that are relatively common. Sample LWD 10 also contains mostly aquatic molluscs, whereas LWD 13 contains a mixture of terrestrial and aquatic molluscs. The ostracodes in these samples indicate the depositional environment was

likely a seep with seasonally variable flux. The ostracodes from these two samples are not limited to a specific major dissolved ion composition, so they could have been living in water derived from the dissolution of limestone or volcanic rock. Their TDS tolerance is also quite wide ranging from values below 100 mg/l to values as high as 17,000 mg/l. Common values would fall between about 750 mg/l and 3000 mg/l.

The assemblage in LWD-8 contains some ostracode species that commonly live in seeps and others that commonly live in pools. The sample also contains both terrestrial and aquatic molluscs. The mixture of ostracode species may indicate a seep-supported pool developed at this site. The water chemistry of that pool could have been derived from either dissolution of limestone or volcanics, as noted above for other samples from this site, but the TDS may have been lower, perhaps remaining below 1000 mg/l.

The ostracode assemblage from the remaining two samples from the LWD locality, LWD-7 (lower unit), and LWD-12, appear to indicate the existence of a flowing spring. Both samples contain terrestrial and aquatic molluscs. There are different ostracode species in the two samples and the various species imply permanence and greater flow at the LWD-12 sample site than at the LWD-7 (lower unit) sample site. Water chemistry could come from either limestone or volcanic rock dissolution and TDS was likely below 1000 mg/l and likely was lower at the site sampled by LWD-12 than at LWD-7 (lower unit).

4.1.2 Crater Flat Deposit: Two of the CFD samples contain few ostracodes, so those rare ostracodes may or may not be representative of the depositional environment. One of those samples, from a grey sediment about 10 meters from the dated section (Figure 9) contains a taxon (Candona n. sp.). Candona n. sp. species lives in the region today in spring supported pools and wetlands such as the pond at Fish Lake Valley and some wetlands in the Pahranagat Valley. Sample Site-199-Station-8-sample G also contained few ostracodes. That sample contains a taxon (Cavernocypris wardi) indicative of very cold water seeps and springs (T°C < 12°C). Sample Site 199-H Station 7, from about 1.5 m above the stream bed, contains a diverse and abundant assemblage of ostracodes as well as common aquatic molluscs. The species assemblage is indicative of a spring supported wetland. The solute composition of the water most likely was derived from volcanic rock and hence the most common dissolved ions were probably sodium, (bi)carbonate, and chloride. A typical TDS for this assemblage would be between 1000 and 2000 mg/l. Most of the species found in the assemblage live in the region today or in northern Nevada.

4.1.3 Stateline Deposits: The ostracodes found in three samples from ground or near ground surface samples of a site located near the modern-day Amargosa River provide a preliminary indication of the nature of the environment in this area of the flow system. Two of the samples (NV94RMF83B, 0 to -5 cm, -25 to - 29.5 cm) represent the top and bottom 5 cm from a 30 cm core taken by hand-driving a PVC pipe. The third sample (NV94RMF82) comes from a site where molluscs were collected for radiocarbon and uranium series dates. The latter site is about 5 m from site 83. The ostracodes found in sample NV94RMF83B -25 to -29.5 cm, suggest the presence of a mixture between a flowing spring and a pool/wetland environment. The sample from the top of this sequence (0 to -5 cm), however, is a pool/wetland setting with some flow probable. The major-ion chemistry of the latter two samples like the samples above could have come from either the dissolution of limestone or volcanics and likely had a TDS below 1000 mg/l. Sample site NV94RMF82 contains an ostracode assemblage similar to that from NV94RMF83B 0 to -5cm, and like that sample implies this nearby site also is a pool/wetland environment with a flow aspect. Chemistry of the water is also similar. All three samples contain abundant aquatic molluscs suggesting the presence of wetland settings.

4.1.4 Paleoenvironmental interpretations: Paleontological analyses (ostracodes) of samples collected from the LWD, CFD, and Amargosa River site at the SLD show that discharge was common in the past and supported a variety of paleoenvironments. These paleoenvironments may be generally classified as seeps, flowing springs, and spring-supported standing water (pools, wetlands). The ostracode species found in samples from the above sites are listed in Appendix 3. The following discussion of paleoenvironments is based on the observed fossil ostracodes and mollusc assemblages, and the known environments of living examples of the same genera and species.

Seeps were common and characterized by low levels of ground-water discharge, minor surface water flow, high seasonal variability of water temperature and likely water chemistry, and often

occurred within dense stands of emergents (cattails, bulrush), grasses or other vegetation. Seasonal variations in seep discharge probably ranged spatially throughout this complex discharge-environment from highly ephemeral to permanent. Ostracode species found in seeps are tolerant of wide ranges in temperature, total dissolved solids (TDS), major-dissolved ions, and other parameters. These environmentally-tolerant invertebrates may also live in less variable environments such as flowing springs, but, in those cases, they typically occur with other species less-tolerant of environmental variability. Sediments deposited in highly-ephemeral seeps or wet-ground environments may or may not support ostracodes, but often do support other fauna such as terrestrial and semi-aquatic (air breathing) molluscs. At ephemeral seeps, ground water usually resides at or just below earth surface supporting emergent and other vegetation. Even under dry conditions, small, often ephemeral, pools of water and a humid micro-environment exist within the vegetation. The snails live in the pools or on the plants.

Flowing springs were also common and characterized by continuous ground-water discharge sufficient to form small streamlets, which may have been commonly bordered by water loving vegetation. The streamlet temperature and chemistry had low to moderate seasonal variability and that variability likely was inversely proportional to flux. Ostracodes are usually common in and certain species characteristic of flowing springs. Species from aquatic environments connected to the flowing springs such as aquifer-, wetland-, or stream-taxa may also be common in flowing springs. Associated mollusc assemblages will tend to have more aquatics (air and gill breathers) and fewer terrestrial species than in the seepage environments.

Spring supported pools and wetlands were also common in the region, especially notable for latest Pleistocene - earliest Holocene silty deposits near the modern-day Amargosa River north of Franklin Well. These environments must have varied greatly in size, from a few meters in diameter to shallow ponds or lakes hundreds of meters in diameter, based on the fossil ostracodes, on the spatial distribution of the wetland sediments, and on modern analogs such as the wetlands in Pahranagat and Ruby Marsh Valleys. Flow through these environments would typically be minimal with standing water being common in the larger water bodies. Those environments were variously permanent or ephemeral.

4.2 Diatoms:

Diatom and ostracod assemblages have been examined from several of the sites described above. One of the most common and persistent diatoms at the LWD deposit is *Denticula valida*. This species characterizes warm (usually less than 40°C), alkaline and slightly saline springs that are related to volcanic hydrothermal processes. For example, it occurs in springs on Mt. Ranier, WA, and in warm water habitats in Yellowstone National Park. However, it does not necessarily imply warm, hydrothermal water. For example, the species is abundant in shallow, near-shore water and marginal spring seeps at Black Lake (Adobe Valley, Mono County, California). Here the water is near ambient air temperature and saline as a result of evaporation. This species has a wide salinity tolerance, ranging from about 1 ppt to about 15 ppt. The other diatoms at the LWD [species?] suggest that salinity was low, probably about 1 ppt.

Denticula valida and its associates characterize all the localities examined so far at LWD. They are present in the upper as well as lower units and also in the outcrops 200 m or more west of the main badlands area. This diatom association is also present in the SLD near Franklin Well, and is found sparingly at the CFW deposit.

Paleontological analysis of samples from LWD paleodischarge site indicate the presence of a freely-flowing alkaline spring system, probably with multiple spring orifices discharging throughout the history of activity. The spring water was silica-rich, only slightly saline, and possibly warm. In hydrochemical terms, the spring water probably resembled ground water present in the volcanic aquifer today. Spring flow was moderate to strong over much of the time and probably passed through a mass of rush-like vegetation that grew at the site.

5. SOURCE OF GROUND WATER

The source of discharging ground water is of critical importance for relating paleohydrologic responses to climate variations. In particular, discrimination between a source associated with the regional potentiometric surface and a local source associated with a perched water zone is central to modeling the SZ behavior under the wetter climate conditions anticipated during the next 100,000 years. Synchronous paleodischarge at all five studied sites distributed over a broad area with heterogeneous hydrogeological conditions indicates the likelihood of a

wide-spread rise in the regional SZ water table. Additional evidence supporting this concept is available from U, Sr and C isotopic data.

Initial $^{234}U/^{238}U$ activity ratios calculated for all materials analyzed from discharge deposits throughout the Amargosa Valley Data consistently vary between values of about 2.8 and 4.4 (Fig. 20, Table 14) and remained uniform over the last several hundred thousand years. Uranium isotopic compositions of ground waters discharging from the Ash Meadows system at Devils Hole have remained remarkably constant over at least the last 500 ka (Ludwig et al., 1992). The observed high $^{234}U/^{238}U$ values from discharge deposits are clearly distinct from analyses of calcretes in the Yucca Mountain vicinity ($^{234}U/^{238}U$ = 1.3 to 1.8; Paces, et al., 1994; 1995). Similarly-low values of $^{234}U/^{238}U$ are observed for surface runoff waters collected during precipitation events at Yucca Mountain (Paces, unpublished data). Therefore, data from paleodischarge deposits clearly require a hydrologic source not dominated by surface waters or pedogenic processes.

Like U data, Sr isotopes provides additional evidence that a surface-water origin is unfeasible. Strontium isotopic compositions of weak-acid leaches largely from the vicinity of southern Crater Flat and SLD (Peterman, unbublished data; Paces, 1995) yield a bimodal distribution of values based on location. Carbonates from the LWD and CFD sites have $\delta^{87}Sr$ values of 5.03 to 5.20 whereas samples from the SLD (and presumably IPD) deposits contain $\delta^{87}Sr$ values between 10.5 and 13.1. Both groups are distinct from local calcretes that have a range of $\delta^{87}Sr$ from 3.3 to 5.0 (Marshall et al., 1993; Marshall and Mahan, 1994).

Carbon from the inorganically-precipitated carbonate at all sites contains a substantial component of heavy carbon (-4 and +2‰) that is not observed in surface environments where plants control most of the carbon budget. Calcrete throughout the region has $\delta^{13}C$ values of -10 to -5. Waters that obtain their carbon during infiltration through the soil zone will acquire relatively low $\delta^{13}C$ values (-12 to -7). These $\delta^{13}C$ compositions are widely observed in surface and shallow volcanic aquifer waters beneath Yucca Mountain (Benson and McKinley, 1985) and in unsaturated-zone (UZ) carbonates (Whelan et al., 1994, 1996). In contrast, calcite associated with Paleozoic aquifers has $\delta^{13}C$ that reflects marine carbon sources (Coplen et al., 1994; Whelan et al., 1994).

Observed ground-water sources are compatible with data for all three isotopic systems (Table 14). Data for waters from springs and wells span a wide range of isotopic compositions that reflect different spatially-distributed recharge or flow-path rock characteristics. Uranium isotopic compositions are variable in regional and perched ground-water systems in the Yucca Mountain region showing $^{234}U/^{238}U$ activity ratios that range from less than 2 to over 8 (Ludwig et al., 1993; Paces unpublished data). In general, deeper flow systems that interact with the Paleozoic carbonate basement have values of 2.5 to 4, whereas shallow flow systems associated with the volcanic aquifer contain higher activity ratios of 3 to 8. Perched water bodies recently recognized at Yucca Mountain show a similar range in uranium isotopic composition.

Strontium isotopic compositions of modern waters from the Yucca Mountain region have $\delta^{87}Sr$ values ranging from 0 to >+20‰ (Table 14, Figure 24). Ground water associated with shallow volcanic and alluvial aquifers adjacent to Yucca Mountain typically has $\delta^{87}Sr$ between +1 and +4‰. Northward from Yucca Mountain, $\delta^{87}Sr$ ground-water values decrease to 0 in the recharge areas and increase southward into the Amargosa Valley to values as large as +11‰ (Peterman and Stuckless, 1993a). Ground water contacting only Paleozoic carbonate rocks in the regional carbonate aquifer would be expected to have $\delta^{87}Sr$ values in the range of -2 to +3‰ (Table 14) except where the carbonates have been mineralized by hydrothermal solutions, such as at Bare Mountain (elevated $\delta^{87}Sr$ values as large as +23‰, Peterman et al., 1994). The only well penetrating the regional carbonate aquifer at Yucca Mountain is UE-25p#1. Water from this well has a $\delta^{87}Sr$ value of +3.6‰ which contrasts with values of 0 to +0.2‰ obtained from Paleozoic limestones from the core (Peterman et al., 1994). Peterman and others (1994) suggested that the lack of equilibrium between the ground water and the aquifer at this location was likely the result of up-gradient interaction with rocks having substantially larger $\delta^{87}Sr$ values such as the Devonian-Mississippian Eleana Argillite with a mean $\delta^{87}Sr$ of +9.8‰. Such interaction with rocks containing radiogenic Sr appears to be fairly common in the regional carbonate aquifer which indicates that more flow occurs through the fractured Precambrian basement than has previously been modeled (Peterman and Stuckless, 1993a and b). This process may therefore explain elevated values of

$\delta^{87}Sr$ (4.5 and 15‰) at present-day springs at Ash Meadows, Franklin Playa and Death Valley representing discharge from deeper carbonate aquifers.

Possible hydrogenic sources for paleodischarge deposits are summarized in Table 15 on the basis of isotopic data as well as the diatom data. Neither runoff or perched aquifer waters can satisfy the isotopic attributes for discharge carbonate deposits. Paleozoic limestone bedrock proximal to LWD, CFD and SLD deposits are not considered reasonable sources of heavy carbon for local perched aquifers since these rocks would also dominate the Sr budget. The data are most consistent with regional aquifer systems although there is ample overlap of aquifer types. This is especially true of the shallow alluvial systems where a large variety of rock types are present and can provide a mixture of geochemical signals to interacting waters. Samples of ground water beneath the discharge sites are unavailable at most sites with the exception of the Amargosa Farms area. A vertically-zoned aquifer system is present in this area were waters from shallow levels contain $\delta^{87}Sr$ values from 3.1 to 5.5‰ and 9.8to 11.4‰ for deeper levels. The deeper waters with higher $\delta^{87}Sr$ are consistent with values observed in SLD paleodischarge carbonates and indicate that the deeper system was discharging at the surface in the past.

6. WATER TABLE FLUCTUATIONS UNDER YUCCA MOUNTAIN:

Combined isotopic evidence including $^{234}U/^{238}U$, $^{87}Sr/^{86}Sr$ and $^{13}C/^{12}C$, as well as spatial and temporal data, suggests that discharging water at paleospring sites represents regional ground waters rather than local perched systems. This conclusion requires that the regional water table elevation fluctuated in the past as a response to the higher effective moisture availability during pluvial episodes. Currently, the water table elevation beneath the sites closest to Yucca Mountain (LWD, CFW and CFD) are extrapolated from potentiometric surface maps (Waddell et al., 1984; Robison, 1984; Classen, 1985) since no direct measurements are available. These estimates provide a current depth to water of between 80 and 120 m (Paces et al., 1993). Similar deposits are not found at higher elevation in this area suggesting that these deposits represent a maximum water table rise over the last 250 ka. The fluctuations in water table elevation as recorded at paleodischarge sites may be localized by unidentified hydrogeologic features since these deposits are not widespread nor uniformly distributed along areas of equal topographic elevation. However, it is unlikely that they represent the result of an overpressured discharge of a confined aquifer because similar estimates of maximum water table elevations under Yucca Mountain have been made on the basis of fracture-filling secondary minerals (Marshall et al., 1993) and distribution of zeolitization in tuffs (Levy, 1991). An overpressured system would not produce uniform water-table elevation changes over broad areas. A similar rise in the water table altitude in the vicinity of the potential repository block at Yucca Mountain (maximum increase of 130 m) has also been modeled using a 1500 percent increase in recharge relative to modern-day (Czarnecki, 1985). This amount of recharge was roughly obtained by doubling the precipitation throughout the various altitude zones considered in the model.

7. RESPONSE OF THE WATER TABLE TO CLIMATIC VARIATION

One of the main consequences of this work is recognition that higher regional water table elevations of up to 100 to 120 m were common during the last two late pluvial cycles (10 to 60 ka and 100 to 200 ka). A histogram of all $^{230}Th/U$ ages lacking evidence of U-loss or other obvious problems is presented in Figure 25. All deposits contain ample evidence for discharge activity between 10 and 20 ka. The greatest number of analyses occur around an age of 15 ka with only a small number of younger petrified plant remains which do not require soil saturation, or for the lowest portions of the system near Franklin Well. Therefore, the bulk of the youngest cycle (approximately 12 to 8 ka) of activity observed by Quade in deposits flanking the Spring Mountains (cycle E of Quade, 1995) is present, but not well-represented in the Amargosa Valley. Discharge and eolian activity continues at most sites from 15 ka through 40 to 60 ka, although some of these ages are not well-determined. An absence of $^{230}Th/U$ ages exists between 60 and 90 ka, followed by a pulse of activity between about 90 to 140 ka. Data become sparse beyond this age, however a small number of dates from LWD are scattered back to as old as 210 and 240 ka.

Although the current level of understanding of paleodischarge deposits does not allow reconstruction of a detailed record of discharge history, dates correspond remarkably well to other proxy records in the area, most notably the record of saline and freshwater diatoms from Owens Lake (Bradbury, 1996). Very little direct dating has been done in this

core; ages are obtained by assuming constant rates of sedimentation and by calibrating the record using radiocarbon dating of the shallowest materials, and paleomagnetic and tephrochronological data on the deepest materials. A remarkable degree of consistency is observed between the Owens Lake records and the paleodischarge data, in spite of the potential geochronological problems inherent in both data sets. Abundant freshwater diatoms indicate periods of increased effective moisture providing ample, dilute runoff to the lake. Saline diatoms are usually absent during these periods. Conversely, saline diatoms dominate the assemblages when effective moisture is low and the lacustrine system is dominated by evaporative concentration of salts. Freshwater diatoms dominate the Owens Lake record between about 10 and 50 ka, falling off dramatically until about 90 to 100 ka before which they domiante throughout the penultimate glaciation until around 170 ka. Saline diatoms dominate the record between about 50 and 100 ka, and again between 160 and 200 ka.

Other dated records of reinforce the general linkage between climate over the last glacial cycle and higher water table elevations in the Amargosa Valley area. In particular, water table levels were between 5 to 9 meters higher above current levels in Browns Room at Devils Hole between 15 and 50 ka with a rapid decline down to only about 1 meter above current levels by about 8 ka (Szabo et al., 1994). Several important conclusions are apparent from the data presented here as well as these other paleoclimate studies.

First, the close correspondence between surface climate records and discharge records suggests that the saturated zone responds rapidly to changes in climate parameters. There is no apparent lag between the time when water becomes available at the surface to the time when is observable at discharge sites. This indicates rapid readjustment to increased levels of recharge and translation of the increased recharge down-gradient to points of discharge.

Second, much of the late Pleistocene was characterized by higher water table elevations. It is possible that a higher water table elevations may be a normal consequence of Pleistocene climate conditions, and that the lower water table elevations observed today are only typical of the relatively short, anomalously dry interglacial periods.

Third, multiple climate cycle histories are recorded at paleo discharge sites. Therefore, it is likely that water table elevations will rise during subsequent future pluvial cycles, and discharge will again become reactivated. These data conflict with the concepts of a monotonically-decreasing trend in water table elevations and effective moisture availability proposed for the Death Valley region due to tectonic lowering of base levels tied to down-dropping the floor of Death Valley, and increasing the rain-shadow effect by raising the height of the Sierra Nevada and Transverse Ranges to the west during the last several million years (Winograd and Doty, 1980; Winograd et al., 1985; Winograd and Szabo, 1988). Repetition of this hydrodynamic response over the last two glacial cycles strongly indicates that performance models of future saturated-zone conditions must consider the full range climatic possibilities.

8. CONCLUSIONS

8.1 Summary of findings:

Data presented above support a strong linkage between a regional saturated-zone ground-water response to changes in climate-induced effective moisture, net infiltration and recharge over the last 200 ka. Demonstrating this connection verifies the practical importance of understanding how climatic conditions changed in the past and how they might be expected to change in the future.

Collectively, data indicate that regional ground waters commonly discharged at surface during pluvial episodes for at least the past two glacial cycles. In general, ages of deposits span a younger period of about 15 to 60 ka, and an older, albeit less well-defined, period of about 90 to 180 ka. Where observed, the break between these two time spans correlates well to differences in lithology, although much remains to map, describe and date these deposits in detail. Therefore, the distribution of ages indicates that discharge may have been active 60-80% of the time during the last 200 ka. A similar proportion of the global record is estimated to have experienced glacial climates over the past 800 ka (M.D. Mifflin, written communication, 1996). Materials younger than 9 to 15 ka at discharge sites have not been identified indicating that activity ceased around 12 to 15 ka in up-gradient sites, and slightly later (~9 ka) down-gradient at lower elevations.

Stable oxygen isotope data are consistent with cooler temperatures of discharge relative to active high-volume discharge from deep carbonate aquifers, which in turn, is compatible with shallower and shorter flow paths and possible recharge at lower elevations. Ostracode and diatom assemblages are consistent with ground-water discharge and indicate that a variety of paleoenvironments were present similar to modern marsh and wetland deposits found much further to the north. Along with paleontological data, $^{234}U/^{238}U$, $\delta^{87}Sr$ and $\delta^{13}C$ data indicate a regional rather than surface or perched source of ground water.

Record of discharge deposition for the youngest glacial cycle is strongly correlated between all five sites in Amargosa Valley, as well as similar deposits flanking the Spring Mountains (Quade et al., 1995). The framework of geochronologic data also correlates with other regional climate proxies indicative of higher effective moisture and elevated regional water table levels. Sites closest to Yucca Mountain indicate water table rises of up to 100 to 120 m in response to increased recharge during pluvial climates. These fluctuations of the saturated-zone in response to increased recharge appear to be rapidly transmitted to discharge sites with respect to timing of changes in effective moisture documented from surface records. The strong correlation between climate and saturated-zone response indicates that Amargosa Valley paleohydrology over the last several hundred thousand years has been predominantly controlled by pluvial and interpluvial climate cycles rather than by longer-term tectonic processes operating in Death Valley and the Sierra Nevada mountains. Therefore, there is a strong likelihood of recurring high water-table stands during future pluvial episodes.

8.2 Remaining Uncertainties:

Data and interpretations presented above must be considered reconnaissance in nature. Much remains to be learned about the detailed discharge history including duration and timing of active periods, as well as also episodes of non-deposition and erosion. This work requires mapping, trenching and sampling of discharge sites in order to establish a better stratigraphy, geochronology and paleoenvironmental reconstruction. This is particularly true of the older pluvial cycles that are currently only crudely defined at two to three sites. Particular attention should be paid to defining deposits that may belong to even older pluvial cycles (up to 400 ka) and to more-clearly identifying important differences between various pluvial cycles. The primary reasons for these investigations are the recognition that global and regional climate cycles are a response to a complex variety of orbital and secondary conditions that are not invariant. Local climate conditions and the hydrologic response that existed during the 400 ka pluvial may not be identical to the late Pleistocene pluvial. If the next pluvial condition will most closely resemble the 400 ka pluvial (Forester et al., 1996), geologic evidence should be examined for the presence of this cycle. Differences between saturated-zone records during other pluvial cycles may provide important clues that allow more accurate predictions of hydrologic conditions expected in the next pluvial. Also of importance is the recognition that full-glacial conditions are not necessary to induce higher water-table elevations. A detailed understanding of the timing of discharge and its correlation to other climate records will determine the climate parameters that allow increased recharge and higher water-table elevations within the Yucca Mountain flow system.

Ground-water source identity remains a significant uncertainty. In particular, flow-paths and recharge areas are largely left unknown. Contributions from local versus distant recharge as well as possible travel times are particularly important aspects of recharge through Yucca Mountain and the potential for rapid transport of nuclides to surface sites. Preliminary radiocarbon data from aquatic and terrestrial snails can be interpreted as evidence for very fast transport (about 500 to several thousand years). In addition to continued work with the surface deposits, shallow drill holes to water table are required to obtain samples of modern-day ground water for hydrochemical and isotopic characterization, as well as temperatures and accurate position of water table elevations. Coring these holes will also allow an older record of deeper deposits to be obtained.

REFERENCES

Balescu, S. and Lamonthe, M., 1992, The blue emission of K-feldspar coarse grains and its potential for overcoming TL age Underestimation, Quaternary Science Reviews, v. 11, p. 45-51.

Benson, L.V., and McKinley, P.W., 1985, Chemical composition of ground water in the Yucca Moun-

tain Area, Nevada, 1971-84: U.S. Geological Survey Open-File Report 85-484, 10 p.

Berger, G.W., 1985, Thermoluminescence dating of volcanic ash: Journal of Volcanology and Geothermal Research v. 25, p. 333-347.

Bradbury, J.P., (in press), A diatom-based paleohydrologic record of climate change for the past 800 ky from Owens Lake, California. In An 800,000-year paleoclimate record from core OL-92, Owens Lake, California, G.I. Smith and J.L. Bischoff (eds.), Geological Society of America Special Paper 317.

Brennan, R. and Quade, J., 1995, Radiocarbon dating of fossil mollusk shells in the Yucca Mountain region. *in* Conference on High-Level Radioactive Waste Management, 6th, Las Vegas, NV, 1995, Proceedings, American Society of Civil Engineers, p. 182-183.

Broecker, W.S., 1963, A preliminary evaluation of uranium-series inequilibrium as a tool for absolute age measurement on marine carbonates: Journal of Geophysical Research, v. 68, p. 2817-2834.

Claassen, H.D., 1985, Sources and mechanisms of recharge for ground water in the west-central Amargosa Desert, Nevada - A geochemical interpretation: U.S. Geological Survey Professional Paper 712-F, 31 p.

Coplen, T.B., Winograd, I.J., Landwehr, J.M., and Riggs, A.C., 1994, 500,000-year stable carbon isotopic record from Devils Hole, Nevada: Science, v. 263, p. 361-365.

Czarnecki, J.,1985, Simulated effects of increased recharge on the ground-water flow system of Yucca Mountain and vicinity, Nevada-California. U.S. Geological Survey Water Resources Investigation Report 84-4344, 33 p.

Edwards, R.L., Chen, J.H., and Wasserburg, G.J., 1986, ^{238}U-^{234}U-^{230}Th-^{232}Th systematics and the precise measurement of time over the past 500,000 years. Earth and Planetary Science Letters, v. 81, p. 175-192.

Faure, G., 1986, Principles of Isotope Geology, second edition: John Wiley & Sons, New York, 589 p.

Forester R.M., Bradbury, J.P., Carter, C., Elvidge, A., Hemphill, M., Lundstrom, S.C., Mahan, S.A., Marshall, B.D., Neymark, L.A., Paces, J.B., Sharpe, S., Whelan, J.F., and Wigand, P., 1996, The climatic and hydrologic history of southern Nevada during the Late Quaternary: Administrative report 3GCA102M to DOE-YMPSCO.

Frizzell, V.A., Jr., and Schulters, J., (1990) Geologic map of the Nevada Test Site, southern Nevada: U.S. Geological Survey Miscellaneous Investigations Series, Map I-2046.

Ivanovich, M., and Harmon, R.S., 1992, Uranium-series disequilibrium: Applications to Earth, Marine, and Environmental Sciences, second edition: Clarendon Press, Oxford, U.K., 910 p.

Ku, T.L., 1976, The urainum-series methods of age determination. Annual Reviews of Earth and Planetary Science, v. 4, p. 347-380.

Levy, S.S. (1991), Mineralogic alteration history and paleohydrology at Yucca Mountain, Nevada. High-Level radioactive Waste Management Proceedings of the Second International Conference, p. 477.

Ludwig, K.R., Peterman, Z.E., Simmons, K.R., and Gutentag, E.D., 1993, $^{234}U/^{238}U$ ratios as a ground water flow tracer, SW Nevada-SE California: *in* Conference on High-Level Radioactive Waste Management, 4th, Las Vegas, NV, 1993, Proceedings, American Society of Civil Engineers, p. 1567-1572.

Ludwig, K.R., Simmons, K.R., Szabo, B.J., Winograd, I.J., Landwehr, J.M., Riggs, A.C., and Hoffman, R.J., 1992, Mass-spectrometeric 230Th-234U-238U dating of the Devils Hole calcite vein: Science v. 258, p. 284-287.

Marshall B.D., Peterman Z.E., Stuckless J.S., Sr isotopic evidence for a higher water table at Yucca Mountain: *in* Conference on High-Level Radioactive Waste Management, 4th, Las Vegas, NV, 1993, Proceedings, American Society of Civil Engineers, p. 1948-1952.

Marshall, B.D., and Mahan, S.A., 1994, Strontium isotope geochemistry of soil and playa deposits near Yuccan Mountain, Nevada: *in* Conference on High-Level Radioactive Waste Management, 5th, Las Vegas, NV, 1994, Proceedings, American Society of Civil Engineers, p. 2685-2691.

McCrea, J.M., 1950, The isotopic chemistry of carbonates and a paleotemperature scale. Journal of Chemical Physics, v. 18, p. 849-857.

Millard, H.T., and Maat, P.B., 1994, Thermoluminescence Dating Procedures in Use at the U.S. Geological Survey, Denver, Colorado: U.S. Geological Survey Open-File Report 94-249, 112 p.

Paces J.B., 1995, FY1995 studies of paleodischarge deposits: Milestone Report 3GQH520M to DOE-YMPSCO, 27 p.

Paces, J.B., Mahan, S.A., Ludwig, K.R., Kwak, L.K., Neymark, L.A., Simmons, K.R., Nealey, L.D., Marshall, B.D., and Walker, A.W., 1995, Progress report on dating Quaternary surficial deposits: Milestone Report 3GCH510M to DOE-YMPSCO.

Paces, J.B., Menges, C.M., Widmann, B., Wesling, J.R., Bush, C.A., Futa, K., Millard, H.T., Maat, P.B., and Whitney, J.W., 1994, Preliminary U-series disequilibrium and thermoluminescence ages of surficial deposits and paleosols associated with Quaternary faults, eastern Yucca Mountain: *in* Conference on High-Level Radioactive Waste Management, 5th, Las Vegas, NV, 1994, Proceedings, American Society of Civil Engineers, p. 2391-2401.

Paces, J.B., Taylor E.M., and Bush, C.A., 1993, Late Quaternary history and uranium isotopic compositions of ground water discharge deposits, Crater Flat, Nevada: *in* Conference on High-Level Radioactive Waste Management, 4th, Las Vegas, NV, 1993, Proceedings, American Society of Civil Engineers, p. 1573-1580.

Perfect, D.L., Faunt, C.C., Steinkampf, W.C., and Turner, A.K., (1995) Hydrochemical data base for the Death Valley region, California and Nevada: U.S. Geological Survey Open-File Report 94-305, 10 p. + 2 diskettes.

Peterman, Z.E., Widmann, B.L., Marshall, B.D., Aleinikoff, J.N., Futa, K., and Mahan, S.A. (1994) Isotopic tracers of gold deposition in Paleozoic limestones, southern Nevada: *in* Conference on High-Level Radioactive Waste Management, 5th, Las Vegas, NV, Proceedings, American Society of Civil Engineers, p. 1316-1323.

Peterman Z.E., and Stuckless, J.S. (1993a) Isotopic evidence of complex ground-water flow at Yucca Mountain, Nevada, USA: *in* Conference on High-Level Radioactive Waste Management, 4th, Las Vegas, NV, 1993, Proceedings, American Society of Civil Engineers, p. 1559-1566.

Peterman Z.E., and Stuckless, J.S. (1993b) Application of strontium and other radiogenic tracer isotopes to paleohydrologic studies: Paleohydrological Methods and their Applications, Proceedings of the NEA Workshop, Paris, p. 59-84.

Quade, J., Mifflin, M.D., Pratt, W.L., McCoy, W., and Burckle, L., 1994, Spring deposits and water table levels in the southern Great Basin during the late Quaternary: Geological Society of America Bulletin, (in press)

Riggs, A., 1984, Major carbon-14 deficiency in modern snail shells from southern Nevada springs. Science 224, p. 58-61.

Robison, J.H. (1984) Ground water level data and preliminary potentiometric-surface maps, Yucca Mountain and Vicinity, Nye Co., Nevada. U.S. Geological Survey Water-Resources Investigations Report 84-4197.

Rosholt, J.N., and Antal, P.S., 1962, Evaluation of the Pa231/U-Th^{230}Th/U method for dating Pleistocene carbonate rocks. U.S. Geological Survey Professional Paper 450-E, p. 108-111.

Singhvi, A.K., Sharma, Y.P., and Agrawal, D.P., 1982, TL dating of dune sands in Rajasthana, India: Nature, v. 295; p. 313-315.

Stuiver, M. and Reimer, P.J., 1993, Extended ^{14}C database and revised CALIB radiocarbon calibration program: Radiocarbon v. 35, p. 215-230.

Swadley, W.C., and Carr, W.J. (1987) Geologic map of the Quaternary and Tertiary deposits of the Big Dune Quadrangle, Nye County, Nevada, and Inyo County, California: U.S. Geological Survey Miscellaneous Series Map, I-1767.

Szabo, B.J., Kolesar, P.T., Riggs A.C., Winograd, I.J., and Ludwig K.R., 1994, Paleoclimatic inferences from a 120,000-yr calcite record of water-table fluctutation in Browns Room of Devils Hole, Nevada: Quaternary Research, v. 41, p. 59-69.

Taylor, E.M., 1991, Quaternary spring deposits at the southern end of Crater Flat, Nye County, Nevada, abst.: Eos Transactions of the American Geophysical Union, v. 72, p. 162.

Waddell, R.K., Robison, J.H., and Blankennagel, R.K., "Hydrology of Yucca Mountain and vicinity, Nevada-California - Investigative results through mid-1983," U.S. Geological Survey Water-Resources Investigations Report 84-4267, (1984).

Whelan, J.F., Moscati, R.J., Allerton, S.B.M., and Marshall, B.D., 1996, Applications of isotope geochemistry to the reconstruction of Yucca Mountain paleohydrology: Milestone Report 3GQH257M to DOE-YMPSCO.

Whelan, J.F., Vaniman, D.T., Stuckless, J.S., and Moscati, R.J., 1994, Paleoclimatic and paleohydrologic records from secondary calcite: Yucca Mountain, Nevada: *in* Conference on High-Level Radioactive Waste Management, 5th, Las Vegas, NV, 1994, Proceedings, American Society of Civil Engineers, p. 2738-2745.

Winograd, I.J., and Doty, G.C., 1980, Paleohydrology of the southern Great Basin with special reference to water table fluctuations beneath the Nevada Test Site during the late(?) Pleistocene: U.S. Geological Survey Open-File Report 80-569, 91 p.

Winograd, I.J., and Szabo, B.J., 1988; Water-table decline in the south-central Great Basin during the Quaternary: Implications for toxic waste disposal: in Carr, M.D. and Yount, J.C., eds., Geologic and Hydrologic Investigations, Yucca Mountain, Nevada, U.S. Geological Survey Bulletin 1790, p. 147-152.

Winograd, I.J, Szabo, B.J., Coplen T.B., Riggs, A.C., and Kolesar, P.T., 1985, Two-million-year record of deuterium depletion in Great Basin ground waters: Science, v. 227, p. 519-522.

Winograd, I.J, Coplen T.B., Landwehr, J.M., Riggs, A.C., Ludwig, K.R., Szabo, B.J., Kolesar, P.T., and Revesz, K.M., 1992, Continuous 500,000-year climate record from vein calcite in Devils Hole, Nevada: Science, v. 258, p. 255-260.

Wintle, A.G., 1977, Detailed study of a thermoluminescent mineral exhibiting anomalous fading: Journal of Luminescence, v. 15, p. 385-393.

Wintle, A.G. and Huntley, D.J., 1980, TL dating of ocean sediments: Canadian Journal of Earth Sciences, v. 17, p. 348-360.

Wintle, A.G. and Huntley, D.J., 1982, Thermoluminescence Dating of Sediments: Quaternary Science Reviews v. 1, p. 31-53.

Wintle, A.G., 1973, Anomalous fading of thermoluminescence in mineral samples: Nature, v. 245, p. 143-144.

Zeller, E. J., 1955, Thermoluminescence of carbonate sediments: in Nuclear Geology, John Wiley and Sons, New York; p. 180-188.

APPENDIX 1: Sample Locations:

Sample	Bar Code	Site	Station	Comments
U-series samples				
HD1384	SPC00502615	LWD	3	Surface lag: Capping marl unit
HD1385	SPC00502616	LWD	3s	Surface lag: Capping marl unit
HD1464	SPC00500385	LWD	7	Dug out from under diatomite cliff: upper Green sand unit
HD1736	SPC00502916	LWD	6	Base of box pit: Green sand unit
HD1969	SPC00502973	LWD	6	Surface outcrop: Capping marl unit
HD1970	SPC00502974	LWD	6	Cliff-face outcrop: basal Diatomite unit
HD1971	SPC00502975	LWD	6	Cliff-face outcrop: upper Green sand unit
HD1972	SPC00502976	LWD	6	Base of box pit: Green sand unit
HD1973	SPC00502977	LWD	13	Wash-bottom carbonate: Green sand unit
HD1974	SPC00502978	LWD	13	Terrace-level carbonate: Green sand unit
HD1975	SPC00502979	LWD	7	Cliff-face outcrop: Diatomite unit
HD1976	SPC00502980	LWD	9	Surface lag (near outcrop): Green sand unit
HD1977	SPC00502981	LWD	9s	Surface lag (near outcrop): Banded travertine limestone
HD1978	SPC00502982	LWD	8N	60-80 cm hand-dug pit (outcrop): Green sand unit
HD1979	SPC00502983	LWD	8	Box pit wall: Green sand unit
HD1980	SPC00502984	LWD	8N	Slope excavation (outcrop): Green sand unit
HD1606	SPC00503047	CFD	4	~90 cm deep in hand-dug pit
HD1607	SPC00503048	CFD	4	~90 cm deep in hand-dug pit
HD170	SPC00002951	CFD	3	Surface lag
HD1733	SPC00502913	CFD	West trench	North end of exposed trench wall, east side of trench
HD1734	SPC00502914	CFD	6	Surface lag
HD1735	SPC00502915	CFD	6	Surface lag/shallow excavation
HD1750	SPC00502957	CFW	---	Surface lag north of Station 4
HD1706	SPC00503086	SLD	---	Outcrop of upper carbonate cap: 36°25.83'N; 116°27.56'W
HD1708	SPC00503088	SLD	---	Wash-bottom carbonate layer: 36°25.83'N; 116°27.56'W
HD1709	SPC00503089	SLD	---	Arroyo wall, 170 cm depth: 36°25.77'N; 116°27.57'W
HD1711	SPC00503091	SLD	---	Outcrop of upper carbonate cap: 36°25.77'N; 116°27.57'W
HD1716	SPC00503096	SLD	---	Outcrop along railroad grade: 36°29.25'N, 116°32.13'W
HD1737	SPC00502917	SLD	---	Arroyo wall, 300 cm depth: 36°25.81'N, 116°27.60'W
HD1738	SPC00502918	SLD	---	Surface exposure: 36°26.06'N, 116°28.25'W
HD1854	SPC00502956	SLD	---	Surface lag on carbonate cap: 36°25.83'N; 116°27.56'W
HD1981	SPC00502985	IPD	1	Shallow hole: lwr Grn silty unit: 36°38.95'N, 116°41.01'W
HD1982	SPC00502986	IPD	1	Cut-bank wall: uppr Grn silty unit: 36°38.95'N, 116°41.01'W
HD1983	SPC00502987	IPD	1	Cut-bank wall: Siliceous marl: 36°38.95'N, 116°41.01'W
HD1984	SPC00502988	IPD	1	Surface lag: Siliceous marl: 36°38.95'N, 116°41.01'W
HD1985	SPC00502989	IPD	1	Surface lag: Siliceous marl: 36°38.95'N, 116°41.01'W

Sample	Bar Code	Site	Station	Comments
TL samples				
TL-65	SPC00502790	LWD	6	See notes on Table 3
TL-66	SPC00502789	LWD	6	See notes on Table 3
TL-67	SPC00502788	LWD	6	See notes on Table 3
TL-43	SPC00500898	LWD	6	See notes on Table 3
TL-24	SPC00502629	LWD	8	See notes on Table 3
TL-68	SPC00502787	LWD	8w	See notes on Table 3
TL-69	SPC00502786	LWD	13	See notes on Table 3
TL-20	SPC00500894	CFD	4	See notes on Table 6
TL-21	SPC00500895	CFD	4	See notes on Table 6
TL-22	SPC00500896	CFD	West Trench	See notes on Table 6
TL-23	SPC00502630	CFD	West Trench	See notes on Table 6
TL-44	SPC00500897	SLD	---	Arroyo wall, 300 cm depth: 36°25.81'N, 116°27.60'W
TL-45	SPC00502628	SLD	---	Arroyo wall, 300 cm depth: 36°25.81'N, 116°27.60'W
TL-46	SPC00502627	SLD	---	Surface exposure: 36°26.06'N, 116°28.25'W
TL-70	SPC00502785	IPD	1	Cut-bank wall: lwr Grn silty unit: 36°38.95'N, 116°41.01'W
TL-71	SPC00502784	IPD	1	Cut-bank wall: uppr Grn silty unit: 36°38.95'N, 116°41.01'W
O, C samples				
HD1751	SPC00500524	CFW	---	Ledgy outcrop ~200 m SE of Station 4
HD1752	SPC00500523	CFW	---	Ledgy outcrop ~200 m SE of Station 4
HD1989	SPC00502993	CFD	8	Base of natural cut-back
HD1994	SPC00502998	CFW	1	Surface exposure
HD1996	SPC00503000	CFW	2	Top of low outcrop of green hackly unit
HD1457	SPC00500394	CFD	4	Pit 1, ~120 cm depth
HD1458	SPC00500395	CFD	4	Pit 1, 80-90 cm depth
HD1459	SPC00500396	CFD	4	Pit 1, ~60 cm depth
HD1460	SPC00500397	CFD	4	Pit 1, ~35 cm depth
HD1461	SPC00500398	CFD	4	Pit 1, 15-25 cm depth
HD1462	SPC00500399	CFD	4	Surface lag
HD1463	SPC00500400	CFD	West Trench	~41 m south of trench-drainage intersection & 1.4 m deep
HD164	SPC00002945	CFD	---	Approximately at Station 5
HD166	SPC00002947	CFD	---	~60 m NNE of Station 5
HD167	SPC00002948	CFD	---	~70 m N of Station 5
HD168	SPC00002949	CFD	---	~120 m NNW of Station 5
HD169	SPC00002950	CFD	---	Approximately at Station 2
HD1700	SPC00500145	CFD	6	Surface Lag
HD1703	SPC00500148	CFD	6	Surface lag plus upper 10 cm
HD1704	SPC00500149	CFD	6	Surface lag plus upper 10 cm
dh-103		Devils Hole	---	Core DH-11 taken subaqueously

Sample	Bar Code	Site	Station	Comments
dh-180		Devils Hole	---	Core DH-11 taken subaqueously
dh-300		Devils Hole	---	Core DH-11 taken subaqueously
HD505	SPC00003741	Grapevine Springs	---	Upper-spring tufa mound; 37°01'12", 117°23'13"W
HD506	SPC00003742	Grapevine Springs	---	Upper-spring tufa mound; 37°01'12", 117°23'13"W
HD507	SPC00003743	Grapevine Springs	---	Upper-spring tufa mound; 37°01'12", 117°23'13"W
HD508	SPC00003744	Grapevine Springs	---	Upper-spring tufa mound; 37°01'12", 117°23'13"W
HD510	SPC00003746	Grapevine Springs	---	Upper-spring tufa mound; 37°01'12", 117°23'13"W
HD511	SPC00003747	Grapevine Springs	---	Upper-spring tufa mound; 37°01'12"N, 117°23'13 W
HD1856	SPC00500519	LWD	12	Exposure in natural drainage
HD1857	SPC00500520	LWD	12	Exposure in natural drainage
HD1858	SPC00500521	LWD	12	Exposure in natural drainage
HD1859	SPC00500522	LWD	12	Exposure in natural drainage
HD1860	SPC00006347	LWD	12	Exposure in natural drainage
HD1861	SPC00006346	LWD	---	Main "fringe" area between stations 11 and 12
HD1863	SPC00006344	LWD	---	Western apron of main badlands area, 40-80 m west if Station 10
HD1999	SPC00008899	LWD	9s	Surface lag (near outcrop): Banded travertine limestone
HD2000	SPC00008898	LWD	9s	Surface lag (near outcrop): Banded travertine limestone
HD1322	SPC00004822	Nevares Spring	---	Stream-cut, S side of mound: 36°30'47"N, 116°49'16"W
HD495	SPC00003731	Nevares Spring	---	Stream-cut, S side of mound: 36°30'47"N, 116°49'16"W
HD496	SPC00003732	Nevares Spring	---	Stream-cut, S side of mound: 36°30'47"N, 116°49'16"W
HD499	SPC00003735	Nevares Spring	---	Stream-cut, S side of mound: 36°30'47"N, 116°49'16"W
HD500	SPC00003736	Nevares Spring	---	Stream-cut, S side of mound: 36°30'47"N, 116°49'16"W
HD501	SPC00003737	Nevares Spring	---	Stream-cut, S side of mound: 36°30'47"N, 116°49'16"W
HD502	SPC00003738	Nevares Spring	---	Stream-cut, S side of mound: 36°30'47"N, 116°49'16"W
HD503	SPC00003739	Nevares Spring	---	Stream-cut, S side of mound: 36°30'47"N, 116°49'16"W
HD1117	SPC00005478	Rock Valley Mound	---	Crest of mound; 36°37'46"N, 116°19'12"W
HD1118	SPC00005479	Rock Valley Mound	---	Low on N-end of mound; 36°38'11"N, 116°18'51"W
HD1319	SPC00004825	Rock Valley Mound	---	Low hill south of Hwy 95; 36°37'46"N, 116°19'12"W
HD1321	SPC00004823	Rock Valley Mound	---	NE end of mound crest; 36°38'11"N, 116°18'51"W
HD1746	SPC00502925	Rock Valley Mound	---	Mound crest; 36°38'11"N, 116°18'51"W
HD1747	SPC00502527	SLD	River bottom	Surface exposure, brown silts: 36°26.06'N, 116°28.25'W
HD1749	SPC00502528	SLD	River bottom	Surface exposure, brown silts: 36°26.06'N, 116°28.25'W
HD1685	SPC00500127	SLD	High terrace	Part of 2m section, head of arroyo; 36°25'53"N, 116°27'32"W
HD1686	SPC00500128	SLD	High terrace	Part of 2m section, head of arroyo; 36°25'53"N, 116°27'32"W
HD1687	SPC00500129	SLD	High terrace	Part of 2m section, head of arroyo; 36°25'53"N, 116°27'32"W
HD1688	SPC00500130	SLD	High terrace	Part of 2m section, head of arroyo; 36°25'53"N, 116°27'32"W
HD1689	SPC00500131	SLD	High terrace	Part of 2m section, head of arroyo; 36°25'53"N, 116°27'32"W
HD1690	SPC00500135	SLD	High terrace	Part of 2m section, head of arroyo; 36°25'53"N, 116°27'32"W
HD1691	SPC00500136	SLD	High terrace	Part of 2m section, head of arroyo; 36°25'53"N, 116°27'32"W
HD483	SPC00003719	Travertine Point	---	TS2 formation; 36°19'50"N, 116°18'17"W

Sample	Bar Code	Site	Station	Comments
HD484	SPC00003720	Travertine Point	---	TS2 formation; 36 19'50"N, 116°18'17"W
HD485	SPC00003721	Travertine Point	---	Vein exposed in cliff face; 36°19'50"N, 116°18'17"W
Paleontological Samples				
OCI-3; NV94RMF77	SPC00009132	CFD	5	Surface exposure, upper 10 cm
JPB-Site 199-G	SPC00009099	CFD	8	Cut-bank exposure, 1 m below surface
JPB-Site 199-H	SPC00009098	CFD	7	Cut-bank exposure, 1.5 m above stream bed
OCI-20; NV95RMF15 (LWD-7)	SPC00009153	LWD	1	Surface exposure, upper portion of carbonate carapace: Capping marl unit
OCI-21; NV95RMF16 (LWD-7)	SPC00009154	LWD	1	Surface exposure, lower portion of carbonate carapace: Capping marl unit
JPB-8F (LWD-8)	SPC00009097	LWD	8N	Base of excavated section (outcrop): Green sand unit
OCI-23; LWD-10	SPC00008998	LWD	6	Top of measured section; Capping marl unit
JPB-11 (LWD-11)	SPC00009096	LWD	---	20 m NW of Station 11, 0-10 cm
OCI-24; LWD-12	SPC00009000	LWD	8N	Middle of excavated section (outcrop): Green sand unit
OCI-24; LWD-13	SPC00009000	LWD	8N	Middle of excavated section (outcrop): Green sand unit
OCI-8; NV94RMF82	SPC0000913.	SLD	River bottom	Surface exposure, brown silts: 36°26.06'N, 116°28.25'W
OCI-9; NV94RMF83b [0 to -5cm]	SPC00009138	SLD	River bottom	Hand-driven tube-core at 0 to 5 cm depth; brown silts: 36°26.06'N, 116°28.25'W
OCI-9; NV94RMF83b [-25 to -29.5cm]	SPC00009138	SLD	River bottom	Hand-driven tube-core at 25 to 29.5 cm depth; brown silts: 36°26.06'N, 116°28.25'W

APPENDIX 2: Analytical Dating Techniques:

Uranium-series disequilibrium dating: In near-surface environments at Yucca Mountain, uranium is oxidized to the hexavalent state and is readily transported in solution by natural waters as various complexed species. In contrast, thorium remains in the tetravalent state resulting in a negligible solubility. Therefore, essentially all ^{230}Th present in a mineral precipitated purely from aqueous solution arises from decay of ^{238}U and ^{234}U incorporated at the time of formation. The $^{230}Th/U$ dating technique relies on the systematic decay of ^{238}U and its natural daughter-isotopes at constant rates under closed-system conditions (no loss or gain of parent or daughter isotopes other than by radioactive decay). The theoretical and mathematical relations defining the isotopic evolution of the ^{238}U system are well understood (Rosholt and Antal, 1962; Broecker, 1963; Ku 1976; Faure 1986; Edwards et al., 1987; Ivanovich and Harmon 1992).

However, much of the authigenic carbonate in the paleodischarge deposits at Yucca Mountain contains substantial amounts of ^{232}Th indicating the presence of a non-hydrogenic component (usually detrital silicates, such as clays, that cannot be physically separated from the hydrogenic component prior to analysis). The uranium and thorium isotopic contribution from this non-hydrogenic component must be subtracted from the measured analysis before an age for the hydrogenic component can be calculated. The approach for obtaining corrected ages in this report is to estimate the isotopic composition of the ^{232}Th-bearing component and use the abundance of ^{232}Th observed in the analysis to correct the observed $^{234}U/^{238}U$ and $^{230}Th/^{238}U$ to a ^{232}Th-free state. The degree of correction is greatest for samples with high ^{232}Th abundances (i.e., low $^{230}Th/^{232}Th$ activity ratios) and negligible in samples with low ^{232}Th abundances (i.e., high $^{230}Th/^{232}Th$ activity ratios). Therefore, in samples with reasonably high $^{230}Th/^{232}Th$, only small corrections (and propagated uncertainties) on the final age estimates are introduced. An advantage of this approach is that a maximum amount of geochronological information is obtained from the available analytical information. The larger number of age estimates form a population distribution that may contain additional information concerning the reliability of the ages estimated for a given unit. A disadvantage of this method is that the isotopic composition of the detrital phase must be assumed rather than measured. Because of this, samples with high amounts of detrital components do not provide reliable results.

Samples consisted of a variety of calcite- and opal-rich hydrogenic materials introduced into the fine-grained eolian deposits during or after deposition. These include individual plant petrifactions (both calcite and opal), irregular carbonate-rich nodules, thicker carbonate layers assumed to represent algal mats, carbonate-cemented insect burrow casts, bedded limestone and mollusc shells. Typically, larger samples were slabbed and polished photodocumented, and microsampled using carbide dental burs to obtain small amounts (0.02 to 0.2 g) of the densest, most detritus-free materials. Softer, more-porous materials were avoided or removed mechanically.

Aliquots were then weighed, spiked with known amounts of tracer isotopes (typically ^{236}U, ^{233}U, and ^{229}Th) and, in most cases, totally digested in concentrated acids (HF, HNO_3, HCl, and $HClO_4$) in Teflon containers. After complete digestion, uranium and thorium were purified by ion chromatography, loaded on rhenium ribbons, and run as metal ions on a Finnigan MAT 262 multi-collection thermal ionization mass spectrometer with ion-counting capabilities.

Thermoluminescence dating: The thermoluminescence (TL) dating method relies on metastable traps within the crystal lattices of certain minerals (primarily quartz and feldspar) that can be filled with electrons excited by interactions with alpha, beta, gamma and cosmic radiation sources. Trapped electrons are released by additional heat or electromagnetic energy sources (ultraviolet radiation) and are effectively reset by sunlight during eolian transport of fine-grained sediments. Following deposition and burial, the traps systematically refill with electrons as a result of the ambient radiation environment thereby acting as a natural radiation dosimeter. The number of accumulated trapped electrons is proportional to the time the mineral has been exposed to the radiation field. This natural radiation dose arises primarily from the decay of ^{40}K, ^{235}U, ^{238}U, ^{232}Th and their collective radioactive daughters. Cosmic Rays and the decay of ^{87}Rb make lesser contributions. In this study, the 4-11 μm polymineralic silt fraction is used because all three types of radiation can penetrate grains of this size and the subsequent lumi-

nescence can easily escape to be detected upon laboratory heating (Wintle and Huntley, 1982).

When applied to dating sedimentary materials (sand, loess, or silt) thermoluminescence dating relies on the following assumptions: 1) during eolian or fluvial transport, mineral grains are exposed to sunlight of sufficient duration and intensity to clear the defect sites of electrons (reset the clock), and 2) following burial, exposure to natural ionizing radiation gradually repopulates the defect sites with electrons. A thermally-stimulated light emission (referred to as thermoluminescence signal), proportional to the concentration of trapped electrons, can be measured quantitatively in the laboratory. Light emission occurs during the transition of the metastable electrons from their trapped configurations to normal lattice positions occupying lower energy states and can be triggered by heating (Zeller, 1955). If the cumulative thermoluminescence signal can be related to the total radiation dose and dose history, then an age estimate can be directly obtained. In order to estimate the total cumulative dose, increments of known artificial radiation are added to the sample from a calibrated irradiator and the resulting luminescence signal measured. The response of the suite of sub-samples artificially irradiated at different levels is compared to the response of the natural sample (no artificial irradiation) and a sunlight-bleached sub-sample (electron traps reset by exposure to sunlight in order to obtain the total equivalent dose (D_E). Ages are then calculated by dividing the equivalent dose (the estimated radiation dose acquired by the sample [= signal/(signal/unit dose)] in units of Grays) by the dose rate (D_R; natural radiation dose rate in units of Grays/ka). Techniques used in this study closely follow methods outlined in detail by Millard and Maat (1994).

After the fine-silt-sized fraction (4-11 μm, polymineralic) is separated from the bulk sample, it is washed in 4N HCl (to remove carbonate) followed by a 30% H_2O_2 solution (to destroy organic carbonate) and dispersed in a sodium pyrophosphate solution. Fine-silt particles are plated onto 10 mm diameter aluminum disks (slurry taken to dryness by evaporation). All disks are normalized using a brief pulse of infrared light in order to compensate for the effects of unequal sample amounts and distributions between disks resulting from variations inherent during plating. Ideally, four experiments are conducted in order to obtain the final age estimate of a sample including sunlight sensitivity tests, anomalous fading tests (Wintle, 1973), a total bleach experiment (Singhvi and others, 1982) and a partial bleach experiment (Wintle and Huntley, 1980).

Before thermoluminescence measurements are made, disks are preheated at 124°C for 64 hours to remove the low-temperature, unstable electrons that are loosely held in traps (Wintle 1977; Berger 1985). Thermoluminescence measurements were made using a Daybreak Model 1100 Instrument with blue transmitting filters Schott UG-11 and Kopp 7-59. Blue wavelengths include quartz emissions and an apparently stable component of potassium feldspar emissions (Balescu and Lamothe, 1992). A heating rate of 5°C/s was employed and samples were heated in a nitrogen environment after initial evacuation of the glow oven.

Only traps that have effectively retained the accumulated electrons without leakage are useful for dating purposes, which, in practice, equates to measured luminescence given off at temperatures of 300°C or higher. A region of stable TL signal (plateau test) is obtained if the values for equivalent doses (amount of radiation necessary to produce the observed natural TL signal estimated by artificial irradiation of the sample) remain constant over a 50° to 200°C temperature interval, providing an indication that negligible leakage of electron traps has occurred. Failure of the plateau test can be caused by several reasons, however, the result is an incalculable or unreliable age.

In addition to estimating the equivalent dose of radiation that the sample has accumulated, dose rates must be known and constant throughout the history of sediment burial before TL ages are derived. Dose rates have been measured in situ using a field sodium iodide gamma ray spectrometer. However, dose rates are dependent on the degree of water saturation in a sample due to greater radiation absorption by water filled rather than air-filled inter-granular pore space. Bulk samples are also collected for determination of field-moisture contents as (typically 1 to 8 percent by weight) well as saturation moisture contents (30 to 70 percent by weight). Since it is likely that these deposits were at or near saturation during periods of active discharge during the late Pleistocene, and have high water-holding capacities due to an abundance of clays, ages based on dose rates calculated at half moisture-saturation values are

preferred in this report as an approximation to the more-complex saturation history experienced through time in this environment.

Radiocarbon dating: Interactions between cosmic-ray-produced thermal neutrons and ^{14}N nuclei in the upper atmosphere produce unstable ^{14}C which decays back to ^{14}N by beta decay with a characteristic half life of about 5.7 ka. The radioactive carbon is rapidly converted to CO_2 which is incorporated into the carbon cycle by carbon-based life forms or as dissolved bicarbonate in natural waters. Because atmospheric carbon is in equilibrium between the process of production and decay, organic material or meteoric water will contain atmospheric abundances of radiocarbon through respiration or liquid-vapor diffusion. Once this exchange process is terminated through death or isolation from atmosphere, the abundance of ^{14}C atoms will decrease systematically providing a geochronological tool with an upper limit of about 40 ka (seven half-lives).

Radiocarbon analyses of mollusc shells and plant petrifactions in this report were contracted to Beta Analytical, Inc. of Miami, FL for analysis by accelerator mass spectrometry. Samples of calcite were given minimal pretreatment consisting of washing in deionized water to remove adhering matrix and adsorbed ions or dilute acid washes to remove the outermost few microns which may have experienced some exchange with recent atmospheric carbon. Measured ^{14}C abundances were corrected for fractionation based on measured $^{13}C/^{12}C$, and conventional radiocarbon ages were calculated by normalizing $\delta^{13}C$ to a value of -25‰ and the Libby C14 half life of 5568 years. Errors are based on combined measurements of the sample counting statistics, background and reproducibility of reference standards.

Because ^{14}C production rates have not remained constant over time, conventional radiocarbon ages must be calibrated to calendar years for comparison to ages determined by other dating techniques. Calibrated ^{14}C ages were determined by inputting the conventional radiocarbon age and quoted uncertainty determined by Beta Analytical, Inc. into the program CALIB rev 3.0.1 (Stuiver and Reimer, 1993) using their combined bidecadal tree-ring and spline-fit marine coral data set (file INTCAL93.14C) with an 80 year moving average.

APPENDIX 3: Paleontology analytical results

Listing of ostracode species by site. Predominant habitats are indicated by the number(s) following the taxa parenthetically (1 = seep; 2 = flowing sping; 3 = ponds). Molluscs are noted but not identified.

CRATER FLAT DEPOSIT

OCI-3; NV94RMF77
- *Candona* n.sp. (3)

JPB-Site 199-G
- *Cavernocypris* aff. *C. wardi* (1, 2)

JPB-Site 199-H
- *Cypridopsis vidua* (2, 3)
- *Candona* sp. C
- *Candona* n. sp. (3)
- *Candona acuminata* (2)
- *Cyclocypris serena* (3)
- Charophytes (2, 3)

LATHROP WELLS DIATOMITE

OCI-20; NV95RMF15 (LWD-7)
- ostracode valve fragments
- common terrestrial gastropods, some aquatic molluscs

OCI-21; NV95RMF16 (LWD-7)
- *Candona stagnalis* (3)
- *Candona* n.sp.1
- *Cypridopsis vidua* (2,3)
- *Candona* aff. *C.* sp. H.
- Terrestrial and aquatic molluscs

JPB-8F (LWD-8)
- *Heterocypris incongruens* (1)
- *Scottia tumida* (1)
- *Candona rawsoni* (3)
- *Candona* n. sp. (3)
- *Limnocythere paraornata* (2)
- Aquatic and terrestrial molluscs

OCI-23; LWD-10
- *Cypridopsis vidua* (2, 3)
- *Candona* sp. indet.
- *Heterocypris incongruens* (1)
- Aquatic molluscs common

JPB-11 (LWD-11)
- no ostracodes
- Terrestrial and some aquatic molluscs

OCI-24; LWD-12
- *Cypridopsis vidua* (2, 3)
- *Candona* sp. C
- *Candona* n. sp. (3)
- *Candona acuminata* (2)
- *Cypridopsis okeechobei* (1, 2)
- *Strandesia meadensis* (2)
- *Candona* sp. aff. *C. stagnalis* (3)
- Terrestrial and aquatic gastropods

OCI-24; LWD-13
- *Cypridopsis okeechobei* (1, 2)
- *Cypridopsis vidua* (2, 3)
- *Candona stagnalis* group (3)
- Terrestrial molluscs

AMARGOSA VALLEY AT STATE LINE DEPOSITS

OCI-8; NV94RMF82
- *Candona* n. sp. C
- *Candona* n. sp. (3)
- New genus, new species (2)
- *Limnocythere paraornata* (2)
- *Strandesia reticularis* (1, 2)
- Aquatic molluscs

OCI-9; NV94RMF83B [0 to -5 cm]
- *Candona* n. sp. C
- *Candona* n. sp. (3)
- New genus, new species (2)
- *Limnocythere paraornata* (2)
- *Candona* n. sp. aff. sp. 49
- Aquatic molluscs

OCI-9; NV94RMF83B [-25 to -29.5 cm]
- *Limnocythere paraornata* (2)
- *Candona* n. sp. (3)
- *Ilyocypris gibba* (2)
- *Candona stagnalis* (3)
- Aquatic molluscs

FIGURE CAPTIONS

Figure 1: Location map showing paleodischarge deposits (dark-shaded patches with CFD = Crater Flat Deposits; CFW = Crater Flat Wash; LWD = Lathrop Wells Diatomite; IPD = Indian Pass Deposits; SLD = State Line Deposits). Other sites described in text are Rock Valley mound (RVM), Devils Hole (DH), Travertine Point (TP), Nevares Spring (NS), and Grapevine Spring (GS, off map to northwest). Active springs at Ash Meadows and Death Valley are shown with spring symbols. Outlined arrows show generalized ground-water flow paths. Light-shaded polygons represent bedrock highs; intervening unpatterned areas represent alluvial-filled basins. Solid and dashed lines in basins represent fluvial channels and fan boundaries, respectively.

Figure 2: Sketch of air photos showing major morphologic features of the Lathrop Wells Diatomite deposit. Light-colored, fine-grained deposits are shown as light-shaded areas. Area with platy veneer of banded dense limestone shown with darker-shading. Numbered stations are shown with circle/cross symbol. Dash-dot lines represent drainage channels. Light-solid lines within boundary of the main badlands area represent prominent cliffs separating topographically high areas (mostly north half) from low areas (mostly south half).

Figure 3: Measured stratigraphic section at LWD Station 6 with age determinations reported in Tables 1, 2 and 3. All uncertanties quoted at the 95% confidence level. Numbers following U-series dates are calculated initial 234U/238U ratios. TL ages are given for dose rates calculated at half-saturation moisture contents followed parenthetically by ages calculated using field- and saturation-moisture contents. U-series dates to the right of the column are correlated by position within the general stratigraphy.

Figure 4: Stratigraphic sections at LWD stations 8N and 8 with age determinations reported in Tables 1, 2 and 3. All uncertainties quoted at the 95% confidence level. Radiocarbon ages are given in radiocarbon years before present (RCYBP) and have not been calibrated for the effects of non-linear radiocarbon production rates. Details for reported U-series and TL ages are the same as those described for Figure 3. A) Measured stratigraphic section at station 8N. B) Schematic section from pit at station 8.

Figure 5: U-series evolution diagram showing U and Th isotopic data for all analyses from LWD. Curved lines leading from different 234U/238U values on the Y-axis to secular equilibrium values of 230Th/238U on the X-axis represent the foci of isotopic compositions during closed-system, temporal evolution of different materials with different initial uranium isotopic ratios (evolution lines). Straight, sub-parallel lines represent isochrons drawn at 10 ka intervals between 0 and 100 ka, 20 ka intervals between 100 and 200 ka, and 50 ka intervals between 200 and 300 ka. 95% confidence Error ellipses represent measured isotopic ratios corrected for detrital-Th components (see text and Appendix 2 for explanation). Samples represented by square boxes have error ellipses smaller than box dimensions.

Figure 6: U-series evolution diagram showing U and Th isotopic results for LWD data having the least amount of analytical uncertainty due to detrital-Th corrections (i.e., lowest 232Th contents). Diagram is described in Figure 5.

Figure 7: Estimated dose (DE) versus temperature plot for sample TL-65 from LWD. A weighted saturating-exponential regression model was used to calculate DE from luminescence data obtained on a suite of variably-irradiated discs at each tempe rature interval. The flat part of the DE spectrum is called the "plateau" and indicates the temperature region that yields the most stable TL response. Inset shows the natural and artificial glow curves. Data obtained using the total bleach method (see Appendix 2 for further details).

Figure 8: Sketch of air photos showing major morphologic features of the Crater Flat Deposit (CFD). Light-colored, fine-grained deposits are shown as light-shaded areas. Numbered sample stations are shown with small black circles. Dash-dot lines represent drainage channels. North is towards the top of the sketch.

Figure 9: Measured stratigraphic section from Pit 1 at Station 4, CFD, with age determinations reported in Tables 4, 5 and 6. U-series ages for HD1606 and HD1607 are given as a range from 5 individual

determinations on carbonate cement with high detrial-Th corrections and large uncertainties on individual determinations. Data are shown in Figure 10. TL ages are given for dose rates calcualted at half-saturation moisture contents followed parenthetically by ages calculated using field- and saturation-moisture contents. Age data to the right of the column are correlated by position within the general stratigraphy.

Figure 10: U-series evolution diagram showing U and Th isotopic results for data from CFD. Diagram is described in Figure 5. Samples HD1734 and HD170-1 have error ellipses that are about the same size as the square symbols. Samples HD1607 and HD1606 have very large error ellipses due to the high detrital-Th corrections required. However, data from five individual determinations form two resolvable clusters with ages that span limited ranges. Results of weighted averages for each sample are shown as insets. Data scatter for each group is within analytical error of the corrected data.

Figure 11: Estimated dose (D_E) versus temperature plot for sample TL-20 from CFD. See Figure 7 for details.

Figure 12: Sketch of air photos showing major morphologic features of the Crater Flat Wash deposit (CFW). Light-colored, fine-grained deoists are shown as light-shaded areas. Numbered sample stations are shown with small black circles. Dash-dot lines represent drainage channels.

Figure 13: Schematic diagrams illustrating geological relations and geochronological data for two sites at SLD. Age determinations are from Tables 8, 9 and 10. All uncertainties are given at the 95% confidence level. Values following U-series ages are calculated initial 234U/238U ratios. TL ages are given for dose rates calculated at saturation-moisture contents followed parenthetically by the total range of ages calculated using different moisture contents and analytical uncertainties. A) Schematic cross-section of high-terrace spring deposits near Franklin Well. B) Schematic cross-section of brown silty deposits near the Amargosa River northwest of Franklin Well. 12) U-series evolution diagram showing all U and Th isotopic data for State Line Deposits.

Figure 14: U-series evolution diagram showing U and Th isotopic results for data from SLD. Diagram is described in Figure 5.

Figure 15: Estimated dose (D_E) versus temperature plot for sample TL-45 from SLD. See Figure 7 for details.

Figure 16: South-central portion of the Ashton Quadrangle, Nevada-California 7.5 minute series topographic map, showing the approximate location of Station 1 in the central portion of the IPD.

Figure 17: Measured stratigraphic section with age determinations reported in Tables 11 and 12. All uncertainties are given at the 95% confidence level. Values following U-series ages are calculated initial 234U/238U ratios. TL ages are given for dose rates calculated at saturation-moisture contents followed parenthetically by the total range of ages calculated using different moisture contents and analytical uncertainties.

Figure 18: U-series evolution diagram showing U and Th isotopic results for data from IPD. Diagram is described in Figure 5.

Figure 19: Estimated dose (D_E) versus temperature plot for sample TL-70 from IPD. See Figure 7 for details.

Figure 20: Ages determined by $^{230}Th/U$, radiocarbon and thermoluminescence methods for samples from paleodischarge sites. Data are grouped by locations given in Figure 1. Data in upper portion of diagram are $^{230}U/Th$ ages plotted against calculated initial $^{234}U/^{238}U$. The lower two data sets, representing radiocarbon ages and thermoluminescence ages are shown at the same age scale, but do not carry information regarding vertical position.

Figure 21: Stable C and O isotopic compositions of carbonate tufas and travertines from active spring discharge sites in the southern Nevada/Death Valley region. Data are from Table 13 and represent Grapevine (open circles) and Nevares (triangles) springs in Death Valley, Travertine Point (squares) in the Funeral Mountains, and Devils Hole (filled circles) in Ash Meadows. The shaded region represents supporting information from the large data set from Devils Hole core DH-11 from Winograd and others (1992) and

Coplen and others (1994) and is included for comparative purposes. Data from a possible spring mound in Rock Valley (crosses) are also shown

Figure 22: Stable C and O isotopic compositions of carbonates from the paleodischarge deposits that are the focus of this report plotted with different symbols representing each of the five sites. The shaded field represents compositions of tufa and travertine deposits shown in Figure 21.

Figure 23: Stable C and O isotopic compositions of LWD carbonates. Based on preliminary geochronology, samples from the last glacial cycle are shown as filled symbols, samples from the penultimate glacial cycle are open symbols, and undated samples from the deposit fringe are shown as crosses. Fossil mollusc-shell carbonates are shown as diamonds and circles; whole rock cements and nodules are shown as squares; and petrified (calcified) plant matter is shown as triangles. The range of isotopic compositions of samples from the CFD is shown (hatchured) for comparison.

Figure 24: Location of wells and springs analyzed for $\delta^{87}Sr$ (values in ‰ relative to sea-water = 0.70920) from waters. Bedrock ranges are shown in shaded patterns, and alluvial-filled valleys are shown unpatterned. Solid and dashed lines within alluvial valleys represent active channels and alluvial fan boundaries, boundaries. Dark circles represent sample sites classified as Paleozoic aquifer, open circles represent sample sites from volcanic or alluvium aquifers, and circles with hatch marks represent sites classified as Precambrian aquifer.

Figure 25: Comparison of the distribution of $^{230}Th/U$ ages from Amargosa Valley discharge deposits from this report with the distribution of freshwater and saline diatoms in Owens Lake core (data from Bradbury, 1996). Chronology for Owens Lake core is based on an assumed constant sedimentation rate between materials dated at 25 ka with radiocarbon and ash units identified as Bishop (~740 ka). Roman numerals and dotted tie-lines represent glacial terminations based on oxygen isotope record from sea-floor sediments (SPECMAP).

Table 1: Uranium-series disequilibrium results from Lathrop Wells Diatomite (LWD) deposit. All uncertainties quoted at the 95% confidence level.

Sample Name	Sample wt. (g)	Concentration U (ppm)	Concentration Th (ppm)	$^{230}Th/^{232}Th$ activity ratio	Detritus-corrected Age (ka) ± 2σ	Detritus-corrected Initial Activity Ratio $^{234}U/^{238}U$ ± 2σ	Sample Type
HD1384-1A	0.116	4.13	4.95	1.70	16 ± 7	4.0 ± 0.7	Insect burrow cast; whole rock
HD1384-1B	0.094	4.57	4.68	1.96	17 ± 6	3.7 ± 0.5	" ; -325 mesh
HD1384-1C	0.089	3.96	5.10	1.60	15 ± 8	4.0 ± 0.8	" ; +325 to -60 mesh
HD1384-1CL	0.068	4.68	2.23	3.27	14 ± 2	3.7 ± 0.2	" ; +325 to -60 mesh, acetic leach
HD1384-2A	0.169	4.10	3.23	1.77	11 ± 5	3.4 ± 0.3	Nodular Carbonate; whole rock
HD1384-2B	0.137	4.02	3.39	1.84	12 ± 5	3.5 ± 0.4	" ; -325 mesh
HD1385-1-1A	0.156	11.1	0.174	81.0	12.3 ± 0.2	3.91 ± 0.02	Individual Rhizolith
HD1385-1-1B	0.100	10.85	1.00	16.6	14.7 ± 0.6	3.97 ± 0.04	"
HD1385-2A	0.163	5.52	5.34	1.93	13 ± 5	4.3 ± 0.6	Nodular Carbonate; whole rock
HD1385-2B	0.152	6.18	4.36	2.41	13 ± 3	4.3 ± 0.4	" ; -325 mesh
HD1464-M1	0.134	1.33	1.50	6.30	129 ± 10	4.9 ± 0.8	Nodular Carbonate; whole rock
HD1464-M2	0.094	1.42	1.22	8.33	136 ± 8	4.6 ± 0.5	" ; -325 mesh
HD1464-M3	0.130	1.42	1.88	5.82	164 ± 15	5.4 ± 1.2	" ; +325 to -60 mesh
HD1736-A1	0.453	4.85	3.39	18.1	Excess 230Th	Undefined	Nodular Carbonate; whole rock
HD1969-U1	0.082	6.79	0.0423	246	15.47 ± 0.14	3.87 ± 0.02	Individual Rhizolith
HD1969-U2	0.173	5.73	0.337	25.2	14.9 ± 0.3	3.83 ± 0.03	"
HD1969-U3	0.243	9.93	0.126	108	13.88 ± 0.14	3.81 ± 0.02	"
HD1969-U4	0.051	5.04	0.0110	625	14.04 ± 0.13	3.74 ± 0.02	"
HD1969-U5	0.107	6.17	0.191	49.6	16.0 ± 0.2	3.74 ± 0.02	Carbonate w/ plant petrifactions
HD1970-U1	0.132	4.40	4.58	4.52	56 ± 6	4.7 ± 0.7	Composite Rhizoliths
HD1970-U2	0.128	21.6	4.01	19.1	42 ± 2	3.86 ± 0.08	"
HD1971-U1	0.070	1.92	0.446	24.7	115 ± 3	3.39 ± 0.08	Composite Rhizoliths
HD1971-U2	0.167	6.25	1.01	37.1	152 ± 3	3.16 ± 0.05	Nodular Carbonate
HD1972-U1	0.117	9.06	0.618	107	186 ± 3	3.72 ± 0.04	Nodular Carbonate
HD1972-U2	0.055	5.19	0.796	44.8	173 ± 14	3.57 ± 0.12	"
HD1973-U1	0.060	0.943	1.11	8.93	Excess 230Th	Undefined	Nodular Carbonate
HD1973-U2	0.151	4.06	1.67	6.17	27 ± 2	3.79 ± 0.17	"
HD1974-U1	0.108	1.52	1.43	7.04	120 ± 9	4.5 ± 0.6	Nodular Carbonate
HD1974-U1L	0.073	1.14	0.650	14.3	159 ± 6	4.8 ± 0.3	"
HD1974-U2	0.142	1.42	1.69	6.38	155 ± 12	5.1 ± 0.9	"
HD1974-U2L	0.097	1.14	0.673	15.2	193 ± 8	5.2 ± 0.4	"
HD1975-U1	0.083	1.11	3.65	3.01	Excessive 232	Excessive 232	Diatomite
HD1976-U1	0.055	3.41	0.664	32.4	140 ± 3	3.47 ± 0.07	Nodular Carbonate
HD1976-U2	0.093	2.08	0.413	37.8	211 ± 8	3.89 ± 0.11	"
HD1976-U3	0.107	2.87	0.503	43.2	244 ± 7	3.92 ± 0.08	"
HD1977-U1	0.105	2.41	0.110	122	140 ± 3	2.95 ± 0.03	Bedded Limestone
HD1977-U2	0.093	2.04	0.168	78.6	208 ± 5	3.21 ± 0.05	"
HD1977-U2b	0.115	2.05	0.178	74.8	204 ± 4	3.24 ± 0.04	"
HD1977-U3	0.109	2.26	0.229	60.0	172 ± 3	3.10 ± 0.04	"
HD1978-U1	0.024	1.25	0.860	16.4	Excess 230Th	Not determined	Nodular Carbonate
HD1978-U2	0.054	1.07	1.22	10.5	Excess 230Th	Not determined	"
HD1979-U1	0.021	7.88	0.397	115	91 ± 5	3.78 ± 0.05	Individual Rhizolith
HD1979-U2	0.017	0.969	0.749	13.2	361 ± 38	7.4 ± 1.1	"
HD1979-U4	0.044	6.64	9.58	9.03	384 ± 56	13 ± 4	Tooth?
HD1980-U1	0.029	1.20	0.816	14.1	200 ± 15	5.7 ± 0.6	Nodular Carbonate

Table 2: Results of radiocarbon dating from Lathrop Wells Diatomite (LWD) deposit

Lab ID (Beta-#)	Sample ID	Sample Type	Measured ^{14}C age (RCYBP)	$\delta^{13}C$ (‰)	Conventional ^{14}C age (RCYBP)	Calibrated Age (ka)
Capping Marl Unit, Station 3						
76704	HD1385-1-1-A	small plant petrifaction	5,290 ± 120	-0.9	5,690 ± 120	$6.51\ ^{+0.19}/_{-0.11}$
Capping Marl Unit, Station 7						
83708	LWD-7	Terrestrial snail (Succnid)	13,200 ± 120	-7.4	13,480 ± 120	16.2 ± 0.2
83496	LWD-7	Terrestrial snail (Succnid)	13,290 ± 140	-8.5	13,550 ± 140	16.3 ± 0.2
83709	LWD-7	Terrestrial snail (Vertigo berryi)	13,250 ± 120	-8.7	13,510 ± 120	16.2 ± 0.2
83710	LWD-7	Terrestrial snail (Vallonia)	13,630 ± 140	-8.6	13,890 ± 140	16.7 ± 0.2
84448	LWD-7	Aquatic snail (Gyraulus circum)	13,690 ± 140	-8.3	13,970 ± 140	16.8 ± 0.2
83495	LWD-7	Aquatic bivalve (Pisidium)	13,800 ± 120	-7.4	14,080 ± 120	16.9 ± 0.2
Green Sand Unit, Station 8N						
90244	LWD-12	Terrestrial snail (Vertigo berryi)	41,630 ± 1,860	-8.3	41,910 ± 1,860	not available
91922	LWD-12	Aquatic bivalve (Hydrobiidae)	39,710 ± 1,280	-9	39,970 ± 1,280	not available
91923	LWD-12	Aquatic bivalve (Hydrobiidae)	34,840 ± 700	-7.7	35,120 ± 700	not available
91924	LWD-12	Aquatic bivalve (Pisidium)	37,960 ± 1,020	-7.4	38,240 ± 1,020	not available
91925	LWD-13	Aquatic bivalve (mixed)	36,600 ± 900	-7.3	36,880 ± 900	not available

Dates reported as RCYBP (radiocarbon years before present, where "present" = 1950 A.D.). By international convention, the modern reference standard was 95% of the ^{14}C content of the National Bureau of Standards' Oxalic Acid and calculated using the Libby ^{14}C half life (5,568 years). Quoted errors represent 2 standard deviation statistics (95% probability) and are based on combined measurements of the sample, background, and modern reference standards. Measured $\delta^{13}C$ were calculated relative to PDB-1 international standard and conventional RCYBP ages were normalize to -25 per mil. Calibrated ages were calculated using CALIB (Stuiver and Reimer, 1993) and appropriate data sets.

Table 3: Thermoluminescence results from Lathrop Wells Diatomite deposit. All errors quoted at the 95% confidence limit.

Sample Name	Water Content		Dose Rate (Gy/ka)		Total Bleach Equivalent Dose (Gy)	Total Bleach Age (ka)				Partial Bleach Eqivalent Dose (Gy)	Partial Bleach Age (ka)			
	Field Moist. (%)	Saturation Moist. (%)	Field H20	Saturation H2O		field-moist. H2O	½-sat. moist.	sat.-moist. H2O	Total Range		field-moist. H2O	½-sat. moist.	sat.-moist H2O	Total Range
TL-65	3.7	72	6.1±0.4	3.5±0.3	131±5	21±2	29±2	38±3	19-41					
TL-66	3.8	71	9.4±0.6	5.2±0.4	204±39	22±4	30±6	39±8	18-47					
TL-67	1.1	62												
TL-43	1.3	46	11±0.7	6.8±0.5	263±34	25±4	31±5	39±6	21-45	253±34	24±4	29±5	37±6	20-44
TL-24	1.0	45	7.0±0.4	4.6±0.3	187±31	27±5	33±6	41±8	22-49	204±36	29±5	36±7	45±9	24-54
TL-68	5.1	64	8.7±0.6	5.2±0.4	276±37	32±5	42±6	53±8	27-61	244±33	28±4	37±6	47±7	24-54
TL-69	3.9	45	8.7±0.6	5.9±0.4	286±34	33±5	39±6	49±7	29-56					

TL65 [~350 cm above level line : very hard, white "diatomite" silt just above cap.]
TL-66 [~255 cm above level line : loamy, more unconsolidated, white "diatomite" silt .]
TL-67 [Top of box pit, ~160 cm above level line : loamy, more unconsolidated, mud-cracked silt .]
TL-43 [Bottom of box pit, ~50 cm above level line : Green silty-sand lens in an alternating series.]
TL-24 [Upper bench within the mound: very hard, light (almost ashy) layer of green "diatomite", stratigraphically below TL-43.]
TL-68 [West of Sta. 8, 10-20 cm below surface in small saddle or exposed gully: Interpretated by Quade as "spring orifice sand".]
TL-69 [Sta. 13, between lower and upper terrace carbonate layers, 50 cm above lower mat: Interpretated by Quade as "spring orifice sand".]

Table 4: Uranium-series disequilibrium results from Crater Flat Deposit. All uncertainties quoted at the 95% confidence level.

Sample Name	Sample wt. (g)	Concentration U (ppm)	Concentration Th (ppm)	$^{230}Th/^{234}Th$ activity ratio	Detritus-corrected Age (ka) $\pm 2\sigma$	Detritus-corrected Initial Activity Ratio $^{234}U/^{238}U$ $\pm 2\sigma$	Sample Type
HD1606-M1	0.247	1.28	2.04	3.07	104 ± 17	3.8 ± 1.0	Nodular Carbonate; whole rock
HD1606-M2	0.230	1.32	1.92	3.71	113 ± 15	4.0 ± 0.9	" ; -325 mesh
HD1606-M2L	0.154	1.32	1.41	5.00	119 ± 14	3.5 ± 0.5	" ; -325 mesh
HD1606-M3	0.180	1.38	2.47	2.72	108 ± 24	3.8 ± 1.3	" ; -325 to +60 mesh
HD1606-M4	0.224	1.32	1.70	3.76	99 ± 13	3.5 ± 0.6	" ; -60 mesh
HD1607-M1	0.160	1.48	2.66	2.01	53 ± 16	3.7 ± 1.2	Nodular Carbonate; whole rock
HD1607-M2	0.125	1.66	2.30	2.81	62 ± 12	3.6 ± 0.7	" ; -325 mesh
HD1607-M2L	0.130	1.57	1.75	3.59	64 ± 9	3.5 ± 0.5	" ; -325 mesh
HD1607-M3	0.132	1.80	3.02	2.11	55 ± 16	3.5 ± 1.0	" ; -325 to +60 mesh
HD1607-M4	0.161	1.54	2.04	2.78	60 ± 11	3.3 ± 0.6	" ; -60 mesh
HD170-1-D2-A	0.145	1.26	0.435	4.74	21 ± 2	2.9 ± 0.1	Individual Rhizolith
HD170-1-D2-B1	0.070	1.78	0.300	9.01	19.0 ± 1.0	3.03 ± 0.05	"
HD170-1-D2-C1	0.267	1.76	0.177	11.9	15.1 ± 0.6	2.95 ± 0.03	"
HD170-1-E3-A	0.097	2.53	0.306	10.1	15.8 ± 0.8	2.87 ± 0.03	"
HD1733-B	0.162	6.92	0.635	13.9	56 ± 3	1.01 ± 0.03	Individual Rhizolith
HD1734-1A1	0.102	4.39	0.370	9.91	10.3 ± 1.3	2.89 ± 0.03	Individual Rhizolith
HD1734-2A1	0.150	2.64	0.276	9.70	12.8 ± 0.6	2.88 ± 0.03	"
HD1735-A1	0.396	4.20	3.06	2.39	18 ± 5	3.1 ± 0.3	Nodular Carbonate; whole rock

Table 5: Results of radiocarbon dating materials from Crater Flat Deposit paleo discharge site.

Lab ID (Beta-#)	Sample ID	Sample Type	Measured ^{14}C age (RCYBP)	$\delta^{13}C$ (‰)	Conventional ^{14}C age (RCYBP)	Calibrated Age (ka)
Surface exposure, Station 3						
76698	HD170-1 D3	Calcified plant (innermost)	13,020 ± 180	-3.2	13,380 ± 180	16.0 ± 0.27
76699	HD170-1 D3	Calcified plant (outermost)	7,110 ± 120	-1.7	7,490 ± 120	$8.33\ ^{+0.09}/_{-0.16}$
76697	HD170-1 D3&D5	Calcified plant (organic)	5,180 ± 80	-22.3	5,220 ± 80	$6.01\ ^{+0.1}/_{-0.06}$

Dates reported as RCYBP (radiocarbon years before present, where "present" = 1950 A.D.). By international convention, the modern reference standard was 95% of the ^{14}C content of the National Bureau of Standards' Oxalic Acid and calculated using the Libby ^{14}C half life (5,568 years). Quoted errors represent 2 standard deviation statistics (95% probability) and are based on combined measurements of the sample, background, and modern reference standards. Measured $\delta^{13}C$ were calculated relative to PDB-1 international standard and conventional RCYBP ages were normalize to -25 per mil. Calibrated ages were calculated using CALIB (Stuiver and Reimer, 1993) and appropriate data sets.

Table 6: Thermoluminescence results from Crater Flat Deposit (CFD) and west trench. All errors quoted at the 95% confidence limit.

Sample Name	Water Content		Dose Rate (Gy/ka)		Total Bleach	Total Bleach Age (ka)				Partial Bleach	Partial Bleach Age (ka)			
	Field Moist. (%)	Saturation Moist. (%)	Field H20	Saturation H2O	Equivalent Dose (Gy)	field-moist. H2O	½-sat. moist.	sat.-moist. H2O	Total Range	Eqivalent Dose (Gy)	field-moist. H2O	½-sat. moist.	sat.-moist. H2O	Total Range
TL-20	8.2	45	3.0±0.2	2.2±0.2	105±10	34±4	39±5	48±6	30 - 54	140±94	46±31	52±35	64±44	77 - 108
TL-21	3.2	46	3.7±0.3	2.5±0.2	92±6	25±2	30±3	36±4	23 - 40	85±14	23±4	27±5	34±6	19 - 40
TL-22	0.5	20	8.5±1.1	6.8±0.9	17±1.6	2.0±0.[illegible]	2.5±0.4	2.5±0.4	2 - 3	80±11	10±2	12±2	12±2	8 - 14
TL-23	2.8	32	7.6±0.5	5.7±0.4	389±25	51±5	58±6	69±7	46 - 76	472±36	61±6	72±7	83±9	55 - 92

TL-20 [From hand-dug pit into mound of nodular carbonate: 120cm from surface, in clayey, very dense horizon]
TL-21 [From hand-dug pit into mound of nodular carbonate: 10cm from surface, just above reddened, oxidized horizon]
TL-22 [~10 m south of southern end of West Trench: uppermost, sandy Av horizon; atypical of paleodischarge material.]
TL-23 [South wall of West Trench: lower, eolian sandy unit, atypical paleodischarge material.]

Table 7: Uranium-series disequilibrium results from Crater Flat Wash (CFW). All errors quoted at the 95% confidence level.

Sample Name	Sample wt. (g)	Concentration U (ppm)	Concentration Th (ppm)	$^{230}Th/^{232}Th$ activity ratio	Detritus-corrected Age (ka) ± 2σ	Detritus-corrected Initial Activity Ratio $^{234}U/^{238}U$ ± 2σ	Sample Type
HD1750-1A	0.398	3.01	0.403	16.0	19.9 ± 0.6	4.24 ± 0.06	Individual Rhizolith
HD1750-1B	0.248	10.4	0.243	69.2	15.2 ± 0.2	4.15 ± 0.02	Individual Rhizolith

Table 8: Uranium-series disequilibrium results from Stateline Deposits (SLD). All errors quoted at the 95% confidence limit.

Sample Name	Sample wt. (g)	Concentration U (ppm)	Concentration Th (ppm)	$^{230}Th/^{232}Th$ activity ratio	Detritus-corrected Age (ka) ± 2σ	Detritus-corrected Initial Activity Ratio $^{234}U/^{238}U$ ± 2σ	Sample Type
HD1706-A1	0.197	1.53	2.34	6.60	Excess 230Th	Undefined	Greyish-white nodular carbonate
HD1708-A1	0.238	0.286	0.569	3.61	Excess 230Th	Undefined	Dense sandy limestone
HD1709-A2	0.132	1.16	1.47	39.7	Excess 230Th	Undefined	Nodular Carbonate
HD1711-A1	0.216	3.08	0.606	16.4	49.2 ± 1.4	3.09 ± 0.06	Hard, vuggy biogenic limestone
HD1711-A2	0.050	24.10	0.0991	634	37.8 ± 0.3	3.030 ± 0.013	Late opal in biogenic limestone
HD1716-A1	0.154	0.695	1.44	2.09	71 ± 20	4.3 ± 1.9	Dense, greyish-white limestone
HD1737-A1	0.428	9.65	0.359	140	105 ± 6	3.11 ± 0.09	Individual plant petrifaction
HD1737-B	0.154	12.29	0.134	473	104 ± 5	3.07 ± 0.09	Individual plant petrifaction
HD1737-E	0.434	10.51	0.0588	878	96.9 ± 1.0	3.025 ± 0.014	Individual plant petrifaction
HD1738-U1	0.697	3.66	1.55	2.80	11 ± 2	3.3 ± 0.2	Planorbid snail shell
HD1854-1A	0.199	4.58	2.84	3.98	32 ± 4	3.1 ± 0.2	Insect burrow cast

Table 9: Thermoluminescence results from State Line Deposit (SLD)
All errors quoted at the 95% confidence limit.

Sample Name	Water Content		Dose Rate (Gy/ka)		Total Bleach Equivalent Dose (Gy)	Total Bleach Age (ka)				Partial Bleach Eqivalent Dose (Gy)	Partial Bleach Age (ka)			
	Field Moist. (%)	Saturation Moist. (%)	Field H20	Saturation H2O		field-moist. H2O	½-sat. moist.	sat.-moist. H2O	Total Range		field-moist. H2O	½-sat. moist.	sat.-moist. H2O	Total Range
TL-44	2.8	61	9.8±0.6	5.7±0.4	690±120	70±13	94±18	120±23	57 - 143	900±180	92±19	123±26	158±33	73 - 191
TL-45	3.4	58	11.3±0.8	6.7±0.5	224±14	20±2	26±3	33±3	18 - 36	250±13	22±2	30±3	37±3	20 - 41
TL-46	22	45	5.4±0.5	4.4±0.5	65±3	12±1.4		15±2	11 - 17	59±8	11±2		13±2	9 - 15

TL-44 [Carbonate-capped, high terrace just north of Franklin Wells: Arroyo cut exposure which emanate from the toe of the Fortymile Wash alluvial fan, lowest green silt.]
TL-45 [Carbonate-capped, high terrace just north of Franklin Wells: Arroyo cut exposure which emanate from the toe of the Fortymile Wash alluvial fan, silt unit 2m up TL-44.]
TL-46 [Franklin Well, low terrace, Quade's Cycle E: brown, silty deposits associated with 9-11ka snails.]

Table 10: Results of radiocarbon dating materials from State Line Deposit paleo discharge site.

Lab ID (Beta-#)	Sample ID	Sample Type	Measured ^{14}C age (RCYBP)	$\delta^{13}C$ (‰)	Conventional ^{14}C age (RCYBP)	Calibrated Age (ka)
Surface exposure, Station 3						
80361	HD1738 S1-5	Terrestrial snail (Succnid)		-5.9	8100 ± 140	9.02 ± 0.26
80362	HD1738 S6-13	Terrestrial snail (Succnid)		-7	8220 ± 120	$9.24\ ^{+0.17}/_{-0.22}$
80363	HD1738 P1-5	Aquatic snail (Planorbid)		-10.6	9600 ± 120	$10.8\ ^{+0.2}/_{-0.3}$

Dates reported as RCYBP (radiocarbon years before present, where "present" = 1950 A.D.). By international convention, the modern reference standard was 95% of the ^{14}C content of the National Bureau of Standards' Oxalic Acid and calculated using the Libby ^{14}C half life (5,568 years). Quoted errors represent 2 standard deviation statistics (95% probability) and are based on combined measurements of the sample, background, and modern reference standards. Measured $\delta^{13}C$ were calculated relative to PDB-1 international standard and conventional RCYBP ages were normalize to -25 per mil. Calibrated ages were calculated using CALIB (Stuiver and Reimer, 1993) and appropriate data sets.

Table 11: Uranium-series disequlibrium results from Indian Pass Deposits. All errors quoted at the 95% confidence level.

Sample Name	Sample wt. (g)	Concentration U (ppm)	Concentration Th (ppm)	$^{230}Th/^{232}Th$ activity ratio	Detritus-corrected Age (ka) $\pm 2\sigma$	Detritus-corrected Initial Activity Ratio $^{234}U/^{238}U \pm 2\sigma$	Sample Type
HD1981-U2	0.034	5.02	4.24	2.82	28 ±6	3.3 ±0.3	Nodular Carbonate
HD1982-U1	0.046	4.41	4.43	2.39	27 ±7	3.4 ±0.4	Nodular Carbonate
HD1983-U1	0.187	10.5	0.285	32.7	10.9 ±0.2	3.03 ±0.02	*Individual Rhizolith*
HD1983-U2	0.112	6.50	0.556	19.0	20.8 ±1.0	3.08 ±0.03	"
HD1984-U1	0.155	12.1	0.303	49.7	15.9 ±0.3	3.04 ±0.02	Individual Rhizolith
HD1985-U1	0.051	4.30	2.64	2.29	14 ±4	3.1 ±0.2	Nodular Carbonate

Table 12: Thermoluminescence results from Indian Pass Deposit (IPD)
All errors quoted at the 95% confidence limit.

Sample Name	Water Content		Dose Rate (Gy/ka)		Total Bleach Equivalent Dose (Gy)	Total Bleach Age (ka)				Partial Bleach Eqivalent Dose (Gy)	Partial Bleach Age (ka)			
	Field Moist. (%)	Saturation Moist. (%)	Field H20	Saturation H2O		field-moist. H2O	½-sat. moist.	sat.-moist. H2O	Total Range		field-moist. H2O	½-sat. moist.	sat.-moist. H2O	Total Range
TL-70	4.4	49	9.4±0.5	6.1±0.4	306±10	33±2	41±3	50±3	31 - 53					
TL-71	1.5	53	7.5±0.5	4.7±0.3	109±4	14±1.	19±1.4	23±2	13 - 25					

TL-70 [Section from north face of natural exposure, at base: Silty green marl horizon.]
TL-71 [Approximately 170cm above base of natural exposure: Green silty/clayey loam containing fragile rhizoliths.]

Table 13: $\delta^{13}C$ and $\delta^{18}O$ values for calcite from discharge deposit samples. Values in ‰.

Site[1]	HD#[2]	Field Sample #	$\delta^{13}C$	$\delta^{18}O$	Comments
CFW	HD1751a	RCD1-021895-JW	2.5	33.5	secondary calcite
CFW	HD1751b	RCD1-021895-JW	2.4	34.6	secondary calcite
CFW	HD1752a	RCD1-021895-JW	-2.9	23.3	whole rock calcite
CFW	HD1994a	092895-RCD-1B	2.3	38.5	whole rock calcite
CFW	HD1996a	092895-RCD-3	-1.2	24.1	whole rock calcite
CFD	HD1457sa	CFD-P1-01	-2.8	18.4	nodular carbonate
CFD	HD1458sa	CFD-P1-02	-3	18.2	nodular carbonate
CFD	HD1459sa	CFD-P1-03	-2.6	18.9	white soft core
CFD	HD1459sb	CFD-P1-03	-3.9	18.5	dese tan core
CFD	HD1460sa	CFD-P1-04	-2.4	18.9	nodular carbonate
CFD	HD1460sb	CFD-P1-04	-2.5	19.8	nodular carbonate
CFD	HD1461sa	CFD-P1-05	-2.0	18.7	late calcite
CFD	HD1461sb	CFD-P1-05	-2.0	19.2	nodular carbonate
CFD	HD1461sc	CFD-P1-05	-2.1	19.0	nodular carbonate
CFD	HD1462sa	CFD-P1-06	-1.9	20.0	bar calcite
CFD	HD1462sb	CFD-P1-06	-1.9	20.9	bar calcite
CFD	HD1463sa	CFD-ET-01	-2.5	18.8	whole rock cement
CFD	HD1606sa	063094-JP1	-2.8	18.4	late sparry calcite
CFD	HD1606sb	063094-JP1	-2.6	18.4	whole rock calcite
CFD	HD1606sc	063094-JP1	-2.7	18.3	whole rock calcite
CFD	HD1607sa	063094-JP2	-3.6	18.3	late sparry calcite
CFD	HD1607sb	063094-JP2	-3.6	18.3	late sparry calcite
CFD	HD1607sc	063094-JP2	-3.0	18.2	whole rock calcite
CFD	HD1607sd	063094-JP2	-2.8	18.4	whole rock calcite
CFD	HD164-2		-2.9	19.0	whole rock cement
CFD	HD164-2a		-2.9	18.8	whole rock cement
CFD	HD166-1		-1.4	20.5	calcite-cemented whole rock
CFD	HD166-3a		-1.0	20.4	calcite-cemented whole rock
CFD	HD167a		-2.2	20.2	dense calcite limestone
CFD	HD168-1a		-1.6	21.6	whole rock cement
CFD	HD169-1		-1.1	21.4	popcorn nodule calcite
CFD	HD169-1a		-1.1	21.4	popcorn nodule calcite
CFD	HD1700a		-3.9	18.8	root/stem cast whole rock
CFD	HD1700b		-3.9	22.5	root/stem cast whole rock
CFD	HD1703a		0.9	22.3	insect burrow cast whole rock
CFD	HD1703b		1.1	22.5	insect burrow cast whole rock
CFD	HD1704a		-2.3	19.5	whole rock
CFD	HD1989c	092895-CFD-4	-2.2	18.9	nodular carbonate
Devils Hole		dh-103	-1.9	14.0	mamillary travertine
Devils Hole		dh-180	-2.2	14.0	mamillary travertine
Devils Hole		dh-300	-2.2	14.9	mamillary travertine
Grapevine Spring	HD505-2		0.4	14.8	travertine vein
Grapevine Spring	HD505-3		0.2	13.8	travertine vein
Grapevine Spring	HD505-4		-0.1	14.1	travertine vein
Grapevine Spring	HD505-5		0.0	14.1	travertine vein
Grapevine Spring	HD506-1		-0.3	16.0	travertine vein
Grapevine Spring	HD506-2		-0.7	16.1	travertine vein
Grapevine Spring	HD507-1-A		-0.2	17.2	travertine vein
Grapevine Spring	HD507-1-B		-0.6	17.2	travertine vein
Grapevine Spring	HD507-2-C		0.0	16.6	travertine vein
Grapevine Spring	HD507-3-D		0.7	16.9	travertine vein
Grapevine Spring	HD507-3E		0.1	14.7	travertine vein

Site	HD#	Field Sample #	$\delta^{13}C$	$\delta^{18}O$	Comments
Grapevine Spring	HD507-4-F		-0.7	15.6	travertine vein
Grapevine Spring	HD507-4-G		-0.2	14.3	travertine vein
Grapevine Spring	HD508-1		0.0	14.1	travertine vein
Grapevine Spring	HD508-2		-0.1	15.8	travertine vein
Grapevine Spring	HD510-1		-0.8	17.6	travertine vein
Grapevine Spring	HD510-2		-4.6	19.0	travertine vein
Grapevine Spring	HD510-3		-3.6	18.4	travertine vein
Grapevine Spring	HD510-4		-3.5	18.7	travertine vein
Grapevine Spring	HD510-5		-4.5	17.9	travertine vein
Grapevine Spring	HD511		-0.5	18.8	tufa
Grapevine Spring	HD511-A		-0.7	18.7	tufa
IDP	HD1981a	092795-IPD-1	-3.4	19.0	nodular carbonate
IDP	HD1982a	092795-IPD-2	-1.9	18.9	nodular carbonate
IDP	HD1982b	092795-IPD-2	-1.8	18.9	nodular carbonate
IDP	HD1982c	092795-IPD-2	-1.8	18.8	nodular carbonate
IDP	HD1985a	092795-IPD-5	-4.2	20.7	nodular carbonate
IDP	HD1985b	092795-IPD-5	-4.5	20.7	nodular carbonate
IDP	HD1985c	092795-IPD-5	-4.8	20.6	nodular carbonate
LWD	HD1856a	HT-2-050195	-0.9	23.8	calcrete
LWD	HD1856b	HT-2-050195-JW	-0.6	24.9	whole rock calcite cement
LWD	HD1857a	HT-3-050195	-0.5	26.4	calcareous soil, 15cm below ledge
LWD	HD1857b	HT-3-050195-JW	-0.8	24.8	whole rock calcite cement
LWD	HD1858a	HT-4-050195	-1.4	24.2	calcareous soil, 5cm below ledge
LWD	HD1858b	HT-4-050195-JW	-2.0	22.2	whole rock calcite cement
LWD	HD1859a	HT-5-050195	-1.5	21.2	calcareous soil, bottom of ledge
LWD	HD1860a	HT-6-050195	-1.8	20.4	calcareous soil, top of ledge
LWD	HD1860b	HT-6-050195-JW	-3.0	19.9	whole rock calcite cement
LWD	HD1861a	HT-7-050195	-2.7	20.0	bleached-zone calcrete
LWD	HD1861b	HT-7-050195	-3.0	19.1	tan-zone calcrete
LWD	HD1863a	HT-9-050195	-1.8	18.5	bleached-zone calcrete
LWD	HD1863b	HT-9-050195	-1.7	19.4	tan calcrete
LWD	HD1969a	092695-HTD-1A	-6.0	20.0	calcified wood
LWD	HD1969Aa	092695-HTD-1	-5.5	21.4	calcified wood
LWD	HD1969Ba	092695-HTD-1	-3.0	24.8	opaline calcite
LWD	HD1969Bb	092695-HTD-1	-1.9	27.0	whole rock calcite
LWD	HD1969Ca	092695-HTD-1	-8.5	19.8	aquatic snail (planorbid)
LWD	HD1969Cb	092695-HTD-1	-2.7	25.2	whole rock calcite
LWD	HD1972a	092695-HTD-4	-2.7	19.1	whole rock calcite
LWD	HD1972b	092695-HTD-4	-2.7	18.7	whole rock calcite
LWD	HD1973a	092695-HTD-5	-0.8	18.4	dense, tan whole rock
LWD	HD1973b	092695-HTD-5	-0.7	18.8	soft, white whole rock
LWD	HD1974a	092695-HTD-6	-0.9	19.1	whole rock calcite
LWD	HD1976a	092695-HTD-8	-1.6	18.4	dense, whole rock (upper)
LWD	HD1976b	092695-HTD-8	-1.7	18.2	dense, whole rock (middle)
LWD	HD1976c	092695-HTD-8	-1.7	18.3	dense, whole rock (lower)
LWD	HD1978a	092695-HTD-10	-0.5	18.5	dense, interior calcite
LWD	HD1978b	092695-HTD-10	-0.3	18.0	white rim calcite
LWD	HD1978c	092695-HTD-10	-0.8	18.7	dense buff calcite
LWD	HD1980a	092695-HTD-12	-1.5	18.8	nodular carbonate
LWD	HD1980b	092695-HTD-12	-1.5	18.9	nodular carbonate
LWD	HD1980c	092695-HTD-12	-1.4	18.7	nodular carbonate
LWD	HD1999Aa	HT1-950925-JW	1.1	19.0	whole rock calcite
LWD	HD1999Ba	HT1-950925-JW	0.9	17.2	brown calcite, whole rock
LWD	HD1999Bb	HT1-950925-JW	0.8	19.2	white calcite, whole rock

Site[1]	HD#[2]	Field Sample #	$\delta^{13}C$	$\delta^{18}O$	Comments
LWD	HD1999Bc	HT1-950925-JW	0.1	23.6	laminated calcite
LWD	HD1999Ca	HT1-950925-JW	1.0	19.5	whole rock calcite
LWD	HD2000a	HT2-950925-JW	2.3	26.5	late calcite infilling
LWD	HD2000b	HT2-950925-JW	0.7	24.1	channelled calcite
LWD	HD2000c	HT2-950925-JW	0.7	22.1	dense brown calcite
LWD		LWD-12	-9.5	20.1	terrestrial mollusc (Vertigo)
LWD		LWD-12	-7.6	21.5	terrestrial mollusc (Vertigo)
LWD		LWD-12	-6.3	19.5	aquatic mollusc (Pisidium)
LWD		LWD-12	-7.8	19.1	aquatic mollusc (Pisidium)
LWD		LWD-13	-8.8	24.7	aquatic mollusc (Hydrobiid)
LWD		LWD-13	-8.6	20.4	terrestrial mollusc (Vertigo)
LWD		LWD-7	-8.7	21.0	terrestrial mollusc (Pupillid) (upper)
LWD		LWD-7	-9.5	23.8	terrestrial mollusc (Pupillid) (lower)
LWD		LWD-7	-8.1	19.2	aquatic mollusc (Pisidium) (upper)
LWD		LWD-7	-8.0	19.3	aquatic mollusc (Pisidium) (lower)
LWD		LWD-8	-7.1	22.1	terrestrial mollusc (Pupillid)
LWD		LWD-8	-7.8	21.7	terrestrial mollusc (Pupillid)
LWD		LWD-8	-6.1	18.8	aquatic mollusc (Pisidium)
LWD		LWD-10a	-6.9	19.5	aquatic mollusc (Pisidium) (opaque)
LWD		LWD-10a	-6.3	19.9	aquatic mollusc (Pisidium) (opaque)
LWD		LWD-10b	-5.4	20.1	aquatic mollusc (Pisidium) (clear)
LWD		LWD-10b	-7.9	26.8	aquatic mollusc (Pisidium) (clear)
LWD		LWD-10	-9.0	24.8	terrestrial mollusc (Vertigo)
Nevares Spring	HD1322sa	060393-JP1	-2.4	15.0	lattice work
Nevares Spring	HD1322sb	060393-JP1	-2.5	14.7	brown clasts
Nevares Spring	HD1322sc	060393-JP1	-2.5	15.2	dence calcite
Nevares Spring	HD495-A		-2.5	15.4	1.5 m above stream
Nevares Spring	HD496-A		-2.4	15.7	3 m above stream
Nevares Spring	HD499-A		-1.5	17.7	7 m above stream
Nevares Spring	HD500-A		-1.3	18.9	8.5 m above stream
Nevares Spring	HD501-A		-1.6	17.1	drapestone
Nevares Spring	HD502-A		-2.0	15.9	10.5 m above stream
Nevares Spring	HD503-A		-1.4	15.4	massive clean carbonate
Rock Valley Mound	HD1117sa		-1.8	21.2	late sparry calcite - travertine
Rock Valley Mound	HD1117sb		0.0	22.6	buff calcite - travertine
Rock Valley Mound	HD1118sa		-2.5	17.6	travertine
Rock Valley Mound	HD1118sc		-3.6	17.5	light band - tufa
Rock Valley Mound	HD1118sd		-4.7	18.1	late white calcite - tufa
Rock Valley Mound	HD1319sa	060293-JP1	0.7	20.6	non-fluorescing bedded limestone
Rock Valley Mound	HD1319sb	060293-JP1	0.7	18.4	bedded limestone
Rock Valley Mound	HD1321sa	060293-JP3	0.4	22.9	late white calcite - tufa
Rock Valley Mound	HD1321sb	060293-JP3	0.5	22.5	brown calcite infilling - tufa
Rock Valley Mound	HD1321sc	060293-JP3	-0.6	20.7	dense buff calcite - tufa
Rock Valley Mound	HD1746Aa		0.2	21.6	youngest calcite - tufa
Rock Valley Mound	HD1746Ac		0.3	22.5	sucrosic calcite - tufa
Rock Valley Mound	HD1746Ba		-0.3	21.4	buff calcite matrix - tufa
Rock Valley Mound	HD1746Bb		-0.1	22.1	white calcite druse - tufa
SLD	HD1747a		-1.8	21.9	calcite-cemented silty whole rock
SLD	HD1749a		-1.3	19.2	popcorn lag nodules
SLD	HD1685a	AV94-1	-5.5	19.0	whole rock
SLD	HD1686a	AV94-2	-3.5	18.6	whole rock
SLD	HD1687a	AV94-3	-3.5	19.7	whole rock
SLD	HD1688a	AV94-4	-2.8	19.7	whole rock
SLD	HD1688b	AV94-4	-3.4	20.3	brown calcite clasts

Site[1]	HD#[2]	Field Sample #	$\delta^{13}C$	$\delta^{18}O$	Comments
SLD	HD1689a	AV94-5	-2.4	20.4	whole rock white
SLD	HD1689b	AV94-5	-3.6	19.3	whole rock gray
SLD	HD1690	AV94-6	-4.4	18.9	sparry calcite fill
SLD	HD1690b	AV94-6	-2.1	21.0	late laminated fill
SLD	HD1690c	AV94-6	-3.3	19.4	older matrix
SLD	HD1690d	AV94-6	-4.0	19.6	younger matrix
SLD	HD1691a	AV94-7	-3.8	19.4	sparry calcite
SLD	HD1691b	AV94-7	-4.1	19.0	stalactites
SLD	HD1691c	AV94-7	-3.4	19.3	older matrix
SLD	HD1691d	AV94-7	-3.3	19.7	younger matrix whole rock
SLD	HD1708a	110394-FRANK-3	-1.7	19.2	white band calcite
SLD	HD1708b	110394-FRANK-3	-1.8	19.7	whole rock
Travertine Point	HD483-1-A		0.1	15.0	tufa
Travertine Point	HD483-A		0.1	15.7	tufa
Travertine Point	HD484-A		0.4	16.6	tufa
Travertine Point	HD485-A		1.2	15.4	travertine vein

[1] CFW = Crater Flat Wash; CFD = Crater Flat Deposit; LWD Lathrop Wells Diatomite; SLD = State Line Deposit

[2] Hydrogenic Deposits program sample tracking number

Table 14: Characteristic isotopic compositions of paleodischarge deposits, waters and rocks representing possible source materials.

Material	Initial $^{234}U/^{238}U_{activity}$	$\delta^{87}Sr$ (‰)	$\delta^{13}C$ (‰)
Paleodischarge deposits			
inorganic carbonate	2.9 to 4.5	5.0 to 13	-4 to +1
plant/mollusc	"	"	-10 to -5
Aquifers			
Paleozoic	2.5 to 4	3 to >10	-4 to -2 (HCO3-)*
Volcanic/alluvium	3 to 8	1 to 4 (no Precambrian) 7 to >15 (w/ Precambrian)	-13 to -7 (HCO_3^-)*
Perched waters at YM	3 to 7	3.5 to 4.5	-11 to -9 (HCO_3^-)*
Surface Waters at YM	1.4 to 1.8	1.8 to 3.8	
Rocks			
Marine carbonate	~1.0	-2 to +3**	-2 to +2
Calcrete	1.3 to 1.8	3.3 to 5.0	-10 to -5
Volcanics	~1.0	-1.3 to 15	negligible contribution
Precambrian siliciclastics	~1.0	10 to >30	negligible contribution

* At near-surface temperatures, the equilibrium d13C difference between dissolved HCO3- and calcite is ~2‰.

** In areas of Paleozoic limestone that have been hydrothermally-altered, such as Bare Mountain, $\delta^{87}Sr$ values have been elevated to values from +23 to +30 through addition of radiogenic Sr derived from the Precambrian basement (Peterman et al., 1994).

Table 15: Matrix of possible hydrogenic sources and their compatibility with observed data from paleodischarge sites.

Hydrogenic Source	Initial $^{234}U/^{238}U_{activity}$	$\delta^{87}Sr$ (‰)	$\delta^{13}C$ (‰)	Diatoms
Paleozoic Aquifer	possible	possible	possible	unlikely
Volcanic/Alluvial Aquifer	possible	possible	possible	probable
Perched Aquifer	unlikely	NO	NO	NO
Surface Runoff	NO	NO	NO	NO

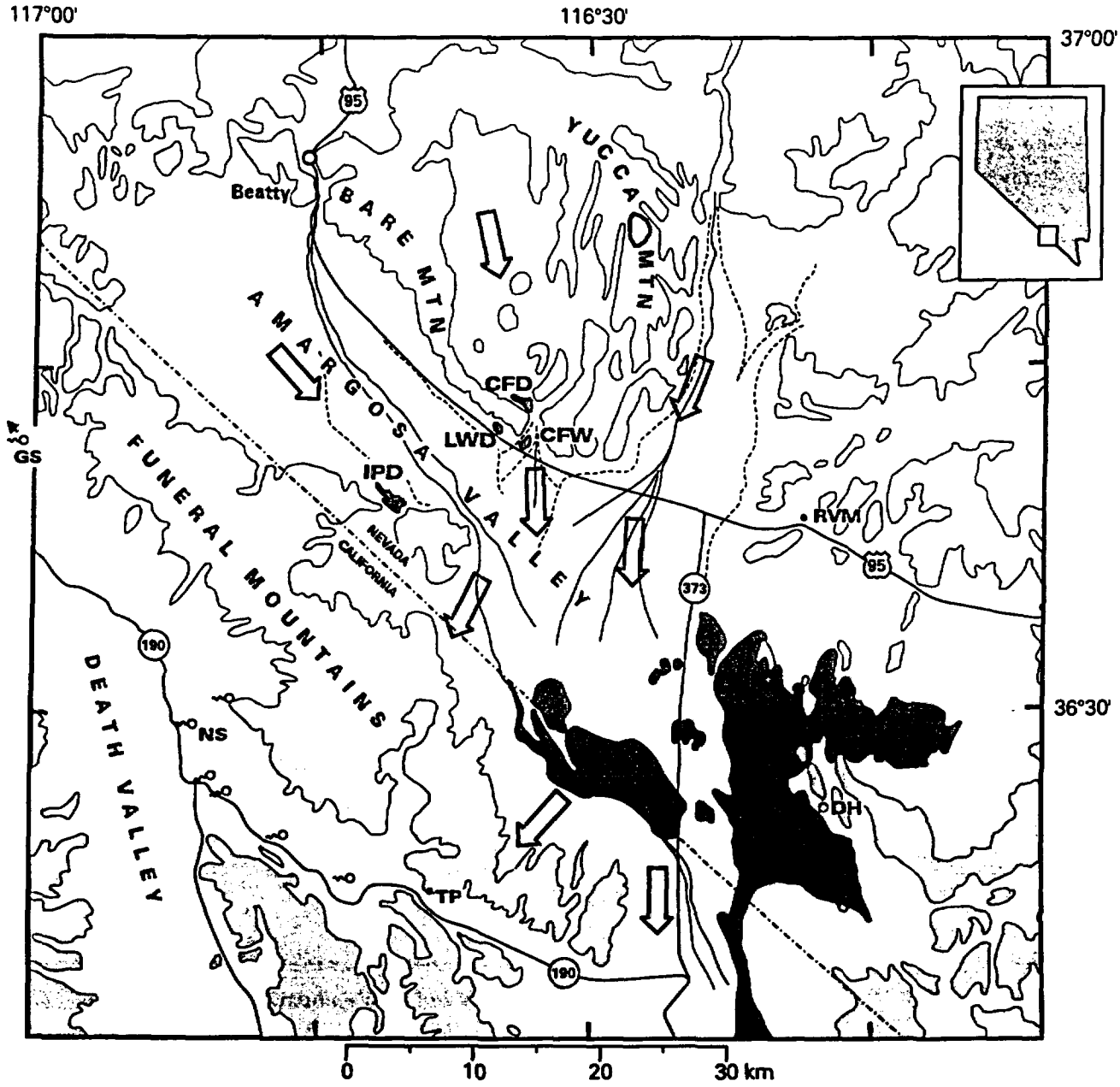

Figure 1: Location map showing paleodischarge deposits (dark-shaded patches with CFD = Crater Flat Deposits; CFW = Crater Flat Wash; LWD = Lathrop Wells Diatomite; IPD = Indian Pass Deposits; SLD = State Line Deposits). Other sites described in text are Rock Valley mound (RVM), Devils Hole (DH), Travertine Point (TP), Nevares Spring (NS), and Grapevine Spring (GS, off map to northwest). Active springs at Ash Meadows and Death Valley are shown with spring symbols. Outlined arrows show generallized ground-water flow paths. Light-shaded polygons represent bedrock highs; intervening unpatterned areas represent alluvial-filled basins. Solid and dashed lines in basins represent fluvial channels and fan boundaries, respectively.

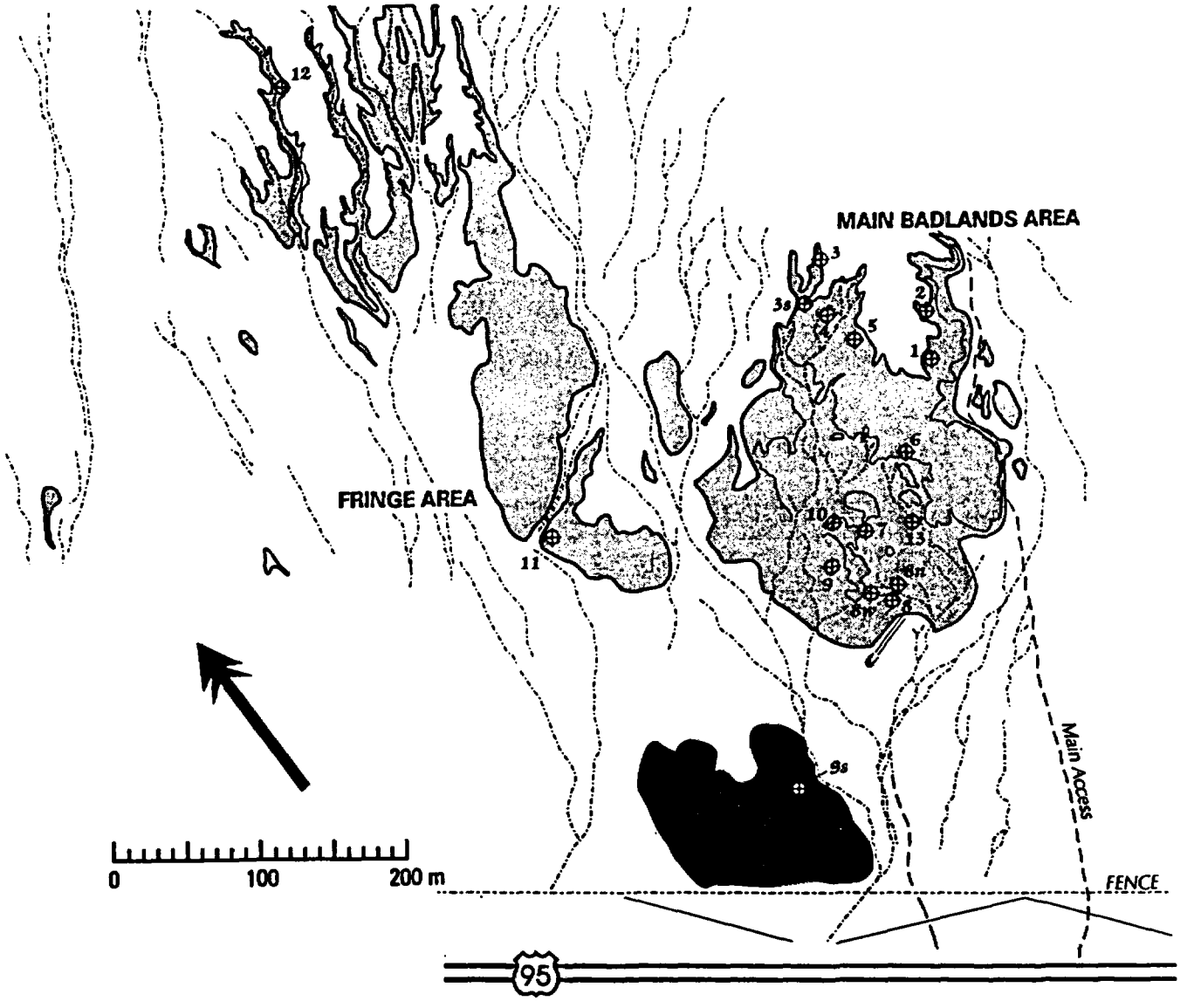

Figure 2: Sketch of air photos showing major morphologic features of the Lathrop Wells Diatomite deposit. Light-colored, fine-grained deposits are shown as light-shaded areas. Area with platy veneer of banded dense limestone shown with darker-shading. Numbered stations are shown with circle/cross symbol. Dash-dot lines represent drainage channels. Light-solid lines within boundary of the main badlands area represent prominent cliffs separating topographically high areas (mostly north half) from low areas (mostly south half).

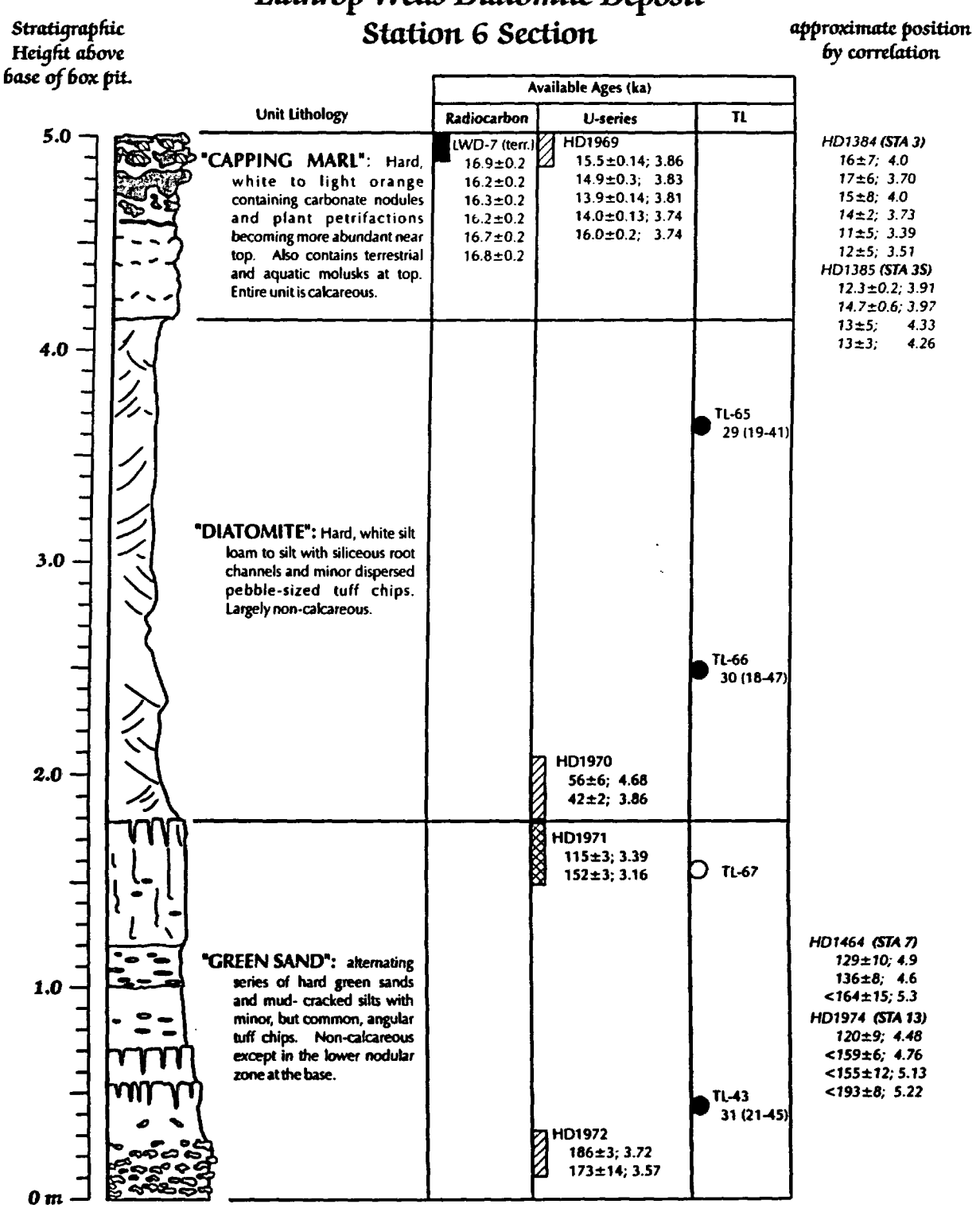

Figure 3: Measured stratigraphic section at LWD Station 6 with age determinations reported in Tables 1, 2 and 3. All uncertanties quoted at the 95% confidence level. Numbers following U-series dates are calculated initial 234U/238U ratios. TL ages are given for dose rates calculated at half-saturation moisture contents followed parenthetically by the total range of ages calculated using moisture contents and analytical uncertainties. U-series dates to the right of the column are correlated by position within the general

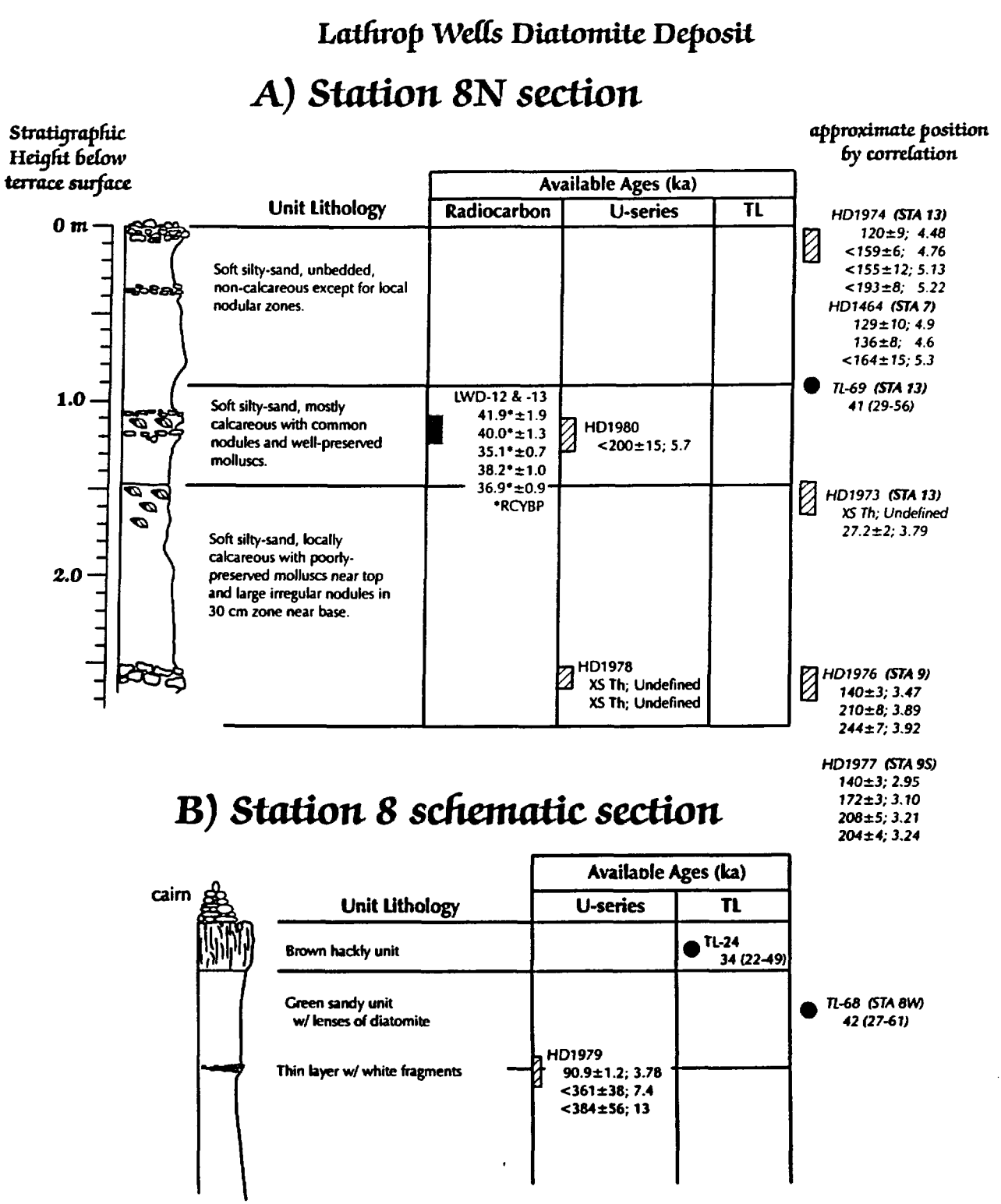

Figure 4: Stratigraphic sections at LWD stations 8N and 8 with age determinations reported in Tables 1, 2 and 3. All uncertainties quoted at the 95% confidence level. Radiocarbon ages are given in radiocarbon years before present (RCYBP) and have not been calibrated for the effects of non-linear radiocarbon production rates. Details for reported U-series and TL ages are the same as those described for Figure 3. A) Measured stratigraphic section at station 8N. B) Schematic section from pit at station 8.

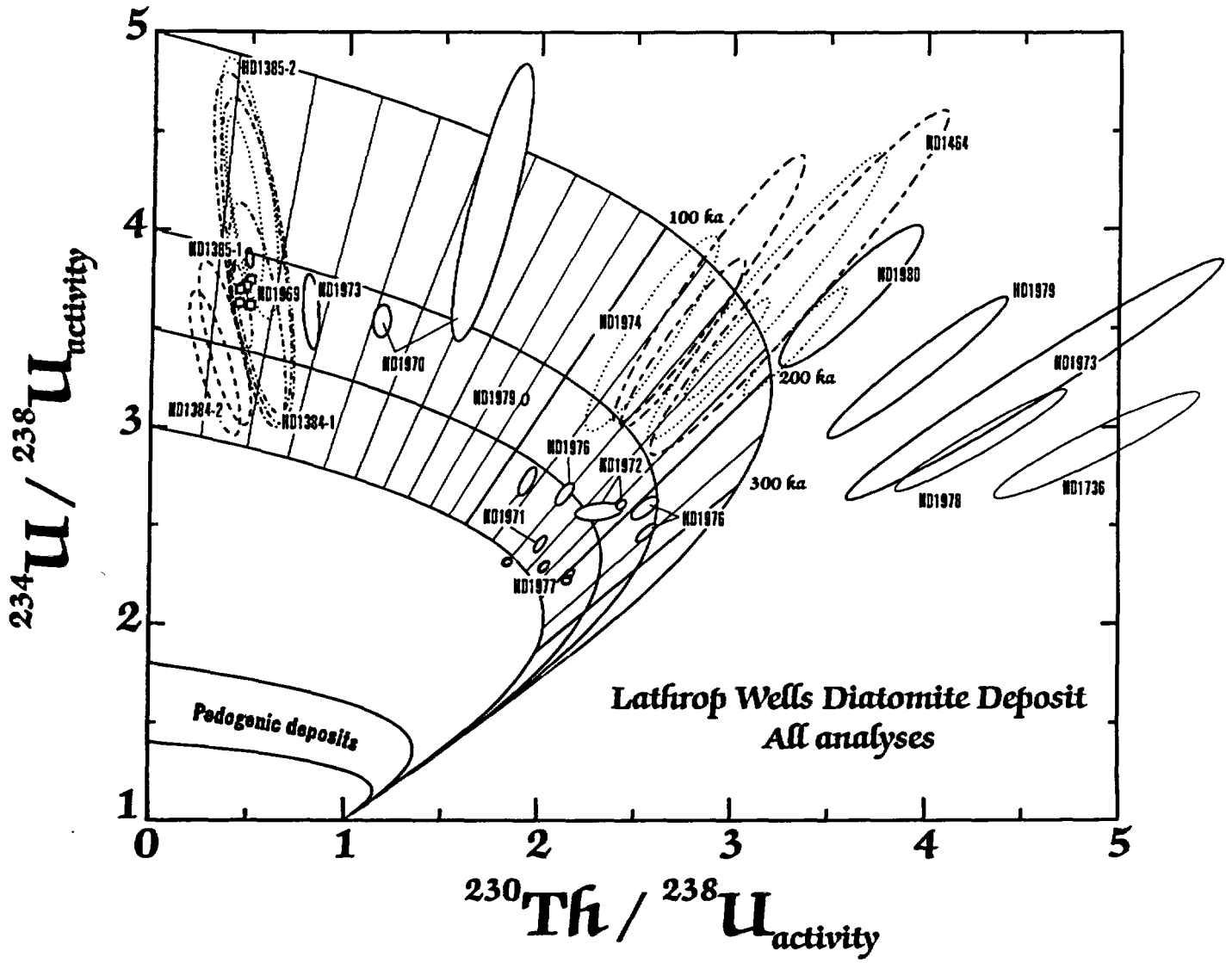

Figure 5: U-series evolution diagram showing U and Th isotopic data for all analyses from LWD. Curved lines leading from different 234U/238U values on the Y-axis to secular equilibrium values of 230Th/238U on the X-axis represent the foci of isotopic compositions during closed-system, temporal evolution of different materials with different initial uranium isotopic ratios (evolution lines). Straight, sub-parallel lines represent isochrons drawn at 10 ka intervals between 0 and 100 ka, 20 ka intervals between 100 and 200 ka, and 50 ka intervals between 200 and 300 ka. 95% confidence Error ellipses represent measured isotopic ratios corrected for detrital-Th components (see text and Appendix 2 for explanation). Samples represented by square boxes have error ellipses smaller than box dimensions.

Concordia-LWD-all.cdr (Aug96)

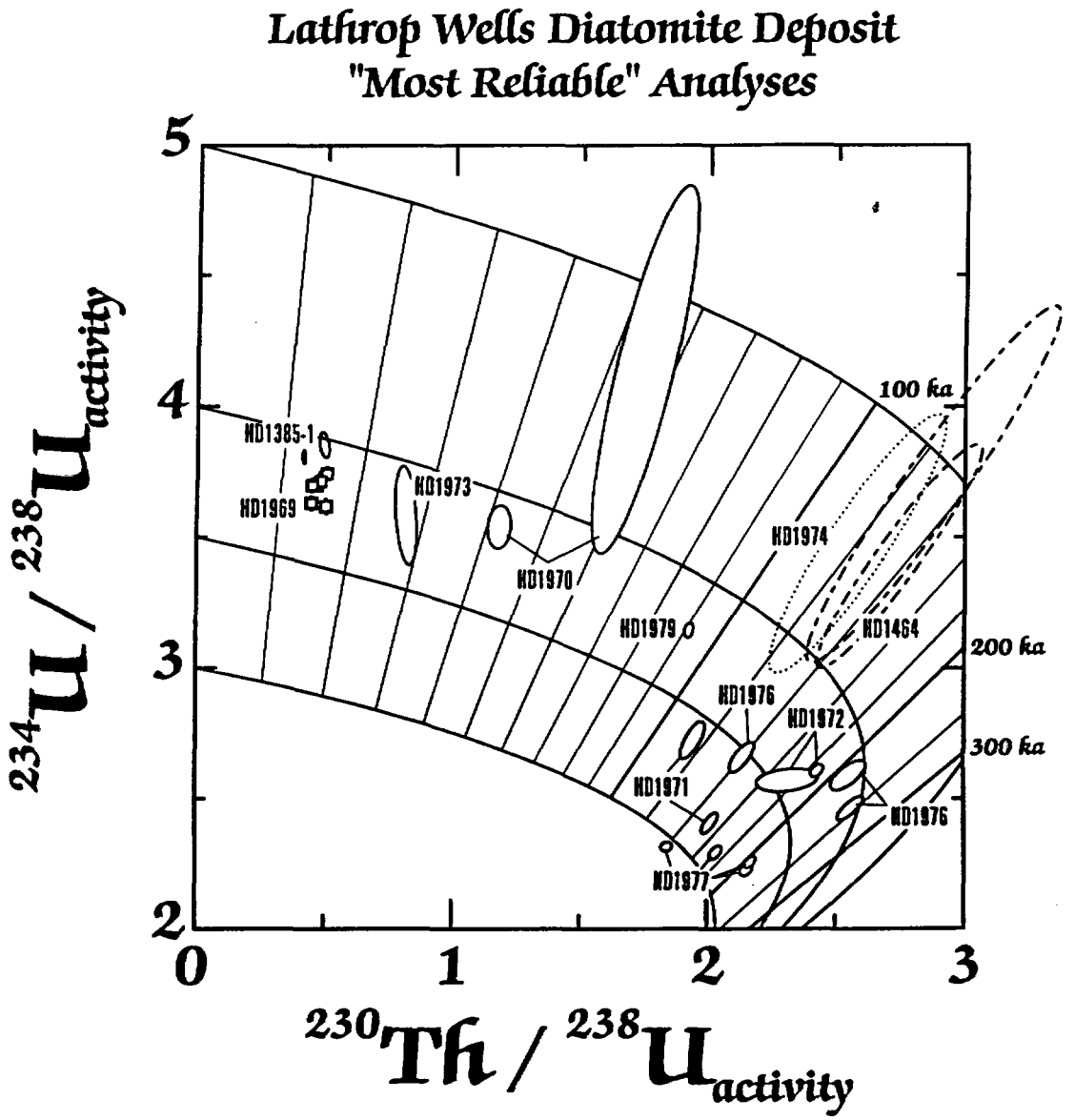

Figure 6: U-series evolution diagram showing U and Th isotopic results for LWD data having the least amount of analytical uncertainty due to detrital-Th corrections (i.e., lowest 232Th contents). Diagram is described in Figure 5.

Concordia-LWD-best.cdr (Aug96)

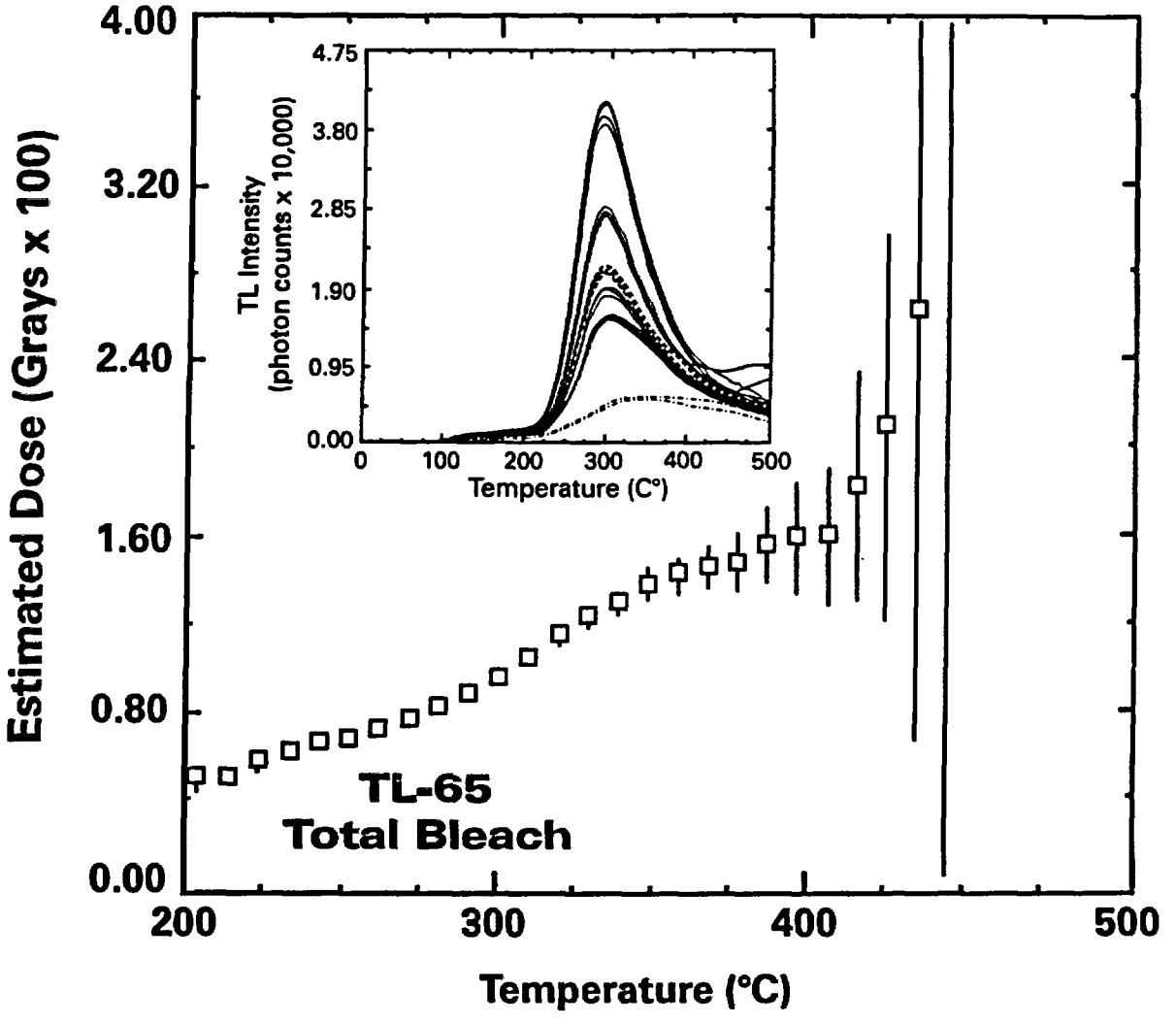

Figure 7: Estimated dose (D_ε) versus temperature plot for sample TL-65 from LWD. A weighted saturating-exponential regression model was used to calculate D_ε from luminescence data obtained on a suite of variably-irradiated discs at each tempe rature interval. The flat part of the D_ε spectrum is called the "plateau" and indicates the temperature region that yields the most stable TL response. Inset shows the natural and artificial glow curves. Data obtained using the total bleach method (see Appendix 2 for further details).

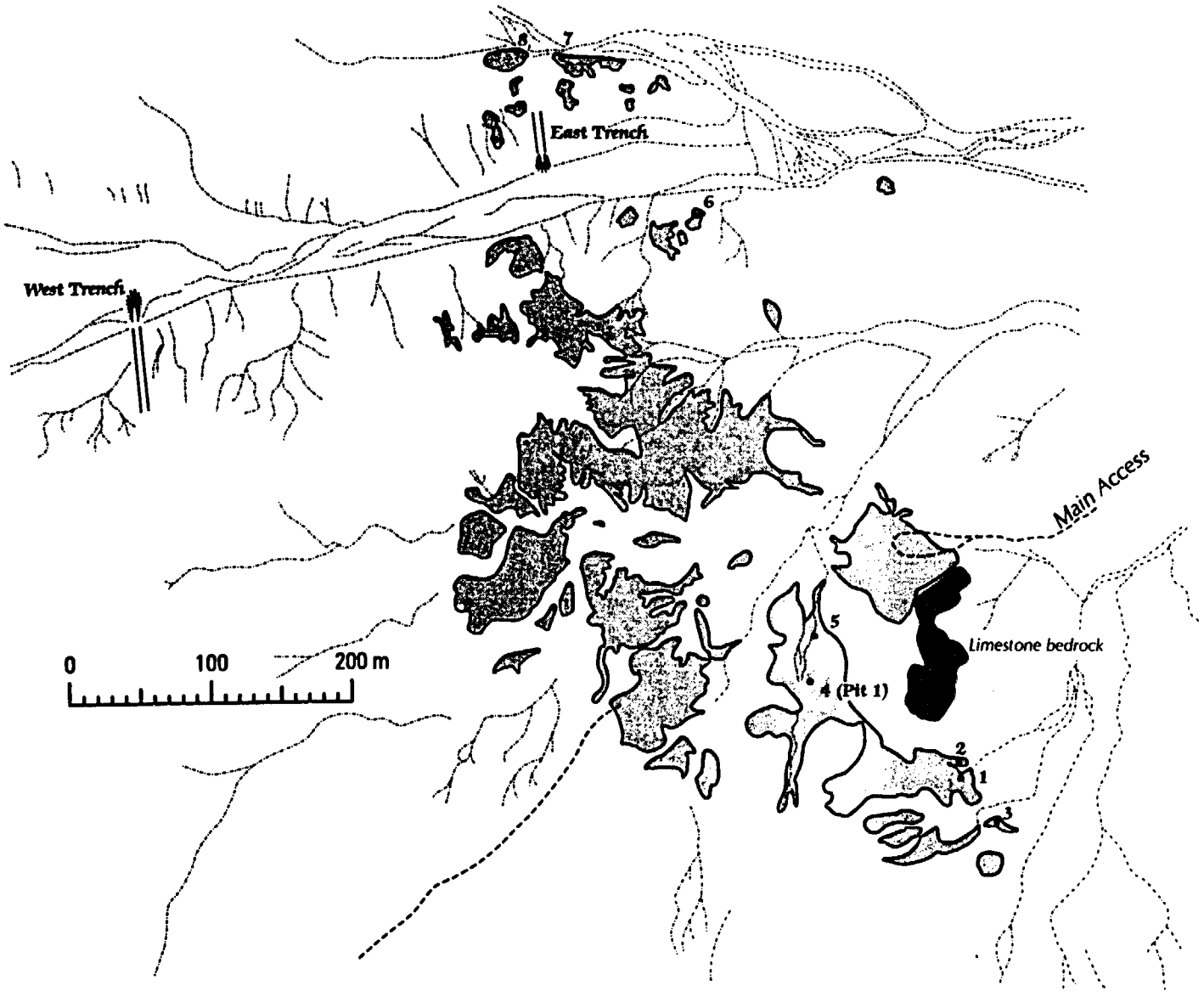

Figure 8: Sketch of air photos showing major morphologic features of the Crater Flat Deposit (CFD). Light-colored, fine-grained deposits are shown as light-shaded areas. Numbered sample stations are shown with small black circles. Dash-dot lines represent drainage channels. North is towards the top of the sketch.

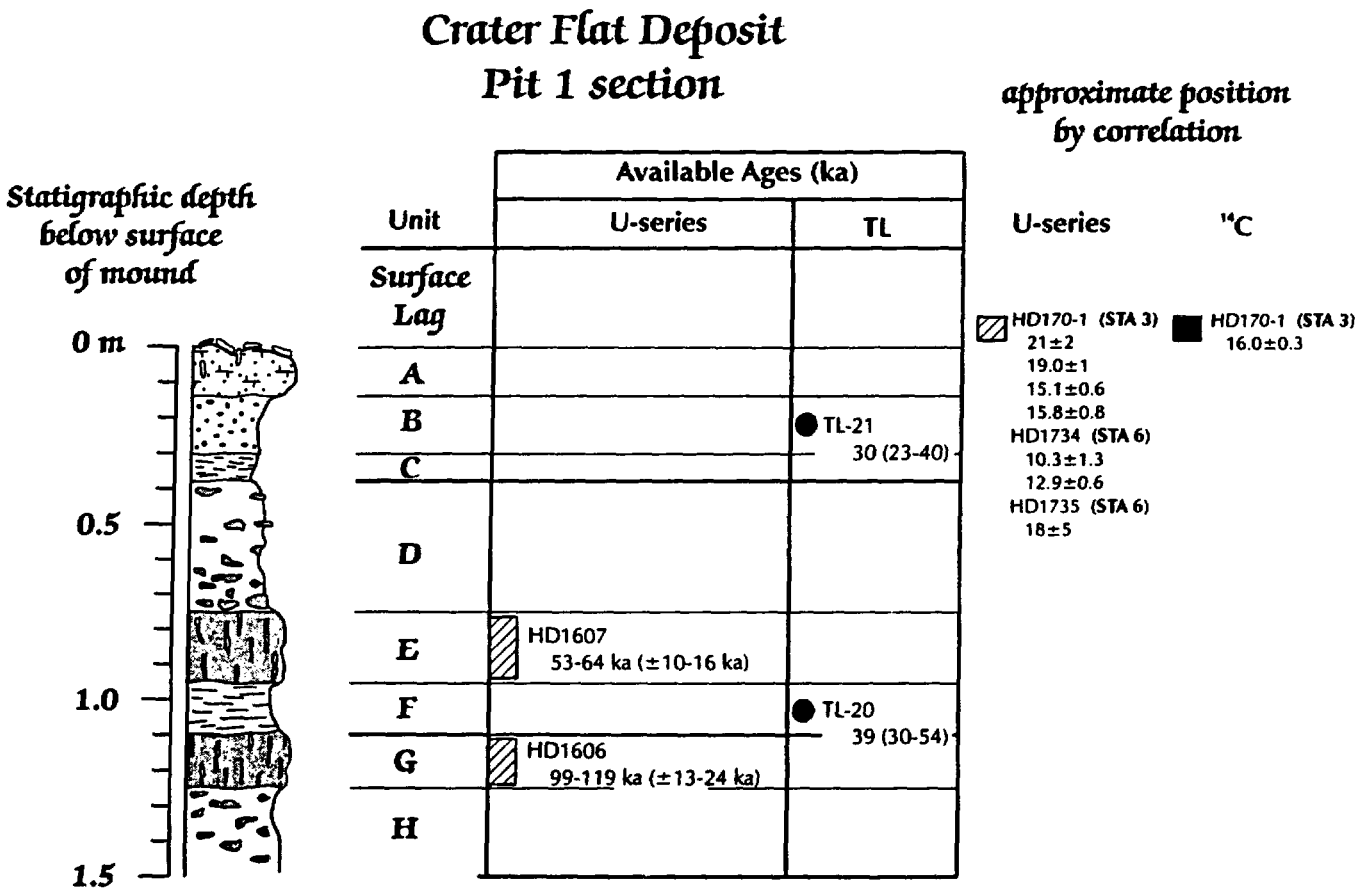

A Partially-cemented sandy loam with reddish-brown oxidized clayey zone at base
B Loose sandy loam, very friable
C Argillic zone containing distinct reddish brown oxidation
D Silty loam with variable amounts of matrix-carbonate and nodular carbonate
E Upper massive carbonate "vegatative mat" with vertically oriented root tubes
F Silty argillic zone
G Lower massive carbonate "vegatative mat" with vertically oriented root tubes
H Silty loam with variable amounts of matrix-carbonate and nodular carbonate

Figure 9: Measured stratigraphic section from Pit 1 at Station 4, CFD, with age determinations reported in Tables 4, 5 and 6. U-series ages for HD1606 and HD1607 are given as a range from 5 individual determinations on carbonate cement with high detrial-Th corrections and large uncertainties on individual determinations. Data are shown in Figure 10. TL ages are given for dose rates calcualted at half-saturation moisture contents followed parenthetically by the total range in ages calculated using different moisture contents and analytical uncertainties. Age data to the right of the column are correlated by position within the general stratigraphy.

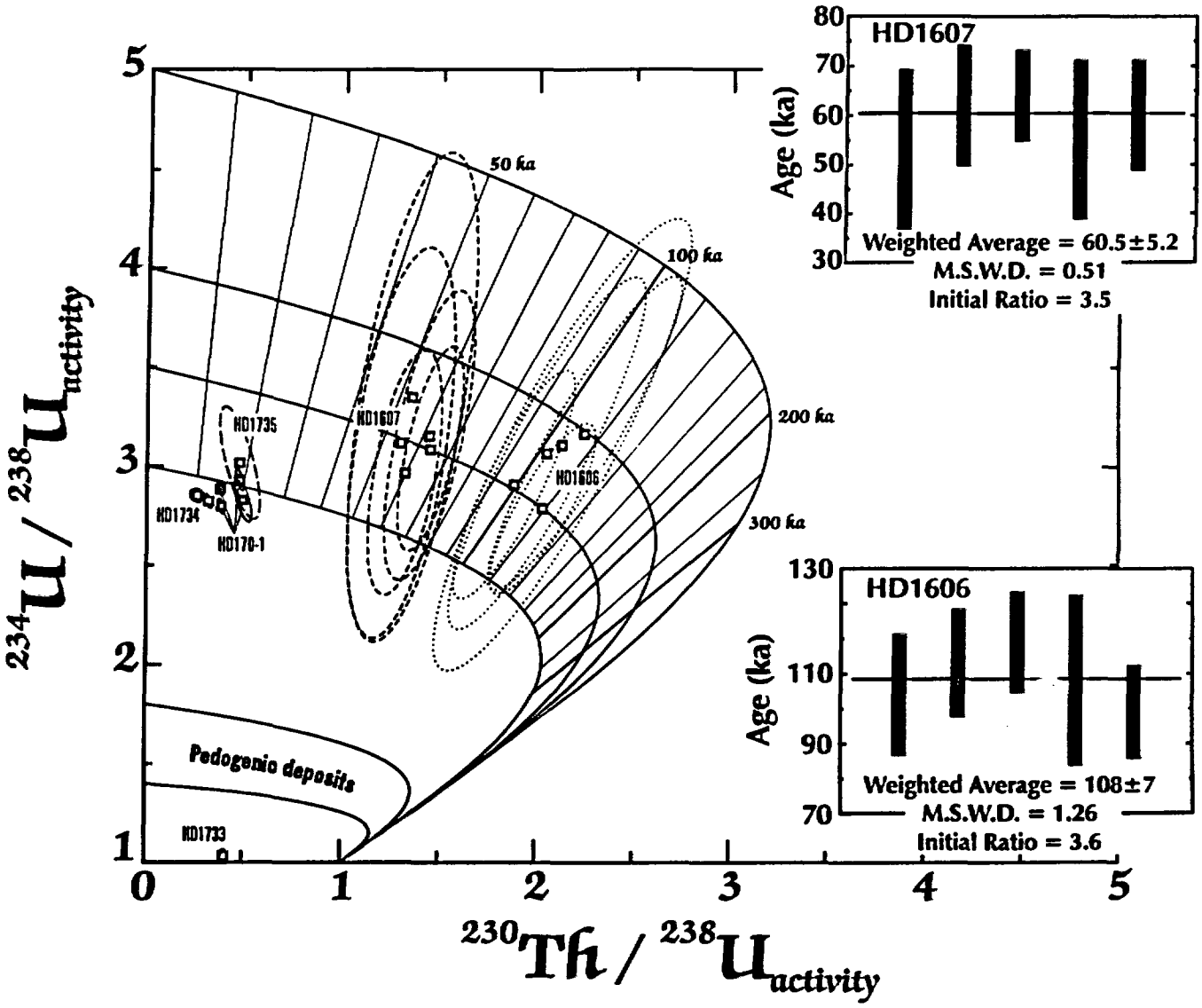

Figure 10: U-series evolution diagram showing U and Th isotopic results for data from CFD. Diagram is described in Figure 5. Samples HD1734 and HD170-1 have error ellipses that are about the same size as the square symbols. Samples HD1607 and HD1606 have very large error ellipses due to the high detrital-Th corrections required. However, data from five individual determinations form two resolvable clusters with ages that span limited ranges. Results of weighted averages for each sample are shown as insets. Data scatter for each group is within analytical error of the corrected data.

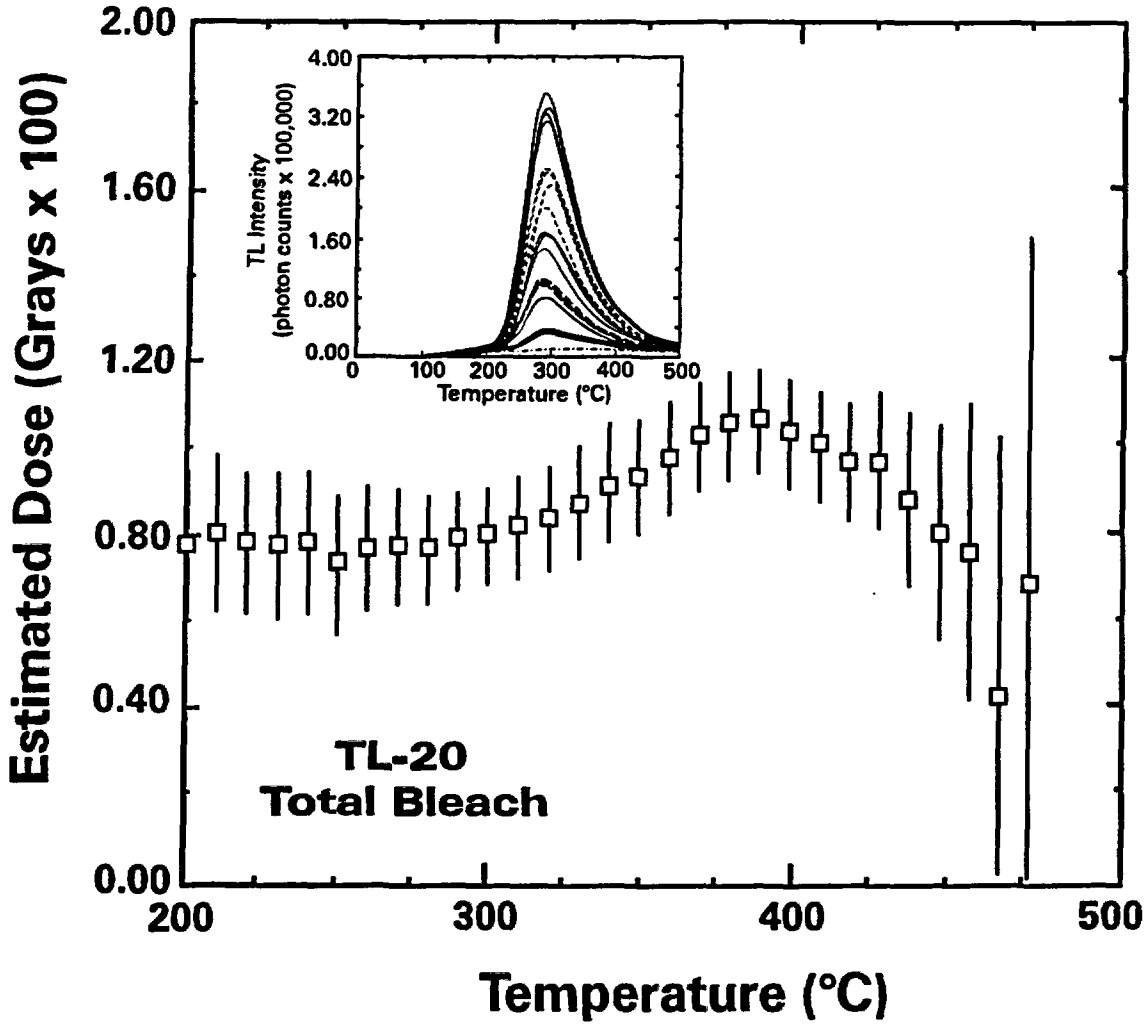

Figure 11: Estimated dose (D_E) versus temperature plot for sample TL-20 from CFD. See Figure 7 for details.

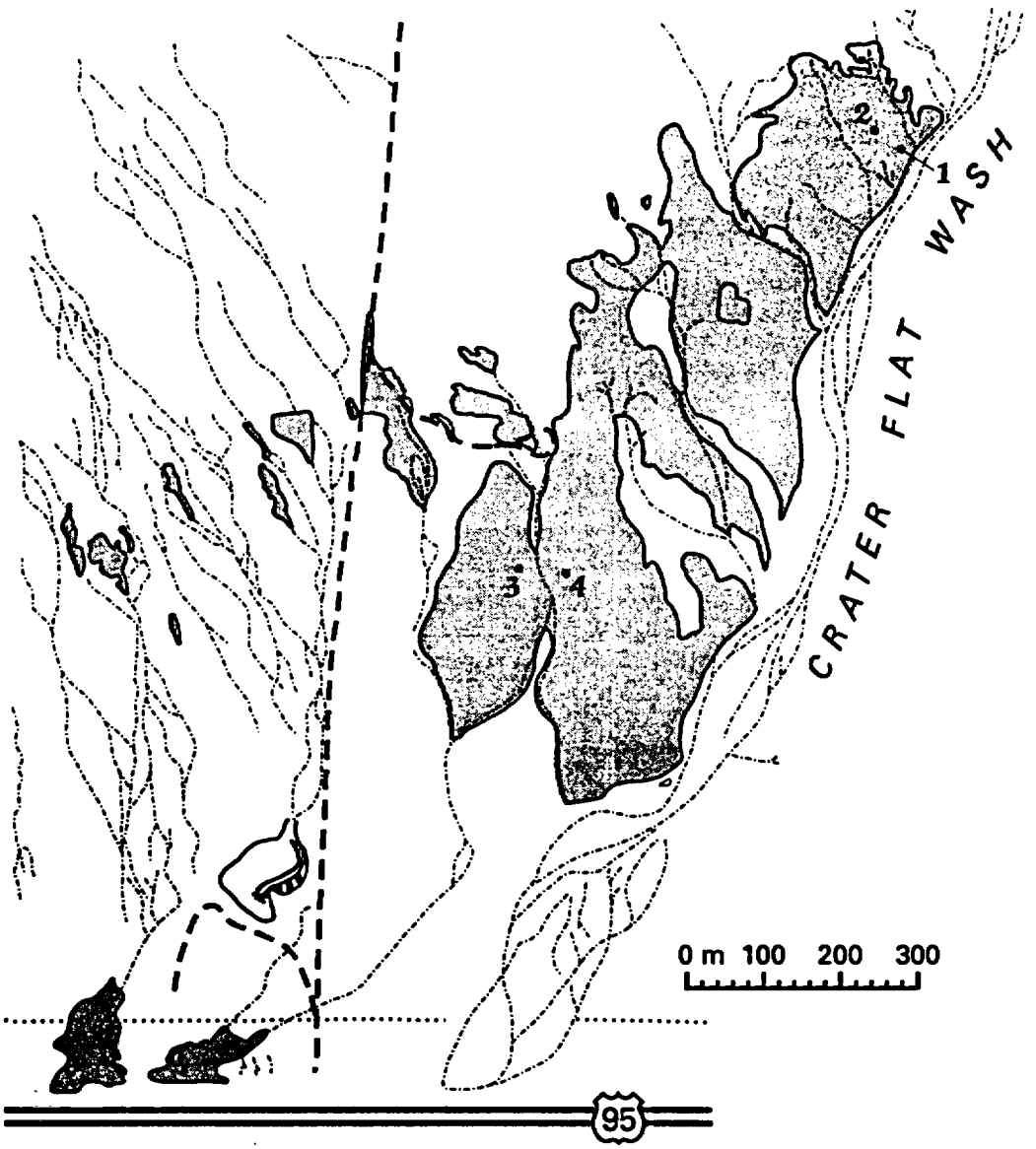

Figure 12: Sketch of air photos showing major morphologic features of the Crater Flat Wash deposit (CFW). Light-colored, fine-grained deoists are shown as light-shaded areas. Numbered sample stations are shown with small black circles. Dash-dot lines represent drainage channels.

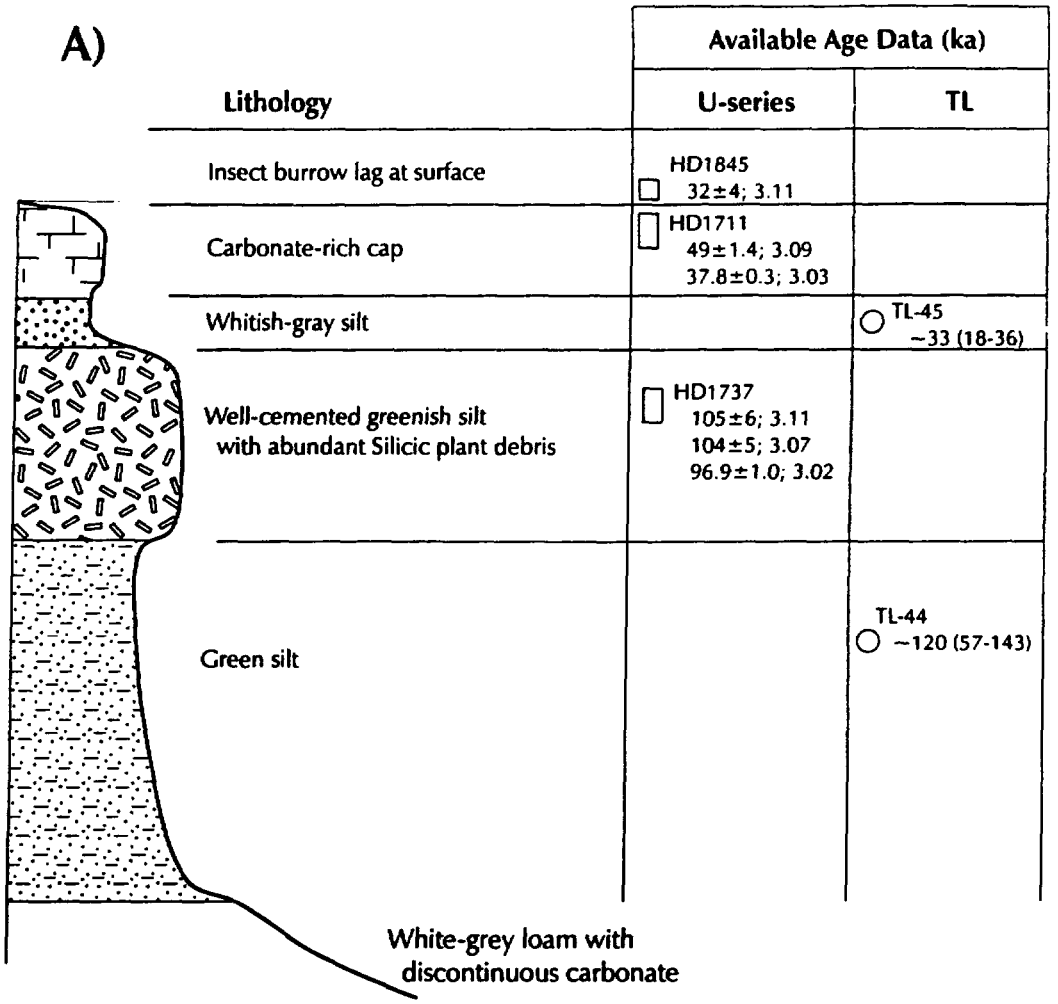

B)

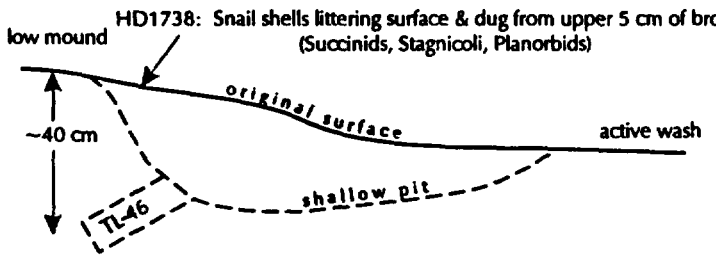

Available Age Data (ka)

Radiocarbon	U-series	TL
terrestrial snails	terrestrial snails	TL-46
9.01±0.25	11±2; 3.34	12 (11-17)
9.23±0.20		
aquatic snail		
10.8±0.24		

Figure 13: Schematic diagrams illustrating geological relations and geochronological data for two sites at SLD. Age determinations are from Tables 8, 9 and 10. All uncertainties are given at the 95% confidence level. Values following U-series ages are calculated initial 234U/238U ratios. TL ages are given for dose rates calculated at saturation-moisture contents followed parenthetically by the total range of ages calculated using different moisture contents and analytical uncertainties. A) Schematic cross-section of high-terrace spring deposits near Franklin Well. B) Schematic cross-section of brown silty deposits near the Amargosa River northwest of Franklin Well.

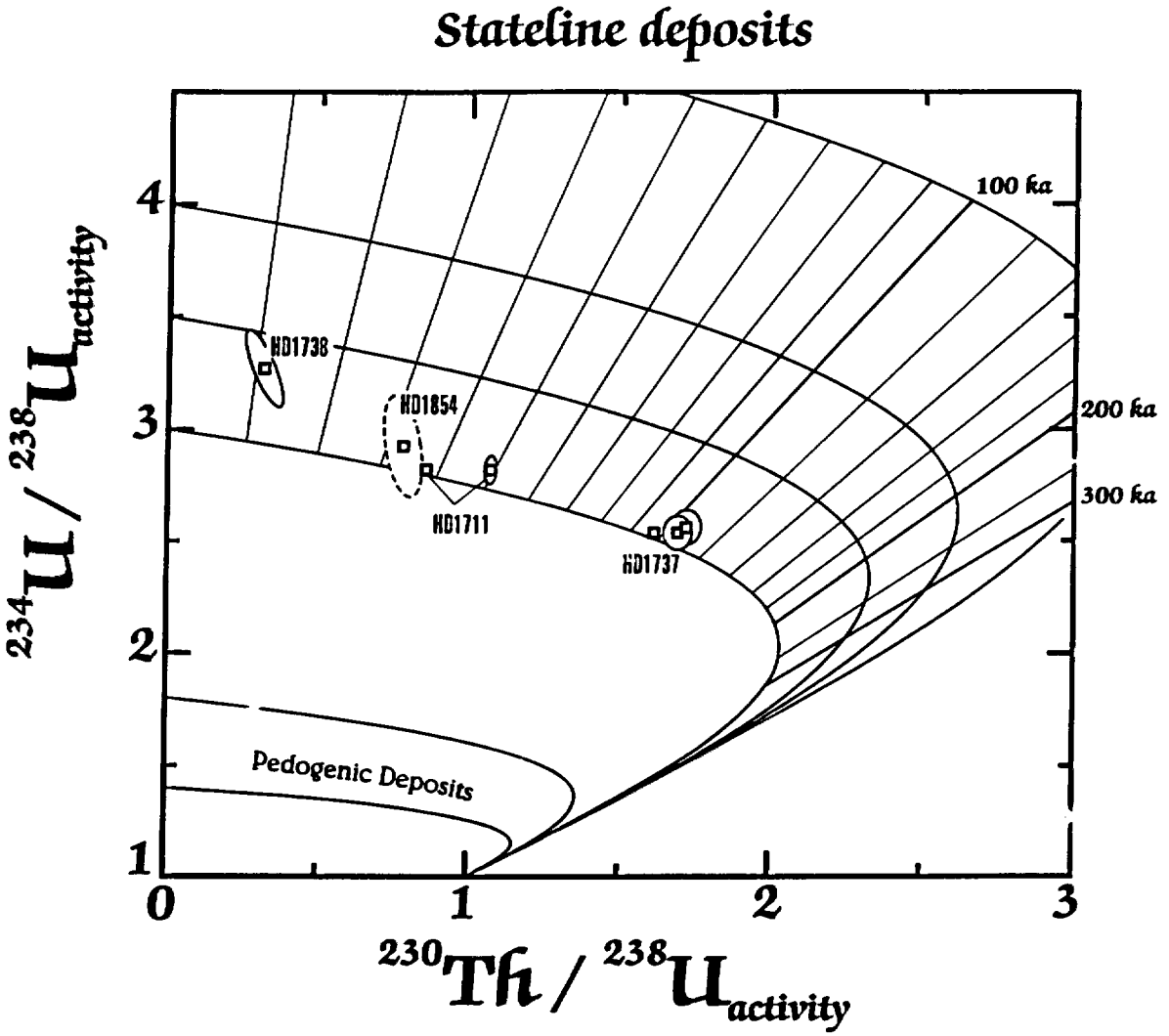

Figure 14: U-series evolution diagram showing U and Th isotopic results for data from SLD. Diagram is described in Figure 5.

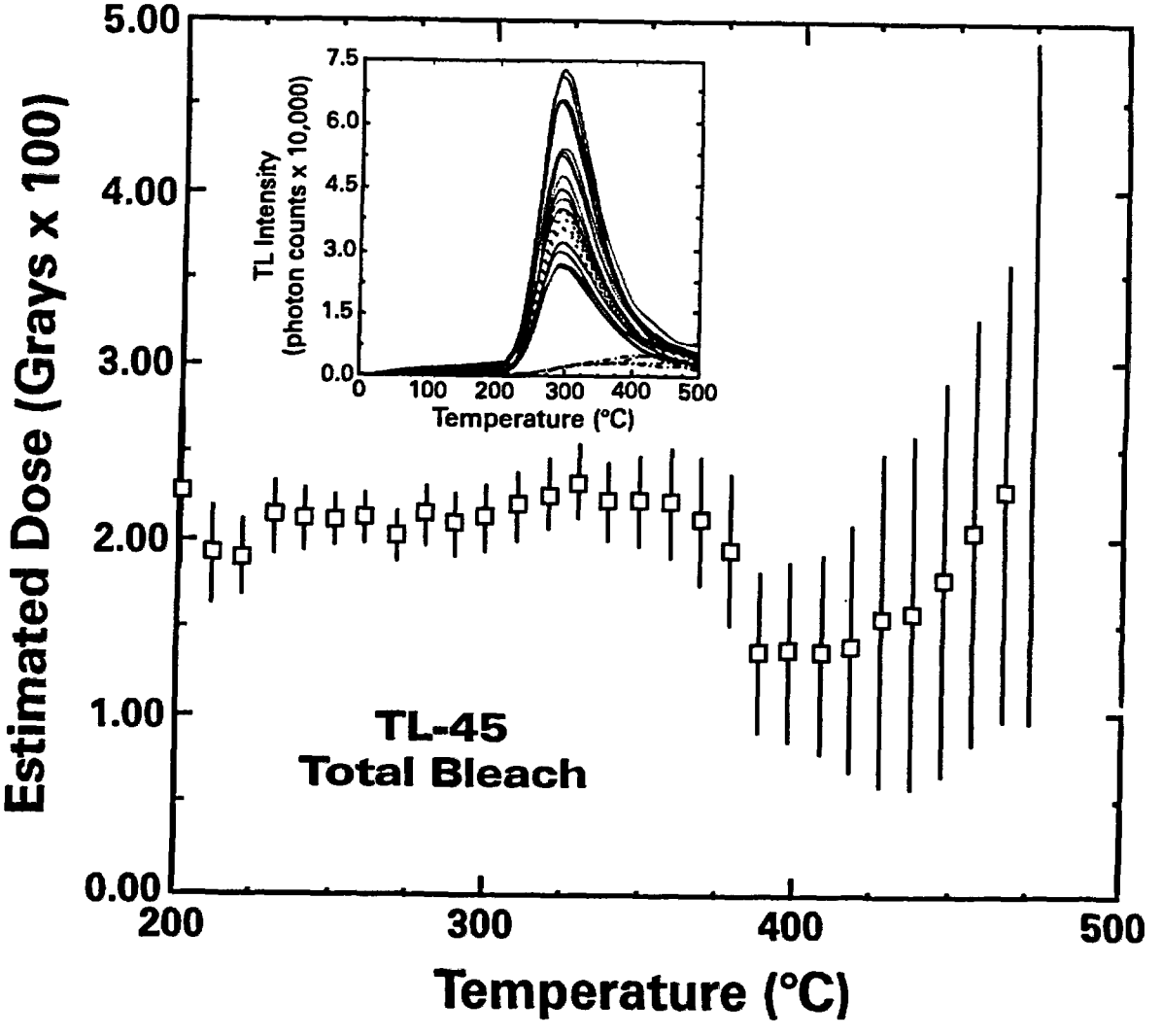

Figure 15: Estimated dose (D_e) versus temperature plot for sample TL-45 from SLD. See Figure 7 for details.

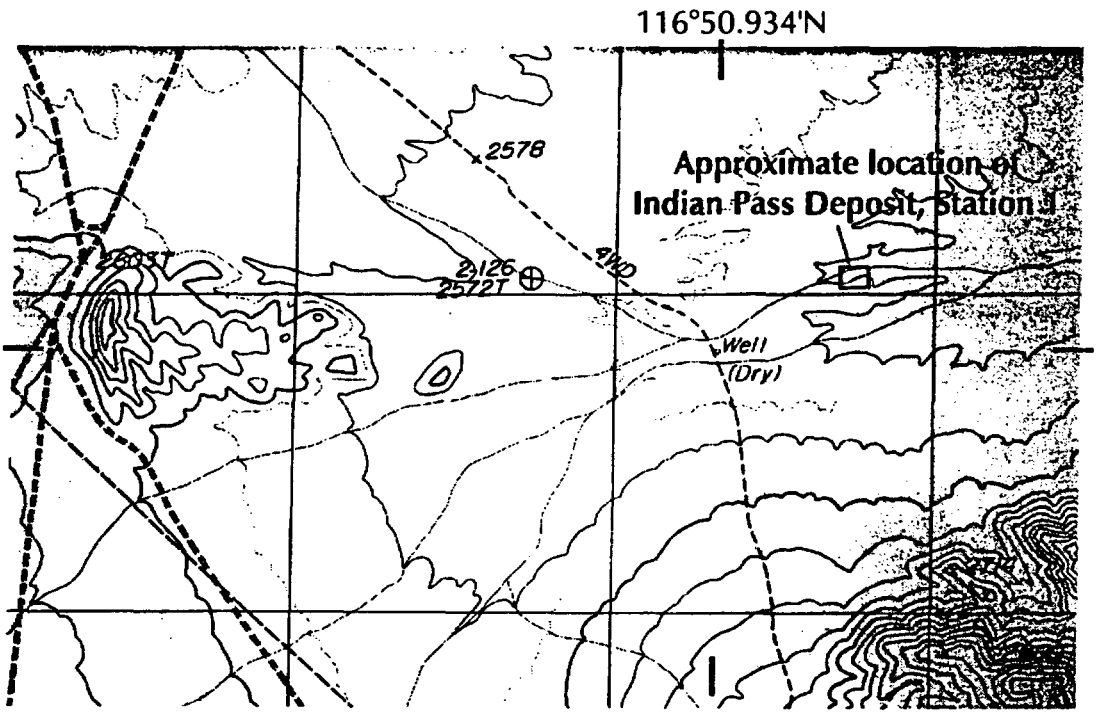

Figure 16: South-central portion of the Ashton Quadrangle, Nevada-California 7.5 minute series topographic map, showing the approximate location of Station 1 in the central portion of the IPD.

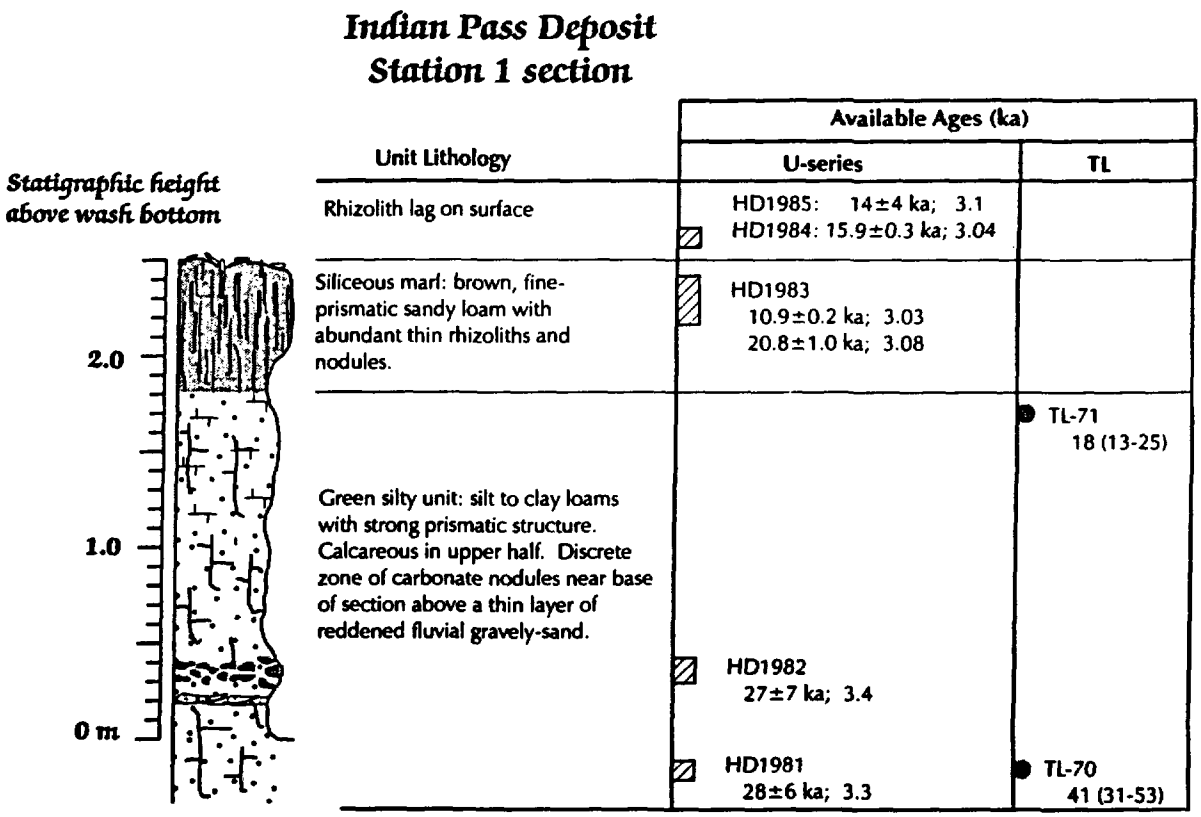

Figure 17: Measured stratigraphic section with age determinations reported in Tables 11 and 12. All uncertainties are given at the 95% confidence level. Values following U-series ages are calculated initial 234U/238U ratios. TL ages are given for dose rates calculated at saturation-moisture contents followed parenthetically by the total range of ages calculated using different moisture contents and analytical uncertainties.

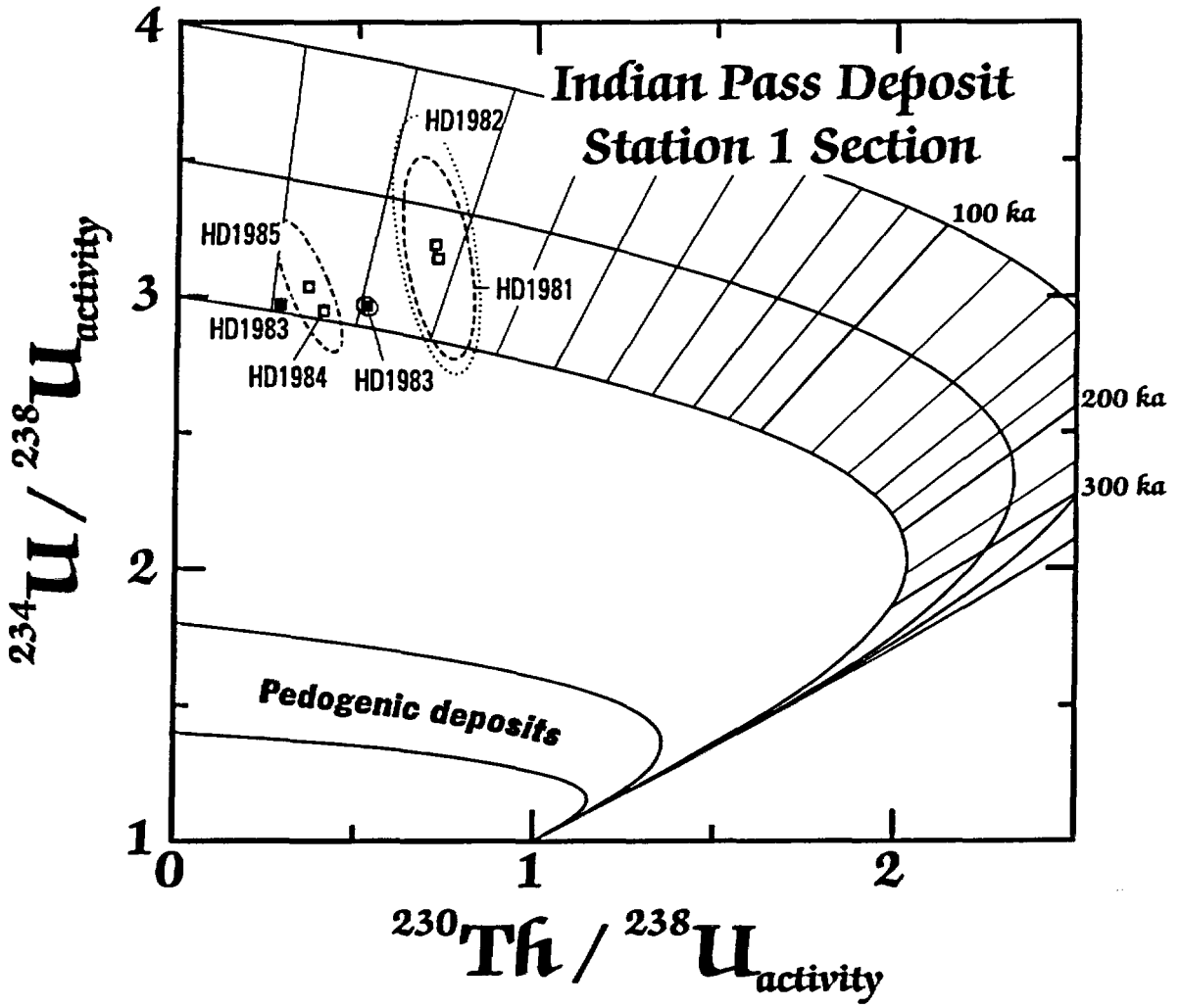

Figure 18: U-series evolution diagram showing U and Th isotopic results for data from IPD. Diagram is described in Figure 5.

Concordia-IPD-all.cdr (Aug96)

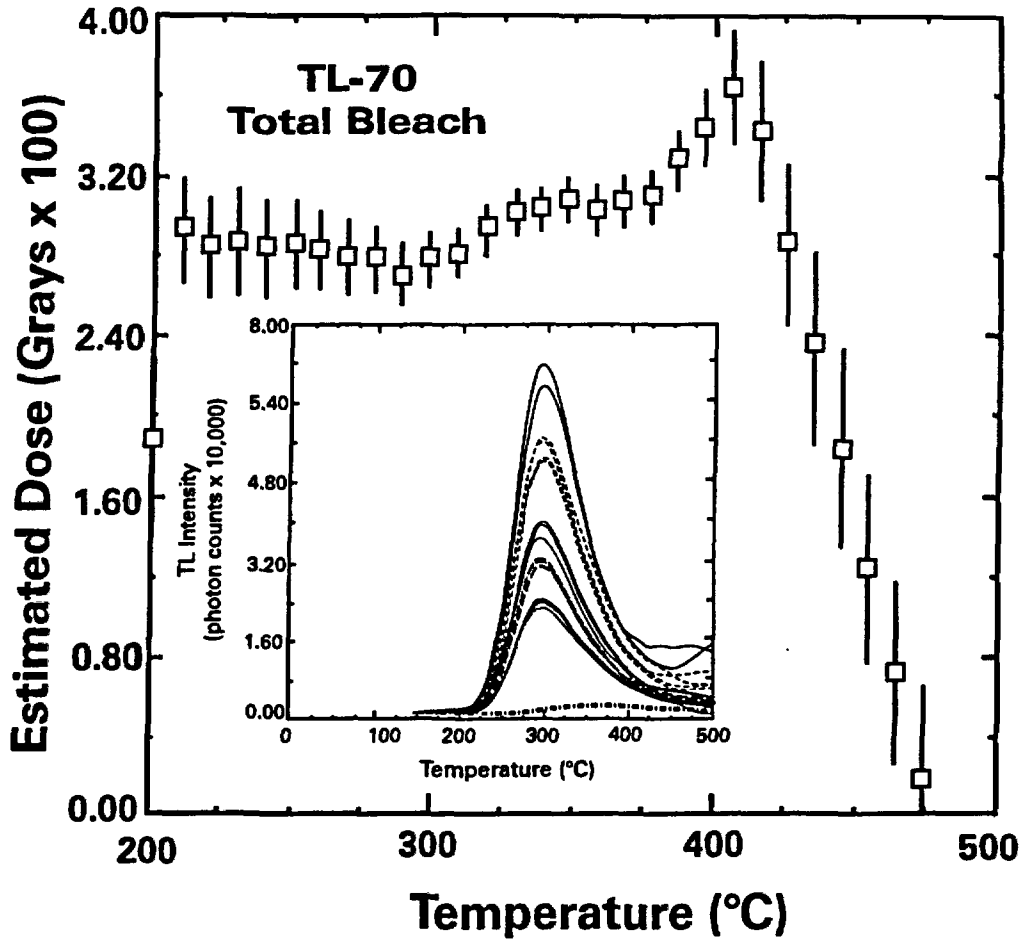

Figure 19: Estimated dose (D_t) versus temperature plot for sample TL-70 from IPD. See Figure 7 for details.

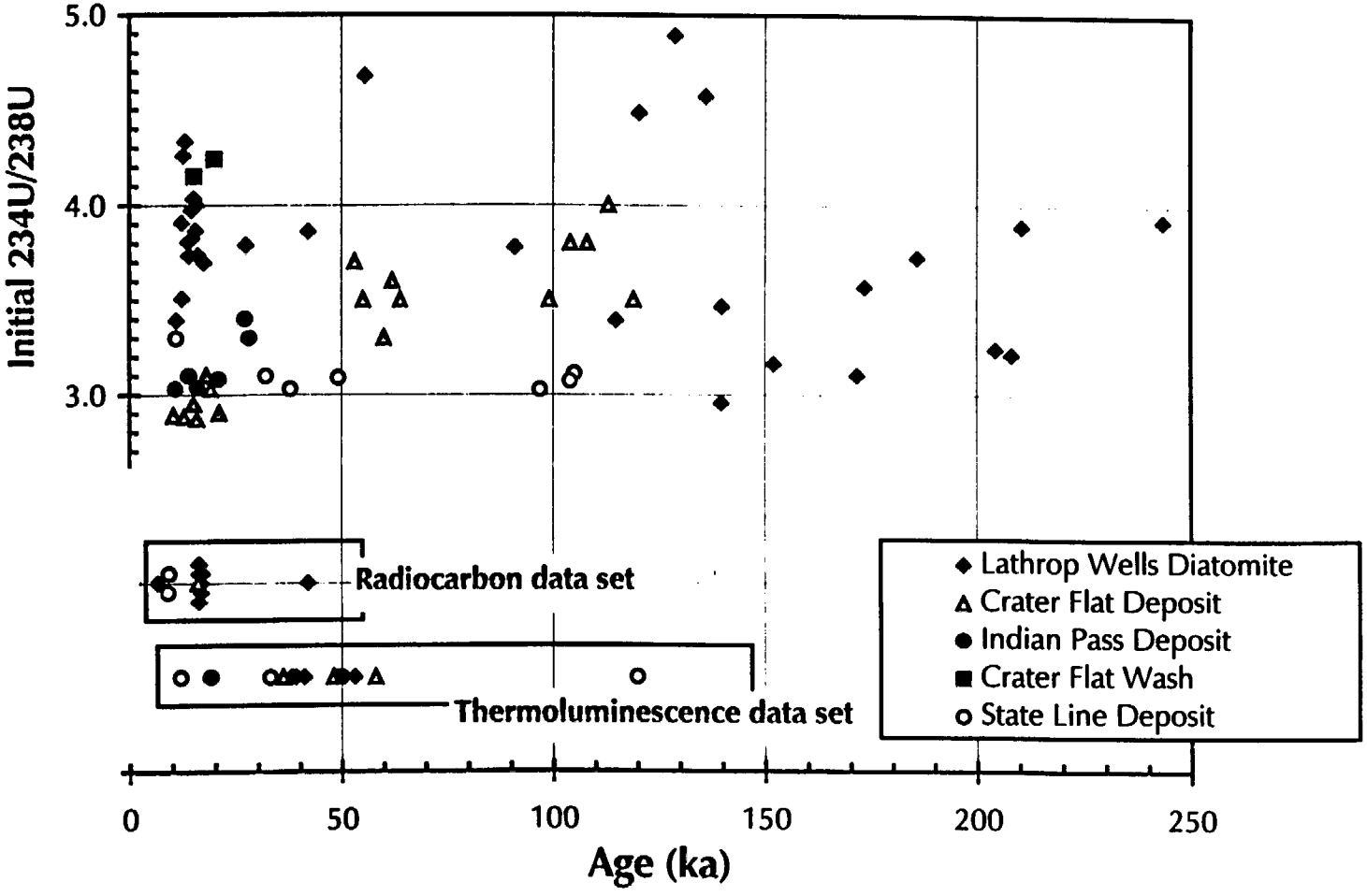

Figure 20: Ages determined by 230Th/U, radiocarbon and thermoluminescence methods for samples from paleodischarge sites. Data are grouped by locations given in Figure 1. Data in upper portion of diagram are 230U/Th ages plotted against calculated initial 234U/238U. The lower two data sets, representing radiocarbon ages and thermoluminescence ages are shown at the same age scale, but do not carry information regarding vertical position.

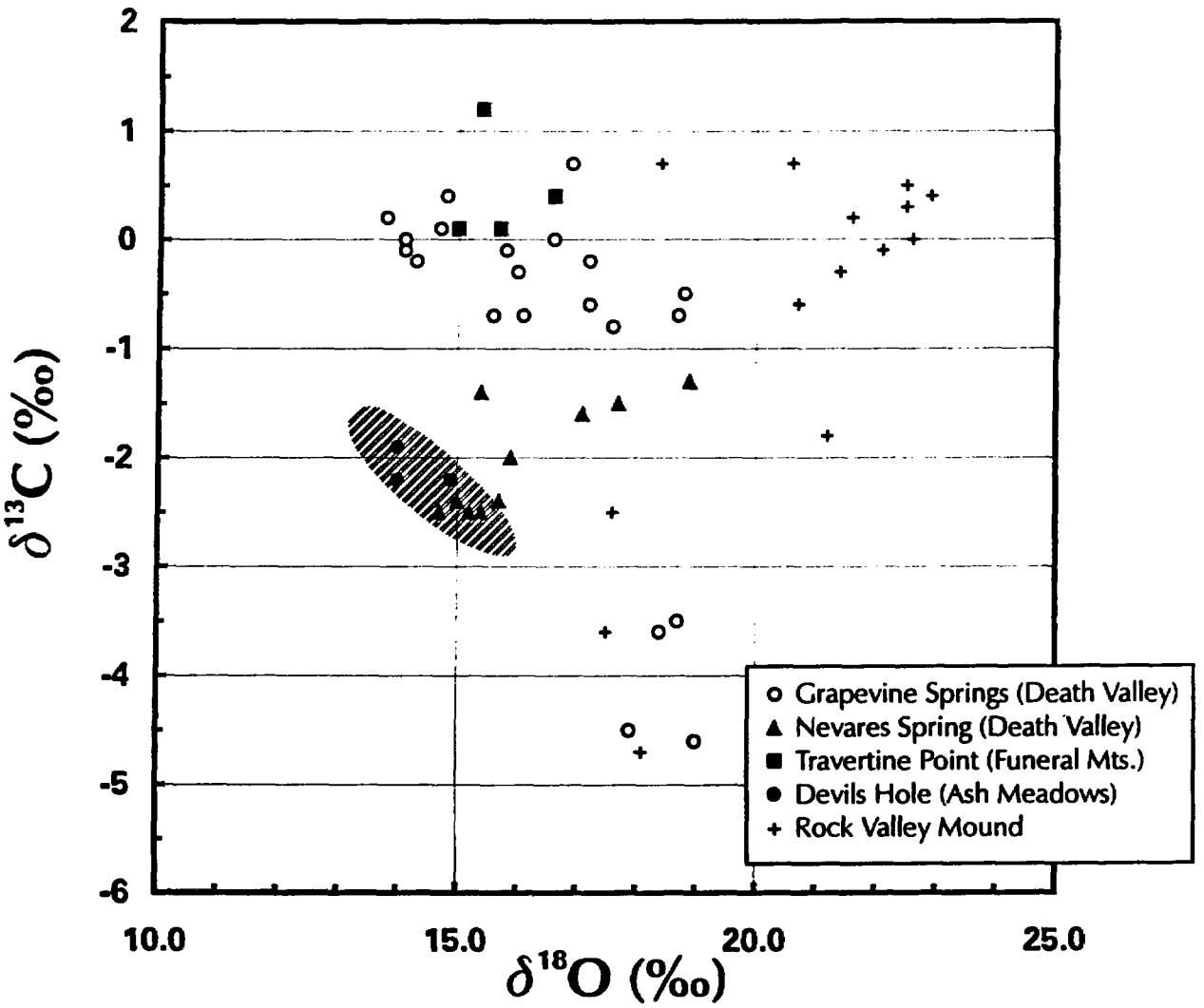

Figure 21: Stable C and O isotopic compositions of carbonate tufas and travertines from active spring discharge sites in the southern Nevada/Death Valley region. Data are from Table 13 and represent Grapevine (open circles) and Nevares (triangles) springs in Death Valley, Travertine Point (squares) in the Funeral Mountains, and Devils Hole (filled circles) in Ash Meadows. The shaded region represents supporting information from the large data set from Devils Hole core DH-11 from Winograd and others (1992) and Coplen and others (1994) and is included for comparitive purposes.. Data from a possible spring mound in Rock Valley (crosses) are also shown

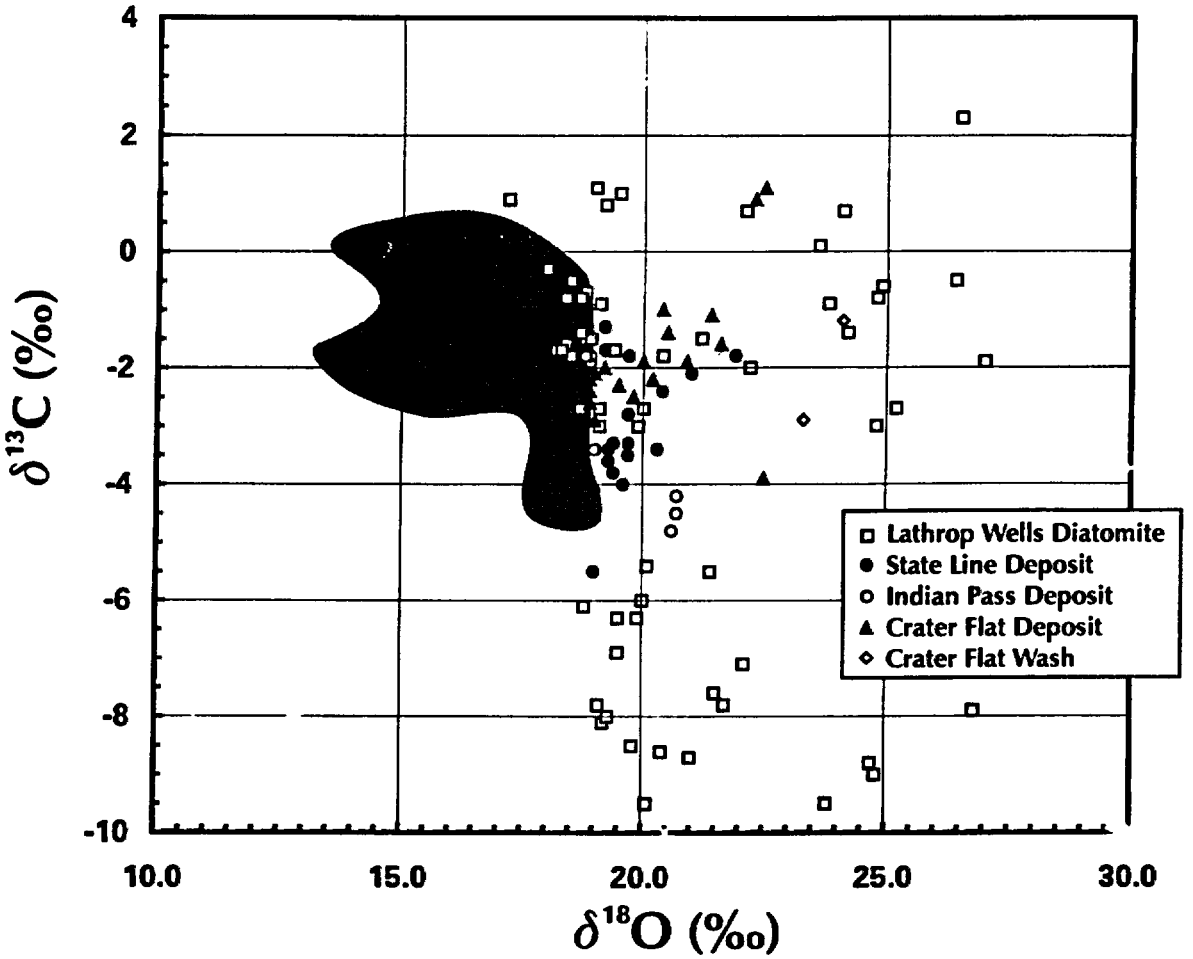

Figure 22: Stable C and O isotopic compositions of carbonates from the paleodischarge deposits that are the focus of this report plotted with different symbols representing each of the five sites. The shaded field represents compositions of tufa and travertine deposits shown in Figure 21.

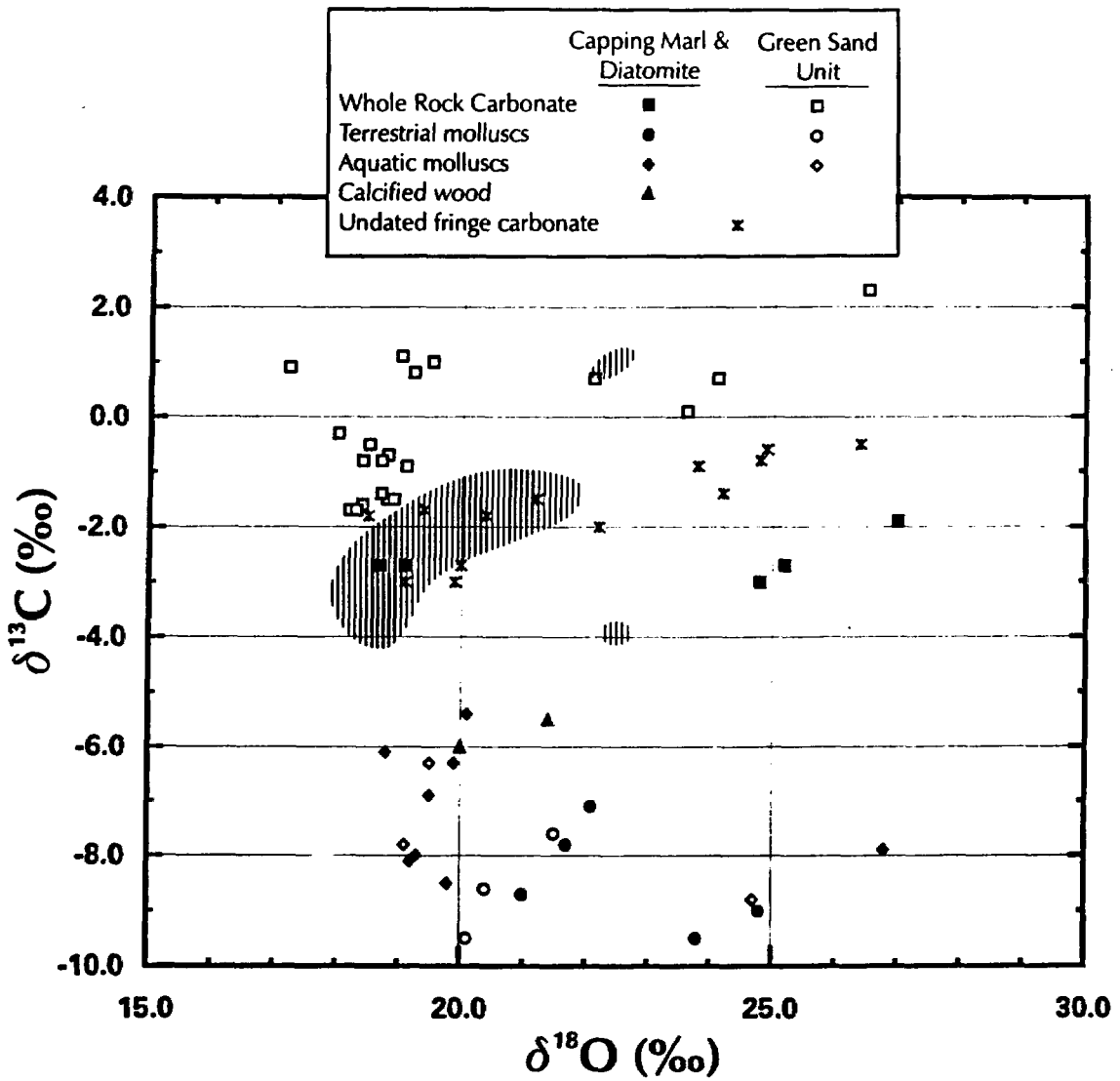

Figure 23: Stable C and O isotopic compositions of LWD carbonates. Based on preliminary geochronology, samples from the last glacial cycle are shown as filled symbols, samples from the penultimate glacial cycle are open symbols, and undated samples from the deposit fringe are shown as crosses. Fossil mollusc-shell carbonates are shown as diamonds and circles; whole rock cements and nodules are shown as squares; and petrified (calcified) plant matter is shown as triangles. The range of isotopic compositions of samples from the CFD is hatchured for comparison.

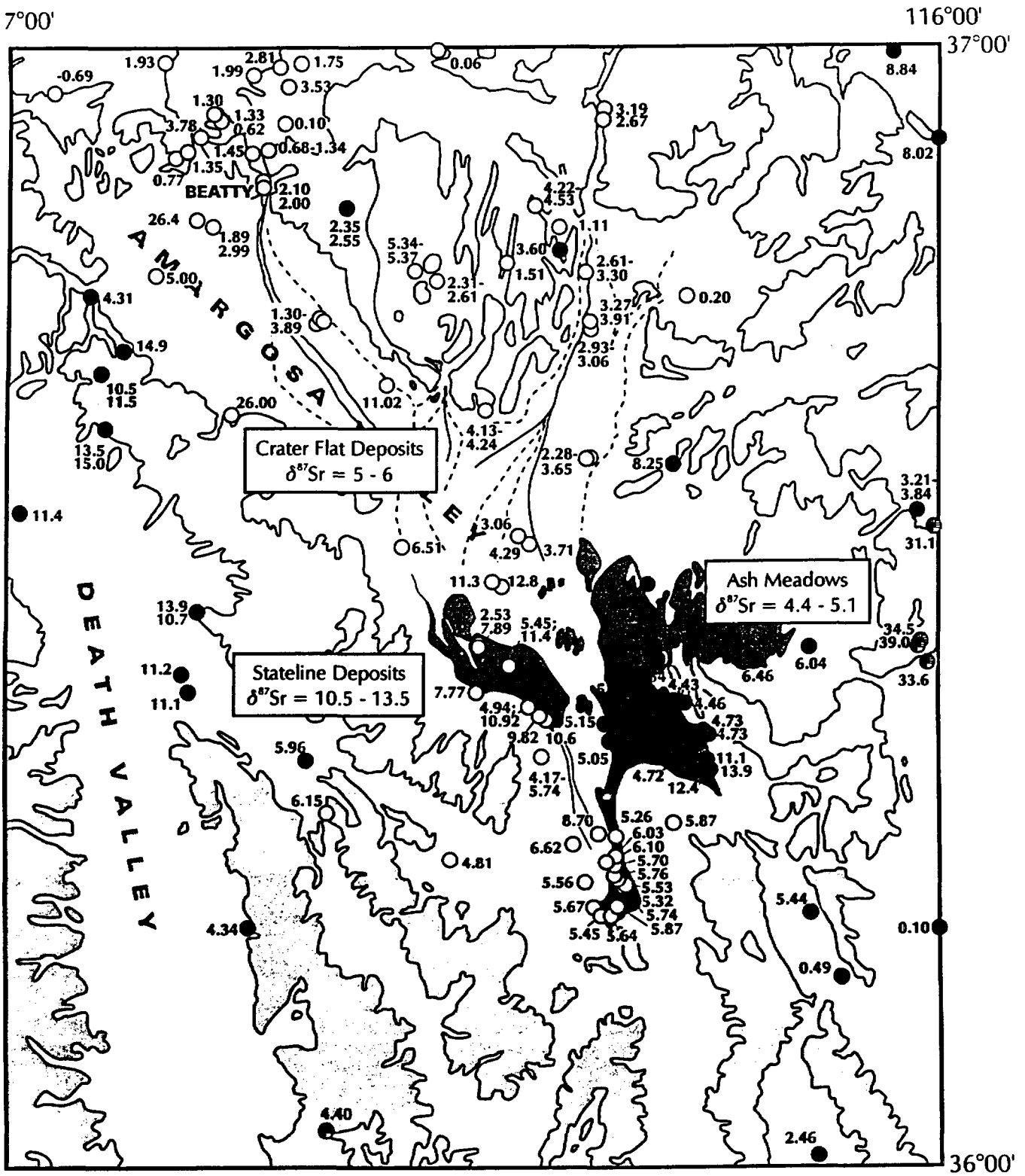

Figure 24: Location of wells and springs analyzed for $\delta^{87}Sr$ (values in ‰ relative to sea-water = 0.70920) from waters. Bedrock ranges are shown in shaded patterns, and alluvial-filled valleys are shown unpatterned. Solid and dashed lines within alluvial valleys represent active channels and alluvial fan boundaries, boundaries. Dark circles represent sample sites classified as Paleozoic aquifer, open circles represent sample sites from volcanic or alluvium aquifers, and circles with hatch marks represent sites classified as Precambrian aquifer.

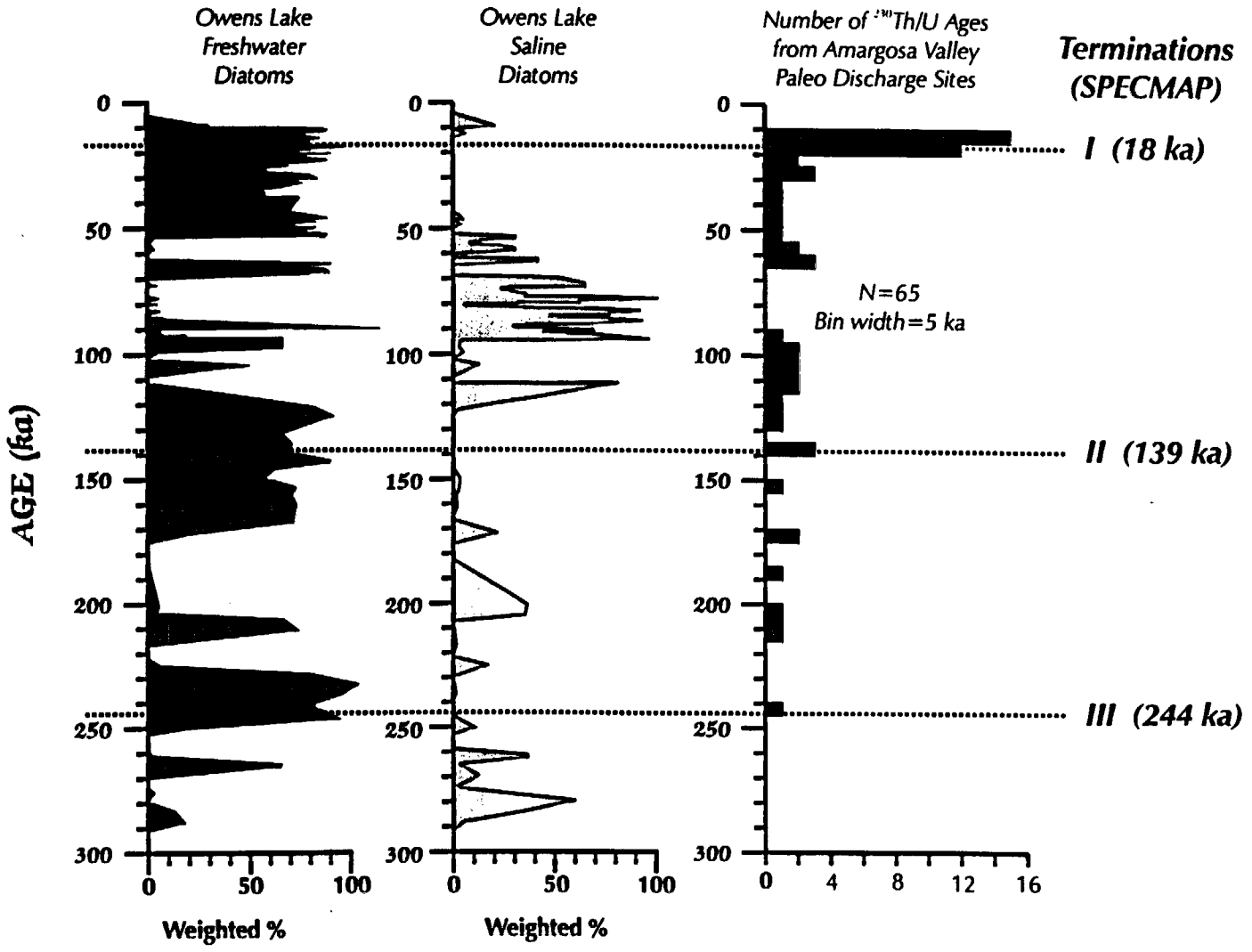

Figure 25: Comparison of the distribution of ^{230}Th/U ages from Amargosa Valley discharge deposits from this report with the distribution of freshwater and saline diatoms in Owens Lake core (data from Bradbury, 1996). Chronology for Owens Lake core is based on an assumed constant sedimentation rate between materials dated at 25 ka with radiocarbon and ash units identified as Bishop (~740 ka). Roman numerals and dotted tie-lines represent glacial terminations based on oxygen isotope record from sea-floor sediments (SPECMAP).